Cyclic Direct Simple Shear Test on Soft Clay at Low Normal Stress

As applicable to offshore pipeline axial walking

BY

YANG AO

BEng (Honours, Civil)
Monash University
Australia

A thesis submitted in fulfilment of the requirement for the degree of Master of Engineering Science (Research)

Department of Civil Engineering
Monash University
Australia

February 2015

To my mother and father,

who are devoted like Eastern parents and liberal like Western parents

Executive summary

Offshore pipelines play a significant role in transporting energy resources such as crude oil and natural gas from offshore platforms to processing facilities. The on-bottom stability of offshore pipelines is influenced significantly by the geotechnical conditions on the seabed. Pipelines undergo a number of thermal cycles during their operational life. At the end of each thermal cycle, some part of the expansion recovers, whereas the irrecoverable expansion accumulates at the free ends and causes the pipe to move axially in one direction, a phenomenon known as axial walking. The test results from the Monash Advanced Pipe testing System (MAPS) imply that pipe axial walking induces relative movements of the soil below the pipe. Since the pipe-soil interaction is extensively influenced by the soil response, the portion of the soil below the pipe which undergoes shearing, characterised as the shear zone, is significant for pipe axial walking assessment and thus needs thorough investigation.

The research program reported here investigates the behaviour of soil within the shear zone in pipe axial walking problems. Cyclic direct simple shear tests on soft clay at low normal stress are performed as applicable to axial walking problems. The soil response in the shear zone is characterised as undrained, partially drained, or drained, based on cyclic shearing velocities and the relationship between residual shear resistance and shearing velocity is investigated. Finite element analyses are also conducted to capture the behaviour of soil within the shear zone, utilising an advanced constitutive soil model. Based on the results from both experimental work and numerical analysis, a set of data is established which can be applied in the calibration of large-scale pipe axial walking modelling, and provide guidance on the design practice of offshore pipelines when considering on-bottom stability in axial direction.

Declaration

I thereby declare that material contained in this thesis has not been published in any other degree or diploma in any other institution. To the best of my knowledge no material presented within has been previously published or written by others except where references are sighted in the text.

[redacted]

Yang Ao
Department of Civil Engineering
Monash University
Australia
February 2015

Acknowledgements

I would like to express my deepest gratitude to my main supervisor, Professor Jayantha Kodikara, for his guidance and support over the past two years. This research program could not have progressed smoothly without his expertise and his assistance throughout the course of the program. Professor Kodikara's generosity and kindness to me has made the past two years one of the most memorable times of my life. I would also like to thank my co-supervisor Dr Dilan Robert, especially for his invaluable guidance in numerical modelling. Many thanks are due to Dr M.Senthilkumar and Dr P.Rajeev, who assisted me greatly at the beginning of the research program.

I would like to thank the staff in the Department of Civil Engineering, Monash University. Our Research and Postgraduate Manager is the incredible Ms Jenny Manson, and I have always been amazed how Jenny manages approximately 100 postgraduate research students all by herself. I thank the laboratory staff who helped me complete the experimental work, Mr Mike Leach and Mr Long Goh, and Dr Ben Shannon who provided the soil properties data and assisted me in setting up the tests. Dr Alex McKnight assisted by proofreading the final version for grammar and style.

I offer many thanks to my fellow postgraduate students, Qianyi Song, Yang Liu, Iris Yan Yang, Bo Zou, Xiao Yang and Andrew Fujia Luo, as my out-of-work time would have been much less fun without you guys. Thanks to my officemates in Room 117 building 36, Michael Von'T Steen, my unofficial career advisor, Asgar Ali, and others too numerous to name individually.

Table of Contents

Executive summary .... **ii**

Acknowledgements .... **iv**

Table of Contents .... **v**

List of Figures .... **viii**

List of Tables .... **xi**

Chapter 1 Introduction **1**

1.1 Background 1

1.2 Research Objectives 3

1.3 Structure of thesis 4

Chapter 2 Literature review **6**

2.1 Offshore pipeline axial walking 6

2.1.1 Axial pipe-soil interaction 6

2.1.2 Drained and undrained soil resistance 7

2.1.3 Cyclic axial response in an effective stress framework 9

2.1.4 Theoretical framework for axial resistance 12

2.2 Shear zone in offshore pipeline axial walking 16

2.3 Generic load-displacement relationship in pipe axial walking 17

2.4 Residual resistance and undrained/drained limits in MAPS 19

2.5 Utilising cyclic direct simple shear test in offshore pipeline axial walking problems 21

2.6 Direct simple shear test 22

2.6.1 Development of direct simple shear test 22

2.6.2 Drained and undrained direct simple shear test 26

2.6.3 Constant-volume undrained equivalent test 27

2.6.4 The advantages of direct simple shear test over triaxial test 27

2.6.5 Non-uniformities in direct simple shear test 28

2.6.6 The effect of side boundaries on the uniformities of stress/strain 29

2.7 Summary 30

Chapter 3 Experimental program and results **31**

3.1 Soil selection 31

3.1.1 General soil properties 31

3.1.2 Specific gravity 32

3.1.3 Particle size analysis 32

3.1.4 Atterberg limits analysis 33

3.1.5 Oedometer analysis 34

3.1.6 Triaxial tests 35

3.1.7 Summary 36

3.2 Experimental set-up 37

3.2.1 GDS direct simple shear testing system 37

3.2.2 Specimen preparation 38

3.2.3 Pore pressure measurement 38

3.3 Test methodology 42

3.3.1 Consolidation and normal stress 42

3.3.2 Shearing velocity and shearing amplitude 43

3.3.3 Summary of test approach 44

3.4 Test results 45

3.4.1 Consolidation stage 45

3.4.2 Cyclic shearing stage 47

3.5 Concluding remarks 55

Chapter 4 Numerical modelling 58

4.1 Finite element model 58

4.1.1 Critical state soil theory and modified Cam-clay model 58

4.1.2 Two-dimensional finite element model 59

4.1.3 Material properties 59

4.1.4 Load and boundary conditions 62

4.1.5 Validation of the finite element model 63

4.2 Finite element analyses results 65

4.2.1 Scope of the analyses 65

4.2.2 Consolidation stage 65

4.2.3 Cyclic shearing stage 70

4.3 Summary of major findings 82

Chapter 5 Conclusions and recommendations 85

5.1 Conclusions 85

5.2 Recommendations for future research 86

References 87

Appendices **91**

A. Critical state soil theory and modified Cam-clay model 91

B. Additional FEA results 98

C. Sample .inp file of the finite element model 105

List of Figures

Figure 2.1 Axial friction resistance schematic with mobilisation displacement and breakout (Bruton et al., 2008) ..... - 7 -

Figure 2.2 Interface shearing: kaolin clay and Storeælt clay till (White and Cathie, 2011, Steenfelt, 1993) ..... - 9 -

Figure 2.3 Time history during cyclic axial pipe testing (White et al., 2011b) ..... - 10 -

Figure 2.4 Friction factor response in cyclic axial pipe testing (White et al., 2011b) ..... - 11 -

Figure 2.5 (a) Total stress interpretation of axial response (b) Effective stress interpretation of axial response (White et al., 2011b) ..... - 12 -

Figure 2.6 (a) Schematic diagram for analysis of velocity effects for planar shearing (b) Stress paths in e-lnσ'_v space (Randolph et al., 2012) ..... - 13 -

Figure 2.7 (a) Example relationships between excess pore pressure and time or shear strain Planar shearing responses for different normalised velocities Variation in resistance with (b)time; (c)displacement (Randolph et al., 2012) ..... - 15 -

Figure 2.8 Shear zone underneath axially-walking pipe (Senthilkumar, 2013) ..... - 16 -

Figure 2.9 (a) Shear zone underneath axially walking pipe and (b) loading pattern of direct simple shear test ..... - 17 -

Figure 2.10 Generic pipe load-displacement curve with emphasis on residual resistance (Senthilkumar, 2013) ..... - 18 -

Figure 2.11 Normalised residual resistance at various displacement rates and pipe embedments for (a) smooth pipe and (b) rough pipe (Senthilkumar, 2013) ..... - 20 -

Figure 2.12 An illustration of the direct shear box (Zekkos et al., 2010) ..... - 23 -

Figure 2.13 Illustrations of direct simple shear test (left) and direct shear test (right) ..... - 24 -

Figure 2.14 S.G.I Direct Simple Shear Device (Kjellman, 1951) ..... - 25 -

Figure 2.15 (a) NGI direct simple shear device (b) Reinforced rubber membrane (Bjerrum and Landva, 1966) ..... - 26 -

Figure 2.16 Stresses acting on test sample: (a) in direct simple shear apparatus; (b) in true simple shear (Airey and Wood, 1987) ..... - 28 -

Figure 2.17 Side view of a plasticine sample after shearing under a normal stress of 12kPa (Roscoe, 1953) ..... - 29 -

Figure 2.18 Three vertical boundary configurations considered (Grognet, 2011) ..... - 29 -

Figure 3.1 Soil sample of Prestige NY and Seabed Silt (Senthilkumar, 2013) ..... - 32 -

Figure 3.2 Particle size distribution curves (Senthilkumar, 2013, Shannon, 2013) ..... - 33 -

Figure 3.3 USGS Charts (Senthilkumar, 2013, Shannon, 2013) ..... - 34 -

Figure 3.4 Consolidation and re-consolidation curves of oedometer tests (Senthilkumar, 2013, Shannon, 2013) .... - 35 -

Figure 3.5 GDS Standard Simple Shear System (GDS-STDSS)........ - 37 -

Figure 3.6 Specimen preparation and insertion .... - 38 -

Figure 3.7 Pore pressure measurement configuration........ - 40 -

Figure 3.8 (a) De-airing water apparatus (b) Water injection........ - 41 -

Figure 3.9 Measuring cylinder connecting to the top drainage port........ - 41 -

Figure 3.10 Variations in horizontal load readings due to rail friction........ - 43 -

Figure 3.11 Consolidation displacement vs. (a) Elapsed time (b) Normalised time .... - 46 -

Figure 3.12 PPT Readings at consolidation stage........ - 46 -

Figure 3.13 Cyclic shearing of the soil specimen........ - 48 -

Figure 3.14 Excess pore pressure development at shearing stage .... - 50 -

Figure 3.15 Continuous consolidation at shearing stage .... - 51 -

Figure 3.16 Shear stress-strain relationship for (a) 0.3mm/s and (b) 0.03mm/s........ - 53 -

Figure 3.17 Shear stress-strain relationship for (a) 0.005mm/s and (b) 0.0005mm/s........ - 54 -

Figure 3.18 Residual resistance versus normalised velocity .... - 56 -

Figure 4.1 Two-dimensional finite element model........ - 59 -

Figure 4.2 Implementation of deformation pattern in cyclic shearing in FEA model........ - 63 -

Figure 4.3 Comparison between experimental and FEA shear stress-strain curves........ - 64 -

Figure 4.4 (a) Vertical displacement vs. normalised time and (b) void ratio vs. normalised time plots at consolidation stage........ - 67 -

Figure 4.5 Excess pore pressure reference element........ - 68 -

Figure 4.6 (a) Excess pore pressure Δu vs. normalised time and (b) $\Delta u/\sigma_n$ vs. normalised time plots at consolidation stage........ - 69 -

Figure 4.7 (a) horizontal displacement function and (b) shear strain definition........ - 70 -

Figure 4.8 Pore pressure distribution at cyclic shearing stage........ - 71 -

Figure 4.9 Excess pore pressure development at cyclic shearing stage for applied vertical stress of 10kPa .... - 73 -

Figure 4.10 Excess pore pressure development at cyclic shearing stage for applied vertical stress of 60kPa .... - 74 -

Figure 4.11 Void ratio versus shear strain plots for applied vertical stress of 10kPa and shear amplitude of 10% of H........ - 76 -

Figure 4.12 Void ratio versus shear strain plots for applied vertical stress of 60kPa and shear amplitude of 10% of H........ - 77 -

Figure 4.13 Shear stress-strain curves for applied vertical stress of 10kPa........................ - 79 -

Figure 4.14 Shear stress-strain curves for applied vertical stress of 60kPa........................ - 80 -

Figure 4.15 Effective stress interpretation of shear stress-strain relationship .... - 81 -

Figure 4.16 Residual resistance versus normalised velocity .... - 83 -

Figure A.1 (a) *e*-log *p'* curve of an isotropic consolidation test and (b) consolidation curve in the *e*-ln *p'* plane (Helwany, 2007) .... - 93 -

Figure A.2 Critical state definition (Helwany, 2007) .... - 94 -

Figure A.3 (a) Normal consolidation and critical state lines in the *e*-ln *p'* plane (b) yield surface of a Cam-clay model in the *q*-*p'* plane (Helwany, 2007) .... - 95 -

Figure A.4 State boundary surface of the Cam-clay model (Helwany, 2007).................... - 95 -

Figure A.5 Excess pore pressure development at cyclic shearing stage for applied vertical stress of 20kPa .... - 99 -

Figure A.6 Excess pore pressure development at cyclic shearing stage for applied vertical stress of 40kPa .... - 100 -

Figure A.7 Void ratio versus shear strain plots for applied vertical stress of 20kPa and shear amplitude of 10% of H.. - 101 -

Figure A.8 Void ratio versus shear strain plots for applied vertical stress of 40kPa and shear amplitude of 10% of H.. - 102 -

Figure A.9 Shear stress-strain curves for applied vertical stress of 20kPa....................... - 103 -

Figure A.10 Shear stress-strain curves for applied vertical stress of 40kPa..................... - 104 -

List of tables

Table 3.1 General soil properties (Senthilkumar, 2013) .... - 31 -

Table 3.2 Specific Gravity of Seabed silt and Prestige NY (Senthilkumar, 2013)............. - 32 -

Table 3.3 Consolidation parameters from oedometer tests (Senthilkumar, 2013, Shannon, 2013) .... - 35 -

Table 3.4 Parameters and properties in triaxial tests (Senthilkumar, 2013,Shannon, 2013)- 36 -

Table 3.5 Geotechnical properties of Seabed silt and Prestige NY kaolinite (Senthilkumar, 2013, Shannon, 2013) .... - 36 -

Table 3.6 Soil properties and test parameters at consolidation stage .... - 45 -

Table 3.7 Test parameters at the cyclic shearing stage .... - 47 -

Table 4.1 Material inputs for the finite element modelling ....- 60 -

Table 4.2 Vertical permeability for different void ratio levels...- 61-

Table 4.3 Variables in finite element analyses...- 63 -

Chapter 1 - Introduction

1.1 Background

Offshore pipelines play a significant role in transporting energy resources such as crude oil and natural gas from offshore platforms to processing facilities. Due to the increasing demand for fossil fuels in recent years, and the development of technology which makes access to deep-sea energy resources possible, the offshore energy industry has grown rapidly. Longer pipelines are laid and such pipelines are required to operate at more extreme conditions. For instance, high operating temperature and pressure need to be applied within some offshore pipelines to prevent petroleum from solidification. Such new technical challenges mean that a better understanding of the behaviour of offshore pipelines is required and the design code for offshore pipelines needs to be upgraded accordingly.

In deep water, pipelines are often left unburied on the seabed. Therefore, the on-bottom stability of offshore pipelines is influenced significantly by the geotechnical conditions on the seabed. Pipeline instability may be caused by the loading from the wave-induced currents (Fujiwara et al., 2011, Myrhaug and Ong, 2011, Chakkarapani et al., 2011). The thermal expansion and contraction corresponding to the production and shutdown cycles of offshore platforms may also cause pipeline instability (Casola et al., 2011). Pipelines undergo a number of such thermal cycles during their operational life. At the end of each thermal cycle, some part of the expansion recovers, whereas the irrecoverable expansion accumulates at the free ends and causes the pipe to move axially in one direction, a phenomenon known as *axial walking*. Consequently, the soil in contact with the pipe is also subjected to both static and dynamic loading, which may affect the long-term mechanical stability of pipelines. The pipe-soil interaction is analogous to structure-soil interaction in foundation problems involving cohesive soils. However, unlike foundations of many structures where flexibility is usually not allowed, offshore pipelines can retain certain flexibility without exceeding the limit state at the centre (Randolph, 2011). Similar to foundation problems, the pipe-soil interaction can be divided into vertical, axial and lateral directions. The pipe-soil interaction in both vertical and lateral directions has been investigated extensively (Merifield et al., 2008, Zhou et al., 2008), whereas the axial pipe-soil interaction, which is regarded as the primary cause of pipeline instability, is yet to be clearly established. Some work has been done, for example, by Bruton et al. (2007), White et al. (2011a) and Randolph (2012). Most recently, a specialised 2-D electric actuator system, the Monash Advanced Pipe-testing System (MAPS), has been developed at Monash University, Australia. The results from scaled axial soil-pipe interaction tests using MAPS have been made available (Senthilkumar, 2013).

The MAPS results imply that pipe axial walking induces relative movements of the soil below the pipe (Senthilkumar, 2013). Since the pipe-soil interaction is extensively influenced by the soil response, the portion of the soil below the pipe which undergoes shearing, characterised as the *shear zone*, is significant for pipe axial walking assessment, and therefore needs to be investigated thoroughly. Cyclic direct simple shear testing is proposed as the preferred testing method to conduct the investigation owing to its various merits, including its loading pattern, allowing the rotation of principal stress axes, the small specimen size required and its shear failure planes.

The results of the current research program will advance the understanding of soil behaviour within the shear zone in pipeline axial walking problems, by performing laboratory soil tests and conducting numerical modelling and analyses. Based on the results from both experimental work and numerical analysis, a set of data will be established which can be applied in the calibration of large-scale pipe axial walking modelling, and provide guidance on the design practice of offshore pipelines when considering on-bottom stability in axial direction.

1.2 Research objectives

The aim of the research program is to investigate soil behaviour within the shear zone in pipe axial walking problems, and to advance the understanding of offshore pipeline instability in the axial direction.

The specific objectives are:

1. Provide a comprehensive literature review to build a conceptual framework upon which the research program is based.

2. Establish an appropriate laboratory testing approach to investigate the soil behaviour within the shear zone.

3. Develop numerical modelling capacity to capture the soil behaviour within the shear zone in finite element analysis.

4. Based on the results from experimental work and numerical analysis, complement and improve the results obtained from MAPS tests.

5. Establish a set of data which can be applied in the calibration of the modelling of large-scale pipe axial walking.

1.3 Structure of thesis

This thesis consists of five chapters, a list of references and appendices. The chapters are summarised below.

Chapter 1 – Introduction

The first chapter contains an introduction to the problem, the scope of the project and the objectives.

Chapter 2 – Literature review

Chapter 2 provides a comprehensive literature review upon which the conceptual framework is built.

Chapter 3 – Experimental program and results

Chapter 3 presents the experimental program and the experimental results. First the soil selected for the experimental program is introduced. This is followed by an elaboration of the experimental set-up and the presentation of the experimental results.

Chapter 4 – Numerical modelling

The numerical modelling work of the current research program is presented in this chapter. The critical state soil theory, upon which the Modified Cam-clay model is based, and the model itself are introduced, followed by the two-dimensional finite element analysis (FEA) of the cyclic direct simple shearing on soft clay. Finally the results of the analyses are presented.

Chapter 5 – Conclusions and recommendations

The major findings of the research program are summarised and conclusions are presented, followed by recommendations for future research.

Appendices

Detailed elaborations of the critical state soil theory and the modified Cam-clay model are provided in Appendix A. Additional finite element analysis results are presented in Appendix

B. An example “.inp” file for the two-dimensional finite element soil model developed is provided in Appendix C

Chapter 2 - Literature review

A comprehensive literature review was conducted to build a conceptual framework upon which the research program was based. First, current research into offshore pipeline axial walking is introduced. An investigation of the shear influence zone induced by axially-walking offshore pipelines is presented. A generic pipe load-displacement relationship that can be applied to characterise pipe axial walking behaviour is discussed. This is followed by the proposal to use cyclic direct simple shear testing to investigate the soil behaviour within the shear zone. A discussion of the relevant parameters in offshore pipeline axial walking is presented. Detailed information about direct simple shear testing is introduced in terms of its development, and variety and uniformity in soil specimens.

2.1 Offshore pipeline axial walking

Offshore pipeline axial walking is a phenomenon of the undesired accumulation of axial displacement of offshore pipelines during operational cycles. Tornes et al. (2000) provided the first comprehensive study of pipe axial walking, and this was followed by analytical solutions linking pipe-soil friction and pipe axial walking presented by Carr et al. (2006). White et al. (2011a) reported some experimental data on pipe-soil axial resistance, demonstrating the influence of drainage and excess pore water pressure. The data indicate that axial resistance, as a portion of submerged pipe weight, can vary from as low as 0.1 to greater than 1. A framework for pipe-soil axial resistance based on an effective stress approach was set out by White & Cathie (2011), covering both undrained and drained conditions. It was argued that axial resistance tends towards the drained values during cycles of pipe movement, regardless of the rate or duration of each movement. This is due to the fact that the soil surrounding the pipe will eventually reach a critical state, at which excess pore water pressure generation will not take place. A reliable prediction of this mechanism could bring significant design benefits, as drained resistance is usually higher than undrained resistance. Consequently, a higher range of axial resistance can be applied, leading to more cost-effective design.

2.1.1 Axial pipe-soil interaction

Bruton et al. (2008) divided axial pipe-soil interaction into two stages as shown by the ‘brittle’ response in Figure 2.1: (i) breakout axial resistance and (ii) residual axial resistance. When the pipe is loaded for the first time, a breakout or peak axial resistance can take place which reduces to a residual axial resistance after breakout. The displacement at which this peak occurs is defined as the mobilisation displacement. A peak is not observed during subsequent loading and this leads to a ductile breakout response, as illustrated by the 'ductile' curve in Figure 2.1.

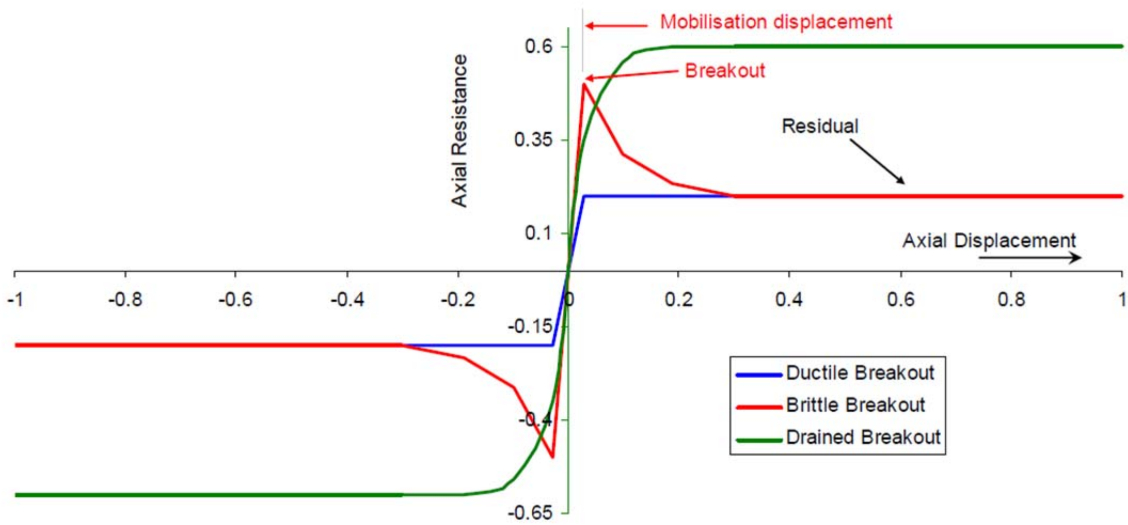

Figure 2.1 Axial friction resistance schematic with mobilisation displacement and breakout (Bruton et al., 2008)

The friction falls away to residual axial resistance when the pipeline reaches larger axial displacement, and the term 'residual' is used by analogy with the residual friction angle which is mobilised within fine-grained soil after continued shearing along a single plane.

The 'drained' response shown in Figure 2.1 corresponds to slow pipe axial displacement, where excess pore water pressure does not build up, and the axial resistance is profoundly higher in this case.

The axial response is thus significantly influenced by the generation and dissipation of excess pore water pressure which leads to undrained and drained soil behaviour. It is likely that the response is between fully undrained and fully drained in typical field conditions.

2.1.2 Drained and undrained soil resistance

Oliphant and Maconochie (2006) presented a method for estimating axial soil resistance using a relative roughness parameter, and made recommendations on the displacements necessary to mobilise peak and residual undrained and drained soil resistance. It is argued that the application of undrained and drained soil resistance will depend on the rate of straining as well as on the duration of pipeline loading for axial resistance.

The dimensionless group vD/c_v can be used to establish the most likely soil response (Randolph and House, 2001), where v is the velocity of the pipeline, D is the pipe diameter and c_v is the consolidation coefficient. The soil response may be bounded by

$$\frac{vD}{c_v} < 1.0 \text{ for the fully drained condition and} \quad (2.1)$$

$$\frac{vD}{c_v} > 20.0 \text{ for the fully undrained condition} \quad (2.2)$$

The value of c_v depends on both the permeability and compressibility of the soil and should be measured at low stress levels, as applicable to offshore pipeline axial walking.

During interface shearing, the response of a fine-grained soil ranges from fully drained to fully undrained for various velocities (White and Cathie, 2011). Figure 2.2 demonstrates the steady residual resistance measured during monotonic shearing of normally consolidated kaolin clay over a rough steel surface at different velocities. The kaolin was normally consolidated to 2.5kPa before shearing. A direct shear box was modified to operate at low stress levels as applicable to the offshore pipeline context. The results from shearing of a concrete-clay till interface at various velocities (Steenfelt, 1993) are plotted in Figure 2.2.

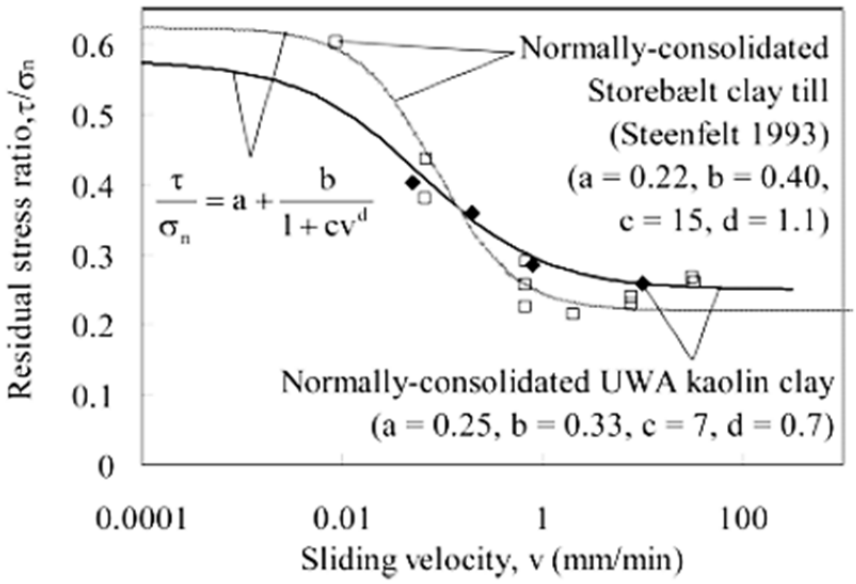

Figure 2.2 Interface shearing: kaolin clay and Storeælt clay till (White and Cathie, 2011, Steenfelt, 1993)

The responses of both the kaolin clay and the Storeælt clay till are close in terms of both the limiting drained and undrained resistances as well as the velocity range over which the transition takes place.

2.1.3 Cyclic axial response in an effective stress framework

The first deep water deployment of the Fugro SMARTPIPE (White et al., 2011b) focused on the axial pipe-soil interaction on soft clay. The tool was equipped with pore pressure measurement capacity on the surface of the test pipe, which allows the cyclic axial response to be interpreted in an effective stress framework.

The time histories of imposed vertical load, imposed axial pipe movement and measured axial resistance are presented in Figure 2.3. A modest peak in axial resistance was observed during the first sweep and ductile response followed during all subsequent sweeps.

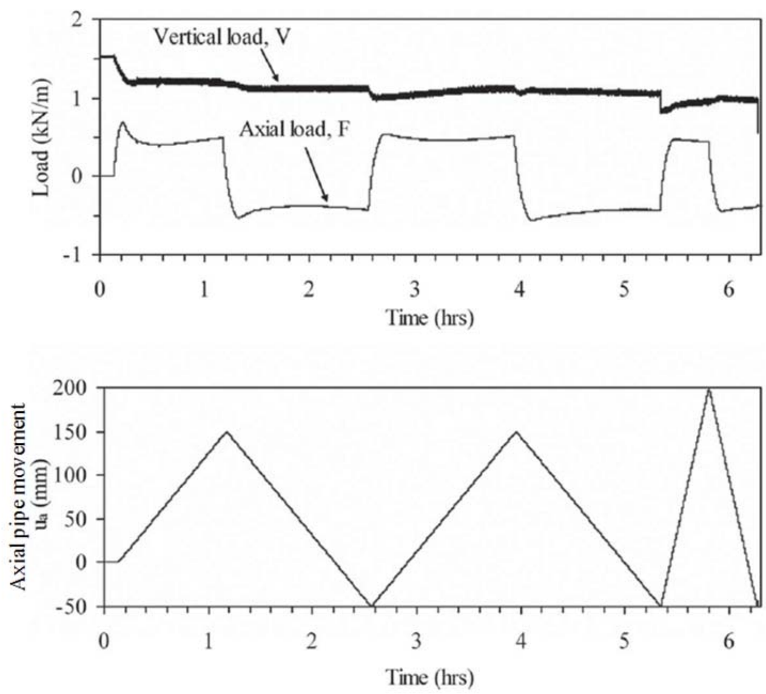

Figure 2.3 Time history during cyclic axial pipe testing (White et al., 2011b)

As it is possible to measure the excess pore pressure at the pipe soil surface, the data obtained from the cyclic axial pipe test can be compared in terms of both total stress and effective stresses. The mean shear stress τ_{av} on the pipe surface is calculated as

$$\tau_{av} = \frac{F}{\pi D/2} \tag{2.3}$$

where F is the axial pipe-soil load per unit length and D is diameter of the model pipe.

The friction factor based on the total stress FF is defined as

$$FF = \tau_{av}/V \tag{2.4}$$

where V is the vertical pipe-soil load per unit length

The friction factor based on effective stress FF' is defined as

$$FF' = \tau_{av}/\sigma'_{n,av} \tag{2.5}$$

where $\sigma'_{n,av}$ is the mean normal or vertical effective stress

The friction factor response during cyclic axial pipe test is shown in Figure 2.4, both in terms of total stress and effective stress. The total stress response is smoother than the effective stress response. This is due to the variations between the excess pore pressures measured by the sensors, which indicate that the excess pore pressure was not uniformly distributed at the pipe soil surface.

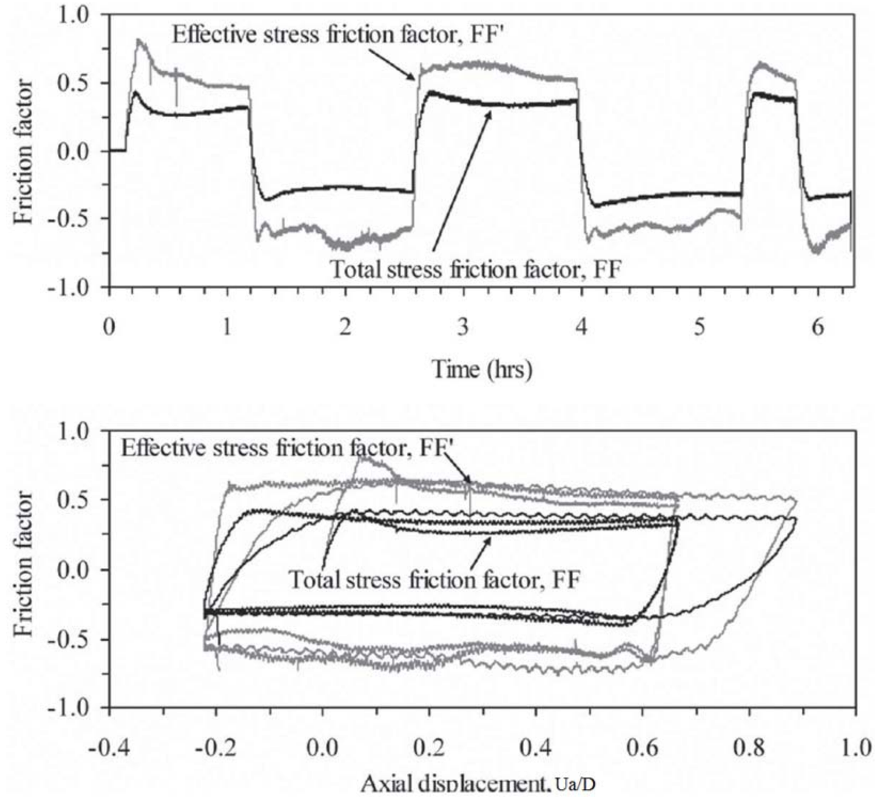

Figure 2.4 Friction factor response in cyclic axial pipe testing (White et al., 2011b)

When the responses are plotted in the form of total and effective stress failure criteria as illustrated in Figure 2.5, the effective stress interpretation is the most consistent. While the axial response in total stress interpretation varies for each cycle, all sweeps in each direction overlie each other in the effective stress interpretation.

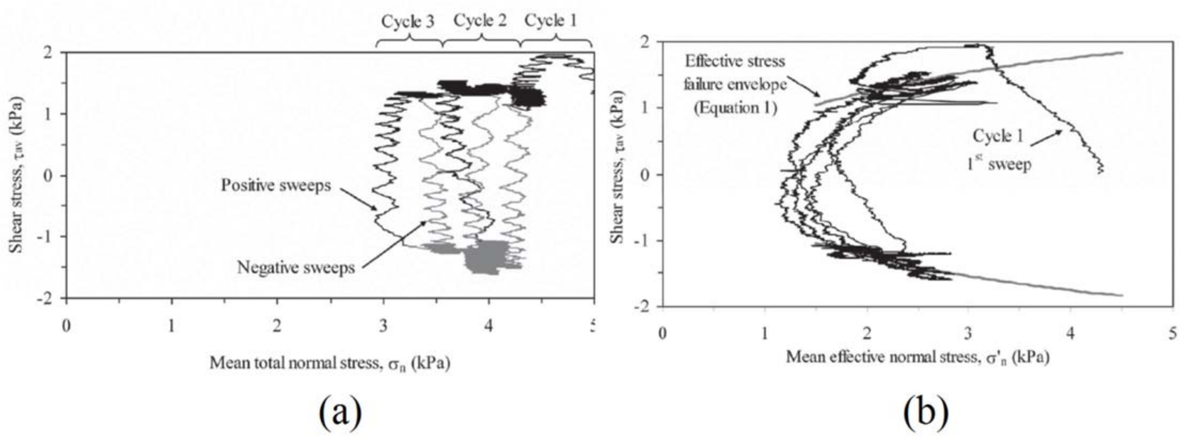

Figure 2.5 (a) Total stress interpretation of axial response (b) Effective stress interpretation of axial response (White et al., 2011b)

Analysis of the field data also suggests that the mobilisation of axial resistance is a time-related process instead of being linked to the distance of shearing. The suggestion is consistent with the excess pore pressure development in the sweeps. In other words, full pipe-soil resistance is only mobilised when steady pore pressures are reached.

2.1.4 Theoretical framework for axial resistance

Randolph et al. (2012) introduced a theoretical framework based on planar shearing to assess the magnitude of axial resistance. In the scenario shown in Figure 2.6(a), a slab is sheared at velocity v across a soil surface. The pressure exerted by the slab on the soil is q, and shearing occurs within a shear band of thickness h_s. Excess pore pressure Δu_s is generated during shearing and a shear strain of γ is reached after a time t = $\gamma\ h_s/v$.

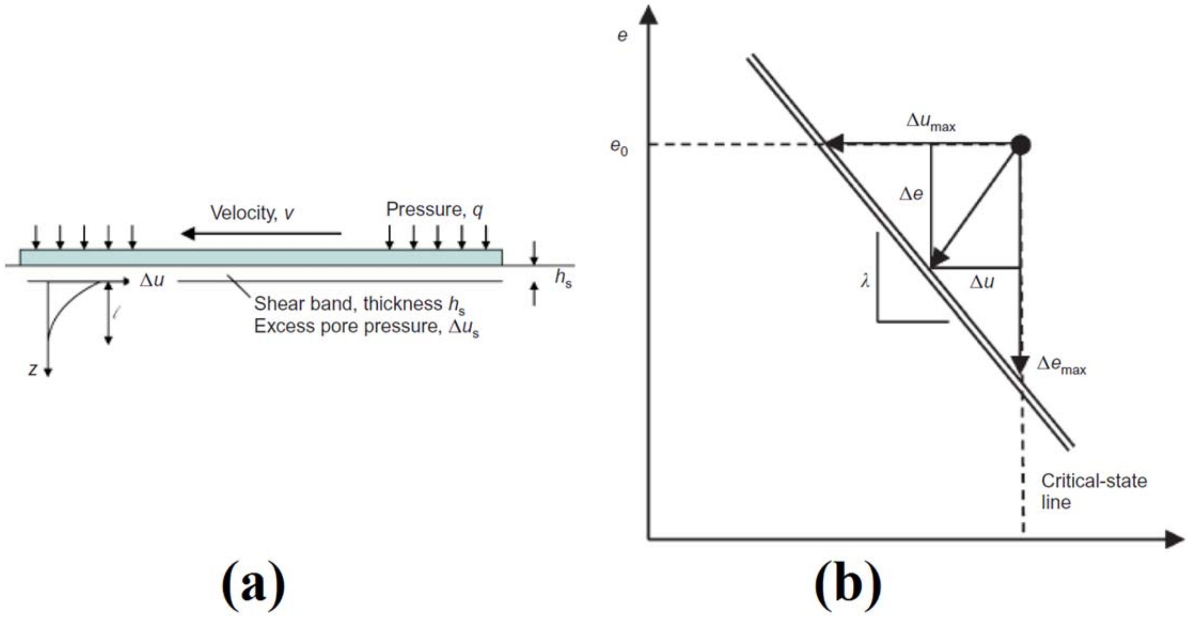

Figure 2.6 (a) Schematic diagram for analysis of velocity effects for planar shearing (b) Stress paths in e-lnσ'_v space (Randolph et al., 2012)

The response of soil within the shear band is presented in Figure 2.6(b). Compression takes place in drained shearing corresponding to an ultimate decrease in void ratio of Δe_{max}, and the volumetric strain in this case is $\Delta\varepsilon_{v,max}$. For undrained shearing, excess pore pressure of Δu_{max} is generated. When the shearing is partially drained or partially undrained, the volumetric strain $\Delta\varepsilon_v$ and excess pore pressure Δu may be related by

$$\Delta\varepsilon_v = -\frac{\Delta e}{1+e_0}$$

$$= \Delta\varepsilon_{v,max} + \frac{\lambda}{1+e_0}\ln(1-\frac{\Delta u}{q}) \qquad (2.6)$$

The corresponding limiting shear stress, τ_f, can be expressed as

$$\tau_f = (q - \Delta u)\tan\emptyset'$$

$$= \mu q(1-\frac{\Delta u}{q}) \qquad (2.7)$$

where $\mu = t\tan\emptyset'$

The zone influenced by excess pore water pressures may be considered to extend a distance of l into the soil, where

$$l = \sqrt{12c_v t} \tag{2.8}$$

Therefore the volumetric strain $\Delta\varepsilon_v$ can be expressed as

$$\Delta\varepsilon_v = \frac{\lambda}{1+e_0}\frac{\Delta u}{q}\sqrt{1.33\frac{c_v t}{h_s^2}}$$

$$= \frac{\lambda}{1+e_0}\frac{\Delta u}{q}\sqrt{1.33\gamma\frac{c_v}{h_s v}} \tag{2.9}$$

Combine this relationship with Equation 2.1 gives

$$\Delta\varepsilon_{v,max}\frac{1+e_0}{\lambda} + \ln\left(1-\frac{\Delta u}{q}\right) = \frac{\Delta u}{q}\sqrt{1.33\frac{c_v t}{h_s^2}}$$

$$= \frac{\Delta u}{q}\sqrt{1.33\gamma\frac{c_v}{h_s v}} \tag{2.10}$$

Figure 2.7(a) provides example relationships between excess pore pressure and time or shear strain divided by normalised velocity vh_s/c_v. Four curves for various values of $\Delta\varepsilon_{v,max}(1+e_0)/\lambda$ are presented. $\Delta\varepsilon_{v,max}(1+e_0)/\lambda$ is a quantity which quantifies the distance of the initial state from the critical state. The upper limit of $\Delta u/q$ is close to unity, resulting in almost zero effective stress on shearing.

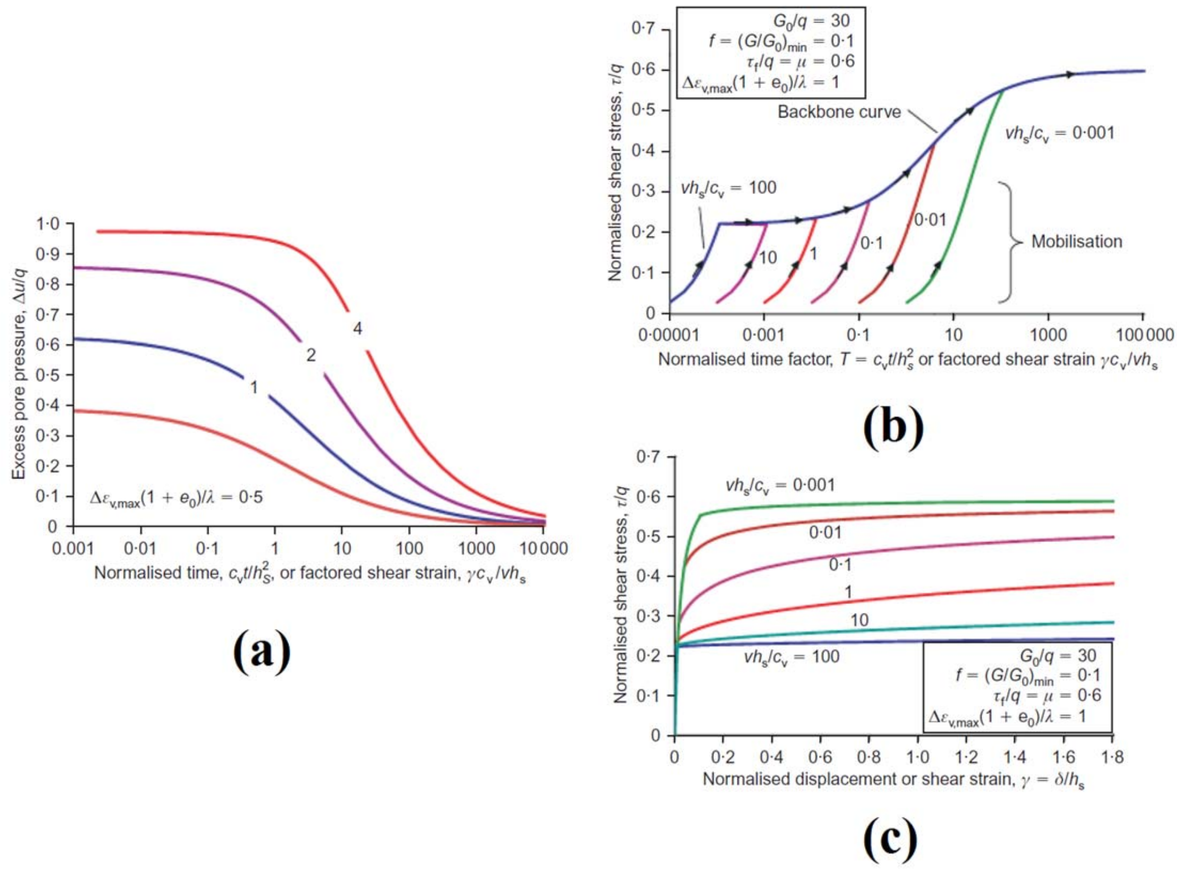

Figure 2.7 (a) Example relationships between excess pore pressure and time or shear strain Planar shearing responses for different normalised velocities Variation in resistance with (b)time; (c)displacement (Randolph et al., 2012)

To develop a complete shear stress-displacement relationship , Randolph et al. (2012) proposed a simple hyperbolic response of the form

$$\tau = \frac{G_0\gamma}{1+R_\mathrm{f}G_0\gamma/\tau_\mathrm{f}} \tag{2.11}$$

with a small-strain shear modulus G_0 and hyperbolic parameter R_f (Duncan and Chang, 1970).

Figure 2.7(b) shows the variation of τ/q with time for different normalised velocities, vh_s/c_v. The responses for various velocities are intercepted by a common backbone curve after failure based on Equation (2.7). The same responses are shown in Figure 2.7(c) as a function of displacement, normalised by the shear band thickness h_s.

2.2 Shear zone in offshore pipeline axial walking

Axially-walking offshore pipelines induce relative movement of the soil underneath the pipe. Since the pipe-soil interaction is extensively influenced by the soil response, the portion of the soil below the pipe which undergoes shearing, characterised as the *shear zone*, is significant for pipe axial walking assessment. To characterise the shear zone, Senthilkumar (2013) applied image correlation analysis in MAPS testing. Based on the observations and results from the experiments conducted, the shear zone can be illustrated as in Figure 2.8.

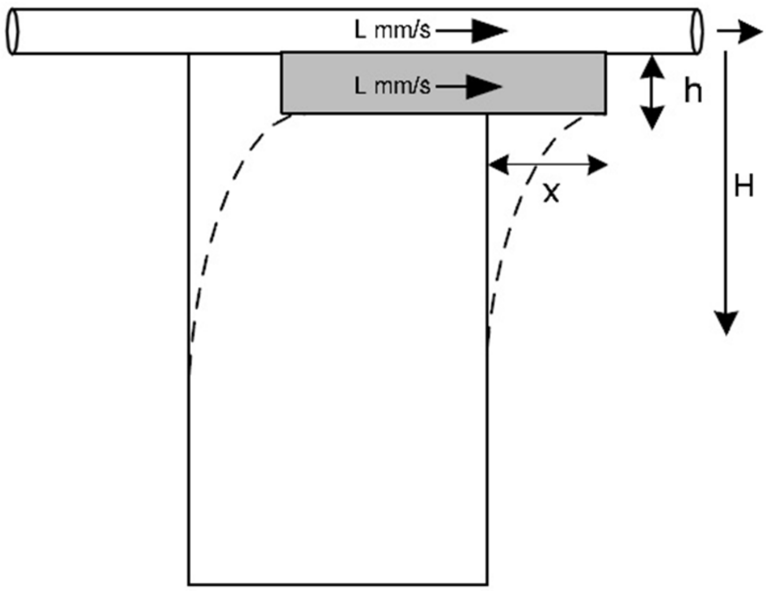

Figure 2.8 Shear zone underneath axially-walking pipe (Senthilkumar, 2013)

The shear zone consists of two parts. The first part, *zone h,* is the soil block from the depth immediately below the pipe to a depth of h. When pipe axial walking takes place, the soil within zone h moves together with the pipe at the same displacement rate. This zone can be considered as the direct failure zone. The second part, *zone H-h*, is the soil block from the depth of h to the depth of H, where H is the limit depth of shear influence. The soil in this zone is mobilised when axial walking occurs, but the soil does not move together with the pipe at the same displacement rate. Instead, the displacement decreases as the depth increases.

The experimental data (Senthilkumar, 2013) suggest that higher axial displacement rate would lead to a deeper shear zone, i.e. a larger value of H. It was found that the depth of zone h increases with both pipe axial displacement rate and pipe embedment. In contrast, the depth of zone H-h increases with increasing axial displacement rate, but it is largely independent of pipe embedment. The axial displacement rate depends primarily on soil axial resistance as well as on the expansion/contraction rate of the pipe wall, which in turn depends on the heating/cooling rate and the properties of the pipe and the soil. If the pipe axial displacement rate can be reduced, the extent of the shear influence on soil can also be reduced.

It is also worth noticing that the soil within the shear zone is subjected to axial loading while under vertical loading due to the pipe's weight. This loading pattern can be closely resembled by the direct simple shear test, as shown in Figure 2.9, in particular for *zone H-h*.

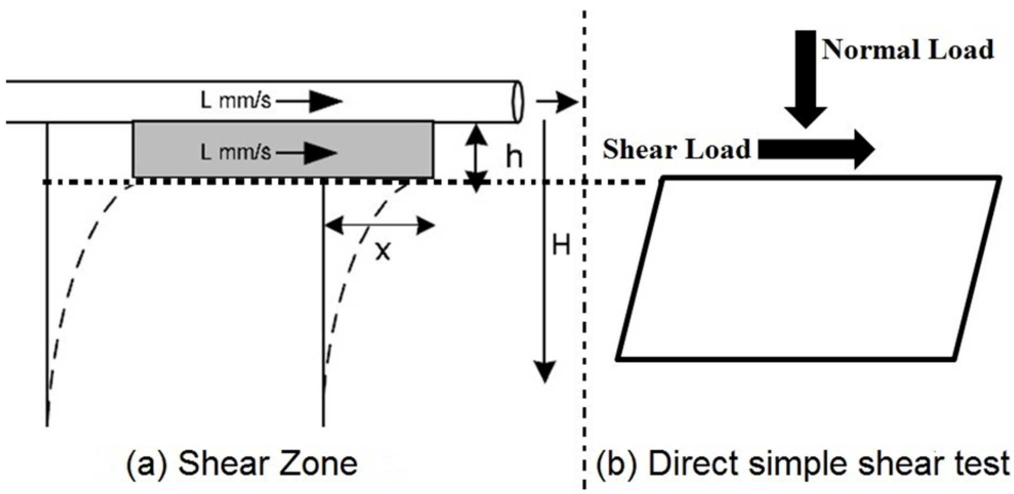

Figure 2.9 (a) Shear zone underneath axially walking pipe and (b) loading pattern of direct simple shear test

.

2.3 Generic load-displacement relationship in pipe axial walking

(Senthilkumar, 2013) proposed a generic pipe load-displacement relationship curve (Figure 2.10), which can be applied to characterise pipe axial walking behaviour. This load-displacement curve was constructed based on the experimental outcomes of physical pipe-soil interaction testing, using the Monash Advanced Pipe-testing System (MAPS).

The load-displacement curve comprises three major components: pre-peak, peak and residual resistance. The experimental results show that at a particular embedment depth, the rate of pipe axial displacement has no or negligible influence on the pre-peak load-displacement relationship. Therefore, in Figure 2.10 the pre-peak portions of the fast/undrained and slow/drained load-displacement curves are the same for a particular embedment depth. However, increasing embedment depth means an increase in contact area, resulting in higher axial resistance.

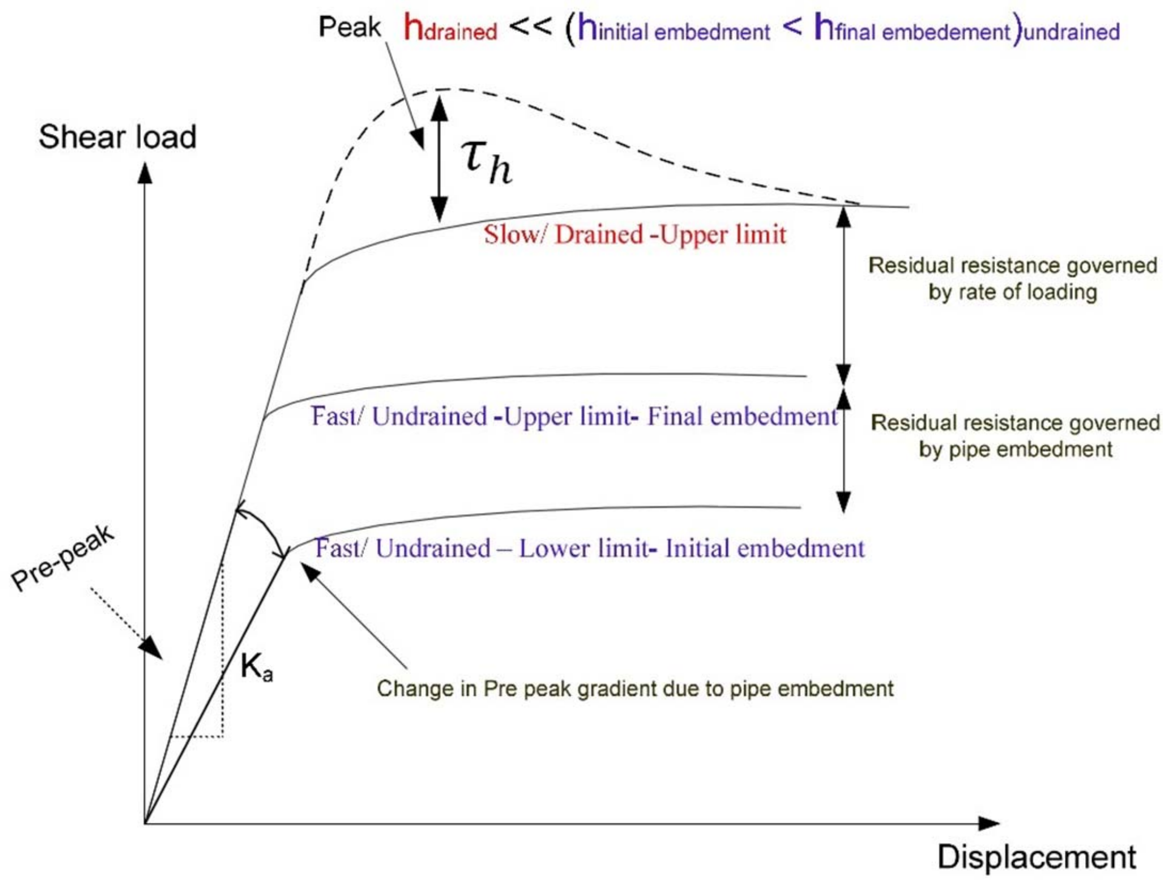

Figure 2.10 Generic pipe load-displacement curve with emphasis on residual resistance (Senthilkumar, 2013)

The peak resistance of the shear load, depicted by τ_h in Figure 2.10, was found at its highest value in the initial shearing cycle based on experimental observation. With increasing number of shearing cycles τ_h weakens gradually and eventually becomes negligible. The peak resistance τ_h was influenced by the embedment of the pipe and was found to be more profound in undrained conditions than in drained conditions.

The residual resistance, which is the primary component in the load-displacement curve, was dominated by pipe axial displacement rate. The fast/undrained residual resistance is defined as the undrained limit, whereas the slow/drained one is defined as the drained limit. The region between the undrained and drained limits is regarded as the transition zone and characterised as *the failure region governed by pipe axial displacement rate*. Furthermore, under undrained conditions, the level of residual resistance was also found to be influenced by pipe embedment. Therefore, the undrained limit of residual resistance is further divided into the upper and lower undrained limits, based on pipe embedment. The region between the lower and upper undrained limits is characterised *as the failure region governed by pipe embedment*.

2.4 Residual resistance and undrained/drained limits in MAPS

The residual resistance levels in MAPS tests at various displacement rates are presented in Figure 2.11 (Senthilkumar, 2013). The axial pipe residual resistance is normalised by the maximum recorded vertical load V_{max} and the axial displacement rate is normalised by the effective pipe diameter D' and the coefficient of consolidation C_v. Figure 2.11(a) shows the residual resistance for smooth pipe surface conditions and Figure 2.11(b) shows the residual resistance for rough pipe surface conditions.

The plots show that the residual resistances at different pipe embedments converge to an unchanged level when the axial displacement rate increases. This limit can be considered as the axial displacement rate beyond which the residual resistance is not affected by the increase of axial displacement rate. In other words, it can be considered as the undrained limit. Similarly, the drained limit of the residual resistance can be obtained from the plots, and it is observed that higher embedment depths result in higher level of residual resistance.

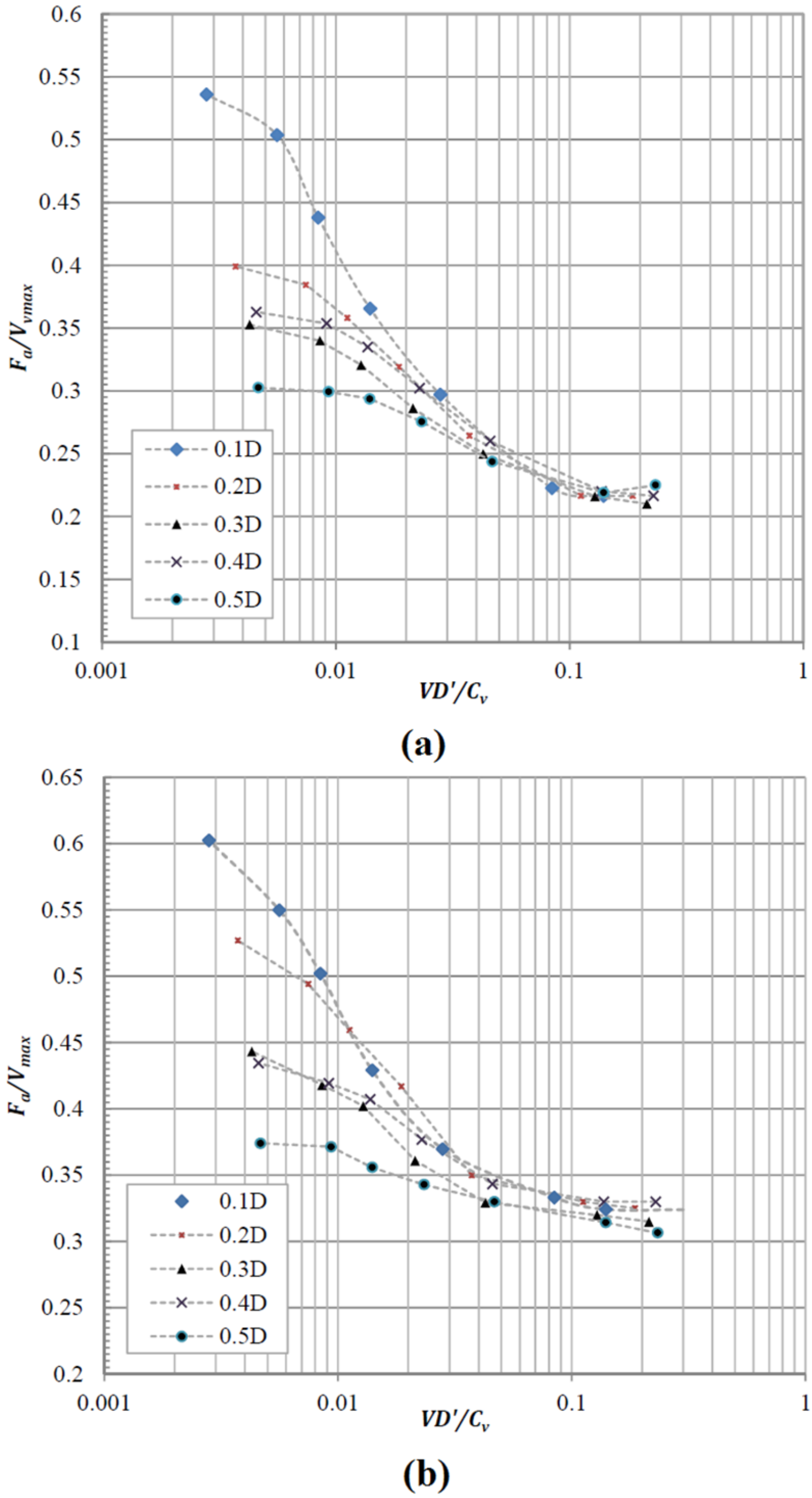

Figure 2.11 Normalised residual resistance at various displacement rates and pipe embedments for (a) smooth pipe and (b) rough pipe (Senthilkumar, 2013)

2.5 Utilising cyclic direct simple shear test in offshore pipeline axial walking problems

In offshore pipeline axial walking problems, the seabed soil underneath the pipe undergoes cyclic shearing with low vertical/normal stress imposed. In order to further investigate the soil behaviour within the shear zone, in particular the load-displacement relationship, cyclic direct simple shear testing was proposed as the preferred testing method. Direct simple shear testing has been used extensively in offshore geotechnical engineering applications. The increasing popularity of the direct simple shear test is mainly due to the relatively small sample size required, and the shearing pattern, which closely resembles the loading condition in offshore geotechnical engineering problems. Particularly for offshore pipeline axial walking scenarios, the soil within the shear zone is subjected to horizontal cyclic shearing while under a vertical load, which is similar to the loading pattern in the direct simple shear test. Furthermore, cyclic shearing can be applied in the direct simple shear test, which can simulate the expansion and contraction in pipeline operation and shutdown cycles. The direct simple shear test also has merits compared with other testing methods. It is the only standard test that allows the rotations of principle stress axes (Airey and Wood, 1987) and unlike in direct shear testing where the shear failure plane is fixed as the horizontal plane, the failure plane in direct simple shear tests is not pre-defined.

When utilising direct simple shear tests in investigating pipeline axial walking problems, it is important to have sound knowledge of the relevant parameters involved. It has been determined that the primary variables are effective normal stress, shearing velocity and shearing amplitude. Some research literature has given guidance on the magnitude of these variables.

Normally the magnitude of the effective normal stress imposed on the soil underneath the pipe is relatively low in pipe axial walking problems. The effective normal stress (σ'_n) equals the total normal stress (σ_n) minus the pore water pressure (u). In drained cases, total normal stress (σ_n) may not be equal to the effective normal stress (σ'_n) since pore water pressure can be very high due to the depth of seabed, which can be in the order of kilometres. Bruton et al. (2007) suggest that the effective normal stress generated by typical pipeline weights is at the levels of 2kPa to 10kPa. The first stage of the Furgo SMARTPIPE project (White et al., 2011b) saw an effective normal stress between 1kPa to 3kPa. In a pipe interface shearing example given by White and Cathie (2011), an effective normal stress of 5kPa was applied.

Regarding the shearing velocities, the magnitude of pipeline velocities ranges from 0.5mm/s to 0.001mm/s, and could even be lower for fully drained conditions. Bruton et al. (2007) advised that the available field data on pipeline velocities were limited, and an example problem provided in the literature showed that pipeline velocities only exceed 0.2mm/s near pipe ends and the durations are very short, and an average velocity of 0.005mm/s was given. In the first stage of the Furgo SMARTPIPE project (White et al., 2011b), 0.04mm/s was applied for sweeps 1-4 and 0.15mm/s for sweeps 5 and 6. In the SAFEBUCK JIP project (White et al., 2011a), where testing was performed on a soft marine clay, 0.5mm/s was used but for sweep no. 22, 0.001mm/s was applied. In a direct shear test (White and Cathie, 2011), where normally consolidated kaolin clay was sheared on a steel interface, 0.003mm/s was applied. In the Monash Advanced Pipe-testing System (MAPS), the maximum velocity was 0.5mm/s and the minimum was 0.01mm/s. The selection of shearing rate in the current research program is intended to cover the undrained, partially drained and drained conditions in pipe axial walking.

No clear guidance is provided on how to transfer the pipe axial walking displacements into the shearing amplitude of direct simple shear tests. The 'Standard Test Method for Consolidated Undrained Direct Simple Shear Testing of Cohesive Soils' (ASTM-D6528, 2007) suggests at least a 20% shear strain for shear strength determination purpose.

2.6 Direct simple shear test

As discussed previously, cyclic direct simple shear testing was selected as the method for investigating the behaviour of soil within the shear zone. In this section, detailed knowledge of the direct simple shear test is presented in terms of its development, variety, uniformities in soil samples and the interpretation of test results.

2.6.1 Development of direct simple shear test

The direct simple shear test (DSS) is an improvement on the direct shear test, and both tests have been developed in order to investigate the shear strength of soil. The direct shear test simulates the effect of shear loads acting on a predetermined failure surface. In these tests a circular or rectangular soil specimen is placed in a split box, as shown in Figure 2.12.

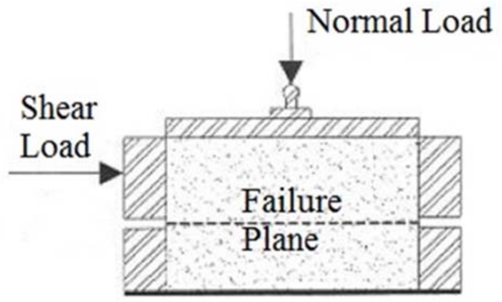

Figure 2.12 An illustration of the direct shear box (Zekkos et al., 2010)

In the first stage a normal load is applied at the top of the box and in the second stage, a shear load is applied at the top or bottom of the split box, which causes the specimen to shear along the predetermined failure plane between the two parts of the split box. During the test, the shear and normal stresses are measured and plotted against the horizontal displacement. A peak in the stress-strain curves is often observed. The progression of the normal displacement versus the horizontal displacement provides information about the contraction or dilation behaviour of the soil specimen (Grognet, 2011). In direct shear tests, the shear stress-strain distribution is highly non-uniform. This is due to a high concentration of stresses developing at the front and back edges of the soil specimen, which creates a progressive failure so that the total shear strength of the specimen is not fully mobilized. In addition, the strain restraints which force the failure in one direction create an unknown state of stress in the specimen (Terzaghi et al., 1996). The direct shear test is useful in determining the shear strength of soils, but not their stress-strain response (Bardet, 1997).

Due to the limitations of the direct shear tests, the direct simple shear test was introduced in order to achieve a more uniform specimen stress-strain distribution. Figure 2.13 illustrates the difference between the direct simple test and the direct shear test. In the direct simple test the soil specimen is confined by a wire-reinforced membrane or stacked rings. At the consolidation stage a normal stress is applied and the specimen is consolidated under one-dimensional conditions. The consolidation phase is followed by the shearing of the soil in one dimension only. This strain condition is called the simple shear strain condition (Dyvik et al., 1987).

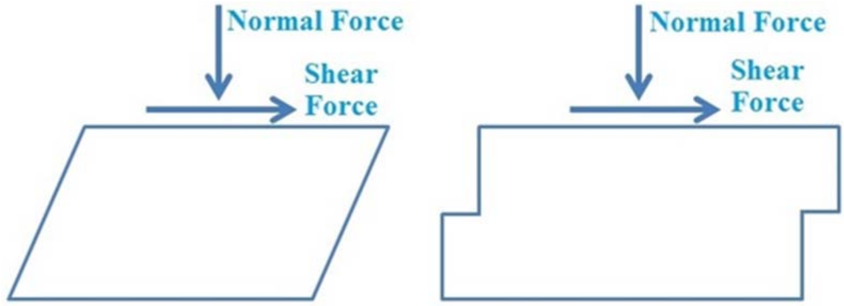

Figure 2.13 Illustrations of direct simple shear test (left) and direct shear test (right)

The first direct simple shear device was developed by the Swedish Geotechnical Institute (S.G.I) in 1936, as illustrated in Figure 2.14 below (Kjellman, 1951). This apparatus was able to test circular soil specimens with a height of 60mm and diameter of 20mm confined by a rubber membrane and aluminium rings. The sample was first consolidated using lead weights and drainage was allowed by placing porous stones at both the top and bottom of the soil specimen. The soil specimen was then sheared from the top plate, while maintaining either a constant load or constant sample height. To avoid slippage between the specimen and the plates, the top and bottom caps were often equipped with teeth. Vertical and horizontal load cells were used to record the normal stress and shear stress, and displacement gauges were applied to measure the vertical displacement and shear strain. The device was able to maintain a constant area of potential sliding during shearing, and to improve the homogeneity of the stress distribution when compared with the direct shear device.

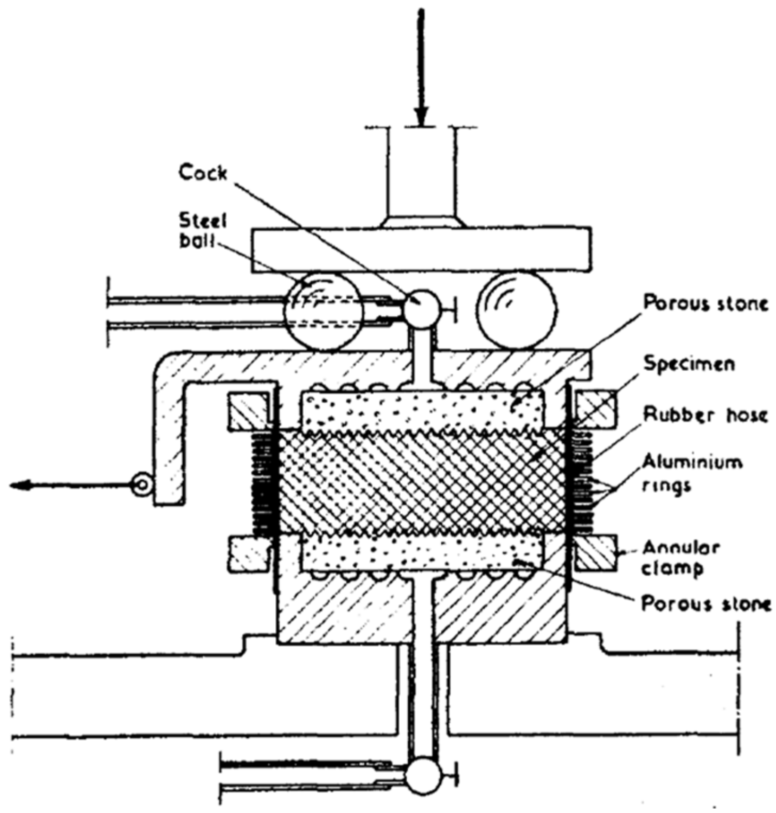

Figure 2.14 S.G.I Direct Simple Shear Device (Kjellman, 1951)

Kjellman's idea (Kjellman, 1951) of using a cylindrical sample confined with a reinforced rubber membrane was further developed by the Norwegian Geotechnical Institute (NGI) (Bjerrum and Landva, 1966), and a photograph of the apparatus is shown in Figure 2.15(a). A soil sample 80mm in diameter and 10mm high was confined in a rubber membrane reinforced with a spiral winding of wire with a diameter of 0.15mm wound at 25 turns per cm, as shown in Figure 2.15(b).

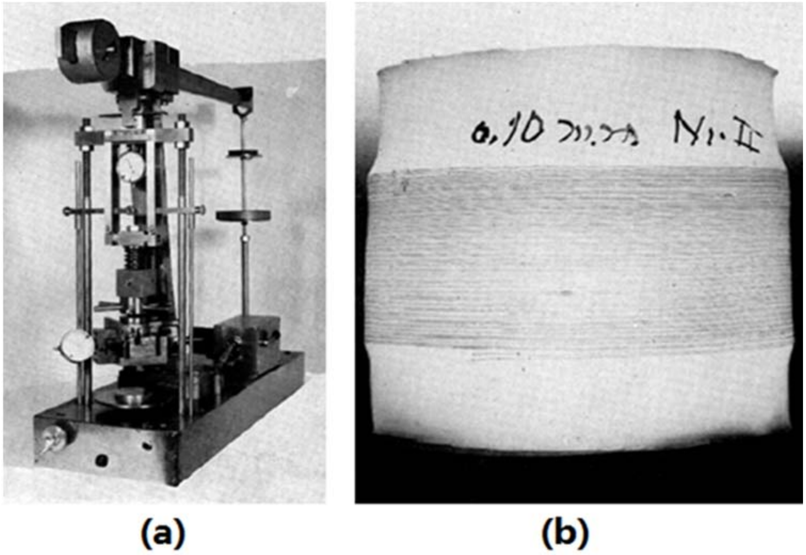

Figure 2.15 (a) NGI direct simple shear device (b) Reinforced rubber membrane (Bjerrum and Landva, 1966)

The confining membrane allows one-dimensional consolidation to occur while maintaining a constant cross-sectional area. At the consolidation stage, the major principal stress σ_1 is equal to the normal stress applied. During shearing a rotation of the principal stress will occur as a result of the increase in shear stress. The NGI direct simple shear device has since become the basis of the design of many later direct simple shear devices.

2.6.2 Drained and undrained direct simple shear test

Drained direct shear conditions are achieved by applying a constant normal load during shearing and applying an appropriate shearing rate so that no excess pore water pressure would build up during shearing. Drained direct simple shear testing is usually performed on granular materials such as sand, since the drained parameters of granular materials are most likely to be investigated.

For cohesive material like clay, the undrained parameters are most likely to be investigated. Therefore, for cohesive materials undrained direct simple shear testing is usually performed. However, several direct simple shear test devices are unable to perform truly undrained testing for two main reasons. Firstly, there may be difficulties in blocking the drainage in a direct simple shear test, because of the lack of pressurised cell which can provide back pressure. Secondly, pore pressure measurement may not be available when using direct simple shear devices.

2.6.3 Constant-volume undrained equivalent test

Since some apparatuses may not be able to perform truly undrained tests, undrained direct simple shear tests were carried out as constant-volume tests (Bjerrum, 1954). Bjerrum and Landva (1966) outlined that 'during the shear phase of the constant-volume tests the specimens were drained and the rate of strain applied was selected such that the pore pressures in the specimen were zero throughout the tests; the height of the specimen was then kept constant by varying the vertical load on the sample'. Therefore, the undrained-equivalent constant-volume test is in essence a drained direct simple shear test with normal load variations.

Further, Bjerrum and Landva (1966) argued that in constant volume tests, the change in applied normal stress equals the change in pore water pressure which would have occurred in truly undrained direct simple shear tests. This argument was verified by Dyvik et al. (1987) for normally consolidated clay. Based on tests results, it was concluded that static undrained-equivalent constant volume tests on normally consolidated clays produce the same results as truly undrained tests. The assumption that the change in applied normal stress equals the change in pore water pressure which would have occurred in truly undrained direct simple shear tests was therefore verified. This is valid for saturated soils. The undrained-equivalent constant-volume direct simple shear test provides undrained parameters of cohesive soils. The American Society for Testing and Materials (ASTM) 'Standard Test Method for Consolidated Undrained Direct Simple Shear Testing of Cohesive Soils'(ASTM-D6528, 2007) is based on the concept of constant volume testing, and many commercially-available direct simple shear devices are built according to ASTM-D6528, such as the GDS Shear base system used in the current research program.

2.6.4 The advantages of direct simple shear test over triaxial test

Airey and Wood (1987) argue that as a standard test the direct simple shear test has apparent merits when compared with the triaxial test. In direct simple shear testing it is relatively easy to set up the soil samples and consolidation takes place at a fast rate due to the small sample height. Furthermore, it is the only standard test that allows the rotations of principle stress axes. Such rotations take place in a large proportion of field situations and lead to a reduction in strength (Symes et al., 1984). However, there has been much discussion about the applicability and suitability of the parameters obtained from direct simple shear testing (Saada and Townsend, 1981, Vucetic and Lacasse, 1982).

2.6.5 Non-uniformities in direct simple shear test

The direct simple shear test apparatus has been particularly criticised because it is unable to impose uniform stress on soil samples (Airey and Wood, 1987). The absence of complementary shear stress along the vertical boundaries of the soil sample means that ideal stress conditions cannot be achieved in the direct simple shear apparatus. As shown in Figure 2.16(a) in the test only the average normal stress, σ, the average shear stress, τ, and in some cases the average radial stress, σ_t are measured along the boundaries. Theoretical and experimental analyses have been conducted to investigate the relationship between the measured stresses and the stresses on a deformed soil sample in direct simple shear, as illustrated in Figure 2.16(b).

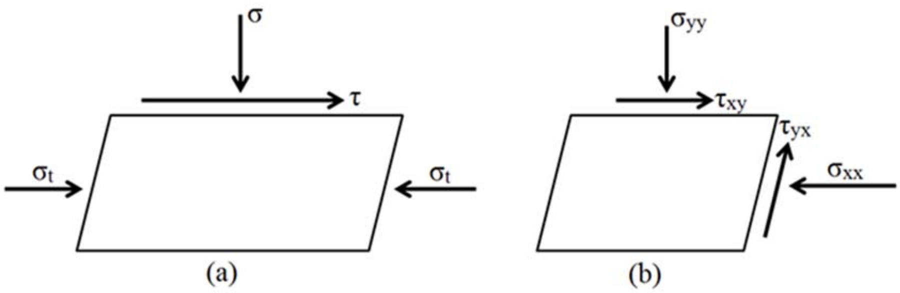

Figure 2.16 Stresses acting on test sample: (a) in direct simple shear apparatus; (b) in true simple shear (Airey and Wood, 1987)

Theoretical analyses have been performed using linear elastic samples (Lucks et al., 1972, Shen et al., 1978, Wright et al., 1978), but the results of these analyses give conflicting pictures of the degree of uniformity of stress. According to Lucks et al. (1972), over 70% of the sample was uniformly stressed, while Wright et al. (1978) concluded that direct simple shear tests cannot provide either reliable stress-strain relationships or absolute failure values. The test results from Vucetic and Lacasse (1982), who performed tests on real soils at various height-to-diameter ratios, showed that the measured soil behaviour is not affected by non-uniformities. In order to have a better understanding of stress non-uniformities, a circular simple shear device in which samples are surrounded by an array of load cells was developed (Budhu, 1979, Airey, 1984), so that the detailed stress-distribution can be measured. A comparison of the uniformity of stress in sands and clays was made by Airey and Wood

(1984) and they concluded that for the more plastic clay samples the uniformity improves significantly. Therefore, the results from direct simple shear tests on clay can be applied with more confidence than the results from tests on sands.

2.6.6 The effect of side boundaries on the uniformities of stress/strain

According to Roscoe (1953), under low normal stress conditions, the non-uniformities of strain are significant with straight vertical side boundaries, as shown in Figure 2.17 below. Despite the fact that the sides were made as smooth as possible, the sample did not deform as a parallelogram and separation could be observed at the corner with acute angles.

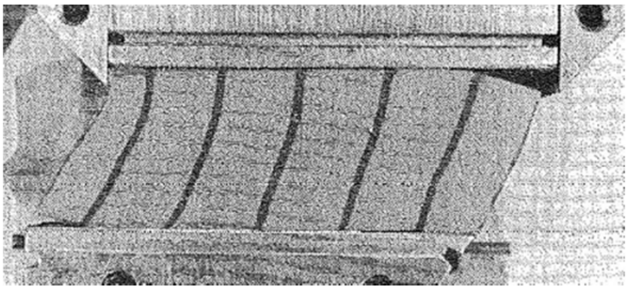

Figure 2.17 Side view of a plasticine sample after shearing under a normal stress of 12kPa (Roscoe, 1953)

Grognet (2011) developed an experimental device to investigate the effect of the vertical side boundaries on the uniformity of stress/strain in direct simple shear tests. Three different vertical side boundary configurations were considered, as shown in Figure 2.18 below.

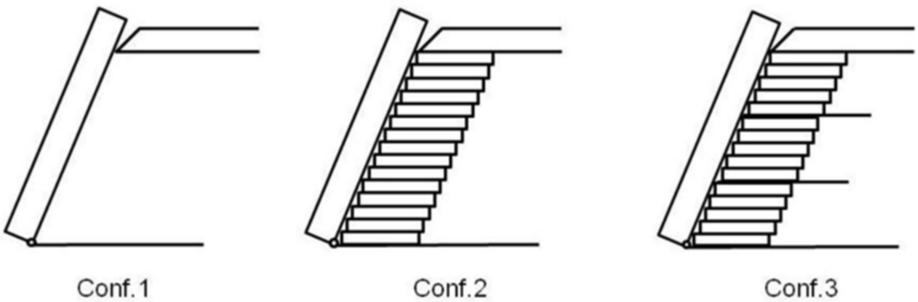

Figure 2.18 Three vertical boundary configurations considered (Grognet, 2011)

Configuration 1 is the conventional straight vertical side boundary, with two PVC plates enclosing the soil specimen. Configuration 2 is vertical boundaries comprising of a series of strips which can slide on top of each other, very similar to the stack of rings used in commercially-available Geonor devices. These strips are added to improve the stress/strain homogeneity by preventing tiling and separation. Configuration 3 is similar to Configuration

2, except that vanes intruding inside the soil specimen are provided, which can increase the number of corners along the vertical boundaries.

Grognet (2011) showed that with the presence of the strips and vanes, the stress/strain uniformity was improved compared with conventional straight vertical boundaries, and separation of the specimen at the acute corner is reduced. Based on the findings, the use of frictionless containing rings in the present commercially-available direct simple shear devices can improve the stress/strain uniformity.

2.7 Summary

A comprehensive literature review was conducted to build a conceptual framework upon which the research program was based. Offshore pipeline axial walking is the undesired accumulation of axial displacement of offshore pipelines during operation cycles. Research indicates that the axial resistance will tend towards the drained values during cycles of pipe movement, regardless of the rate or duration of each movement. A reliable prediction of this mechanism could bring significant design benefits, as drained resistance is usually higher than undrained resistance. Consequently, a higher range of axial resistance can be applied, leading to more cost-effective design. The pipe-soil interaction in pipe axial walking problems is extensively influenced by the soil response. The axial response is significantly influenced by the generation and dissipation of excess pore water pressure which leads to undrained and drained soil behaviour. It is likely that the response is between fully undrained and fully drained in typical field conditions. Analysis of the field data also suggests that the mobilisation of axial resistance is a time-related process instead of being linked to the distance of shearing. This suggestion is consistent with excess pore pressure development in cycles. In other words, the full pipe-soil resistance is only mobilised when steady pore pressures are reached. The residual resistance is the primary component of the load-displacement relationship in pipe axial walking, and it is dominated by the axial displacement rate.

The portion of the soil below the pipe which undergoes shearing, characterised as the shear zone, is significant for pipe axial walking assessment. Cyclic direct simple shear testing was selected as the preferred testing method to conduct an investigation into the soil behaviour within the shear zone owing to its various merits, including its loading pattern, allowing the rotation of principle stress axes, the small specimen size required, and its shear failure planes.

Chapter 3 - Experimental program and results

This chapter presents the experimental program and results. First the soil selected for the experimental program is introduced, followed by an elaboration of the experimental set-up. Finally the experimental results are presented.

3.1 Soil selection

The initial aim of the investigation was to simulate the environment of the petroleum pipelines which were to be laid on the seabed of the North Western Shelf, Australia. However, the use of actual soil material from the field was found to be not feasible due to both accessibility as well as quantity issues. As an alternative, as suggested by researchers at the University of Western Australia (UWA Centre for Offshore Foundation Systems), a kaolinite soil known as Prestige NY from Granville (NSW) was selected as the soil to be tested in the experimental program. Prestige NY kaolinite is commercially available and it was concluded that it exhibits similar characteristics to those of the seabed soil (Senthilkumar, 2013).

Various properties of both Prestige NY kaolinite and seabed silt have been investigated by Shannon (2013) and Senthilkumar (2013), including specific gravity analysis, particle size analysis, Atterberg limits tests, oedometer analysis, mineralogy analysis and triaxial testing.

3.1.1 General soil properties

The general soil properties of the Seabed silt and Prestige NY kaolinite clay are compared in Table 3.1, and the physical appearance of the soils is shown in Figure 3.1.

Table 3.1 General soil properties (Senthilkumar, 2013)

	Seabed silt	**Prestige NY**
Colour	Green	White
Swelling/Non-swelling	Non-swelling	Non-swelling

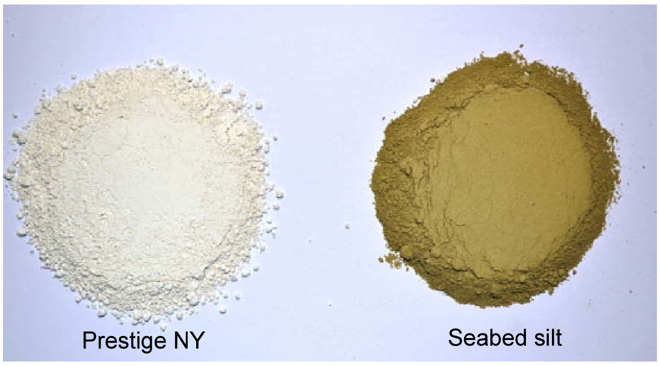

Figure 3.1 Soil sample of Prestige NY and Seabed Silt (Senthilkumar, 2013)

3.1.2 Specific Gravity

Specific gravity analysis was carried out for both soils, using an automatic density analyser. The measured specific gravity of both the Seabed silt and Prestige NY is given in Table 3.2 below.

Table 3.2 Specific Gravity of Seabed silt and Prestige NY (Senthilkumar, 2013)

Seabed silt	2.63
Prestige NY	2.61

3.1.3 Particle size analysis

The average particle size distribution of both soils is given in Figure 3.2. The distribution indicates that for both soils the majority of the particles are clay-sized.

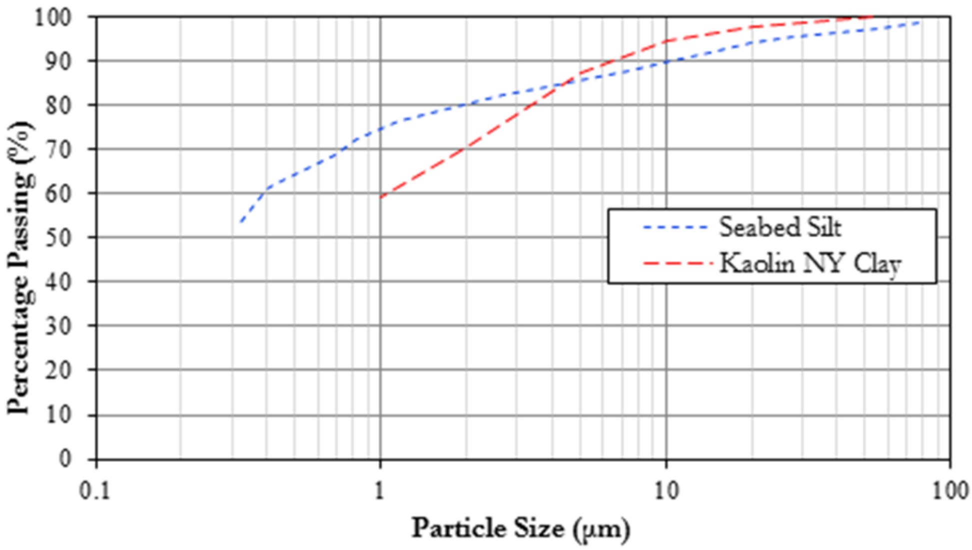

Figure 3.2 Particle size distribution curves (Senthilkumar, 2013, Shannon, 2013)

3.1.4 Atterberg limits analysis

The aims of the Atterberg limits analysis are to determine the liquid limit and plastic limit of the soil. The results are plotted on the USGS chart given in Figure 3.3. Both soils exhibit liquid limits as high as 50% of the gravimetric water content. According to the classification, the Prestige NY kaolinite is classified as inorganic highly plastic clay (CH) but falls close to the boundary of CL soils, whereas the seabed silt is classified as organic silt (MH). Despite the different classifications the two soils fall into, their close proximity on the USGS charts indicates that they exhibit similar wetting characteristics.

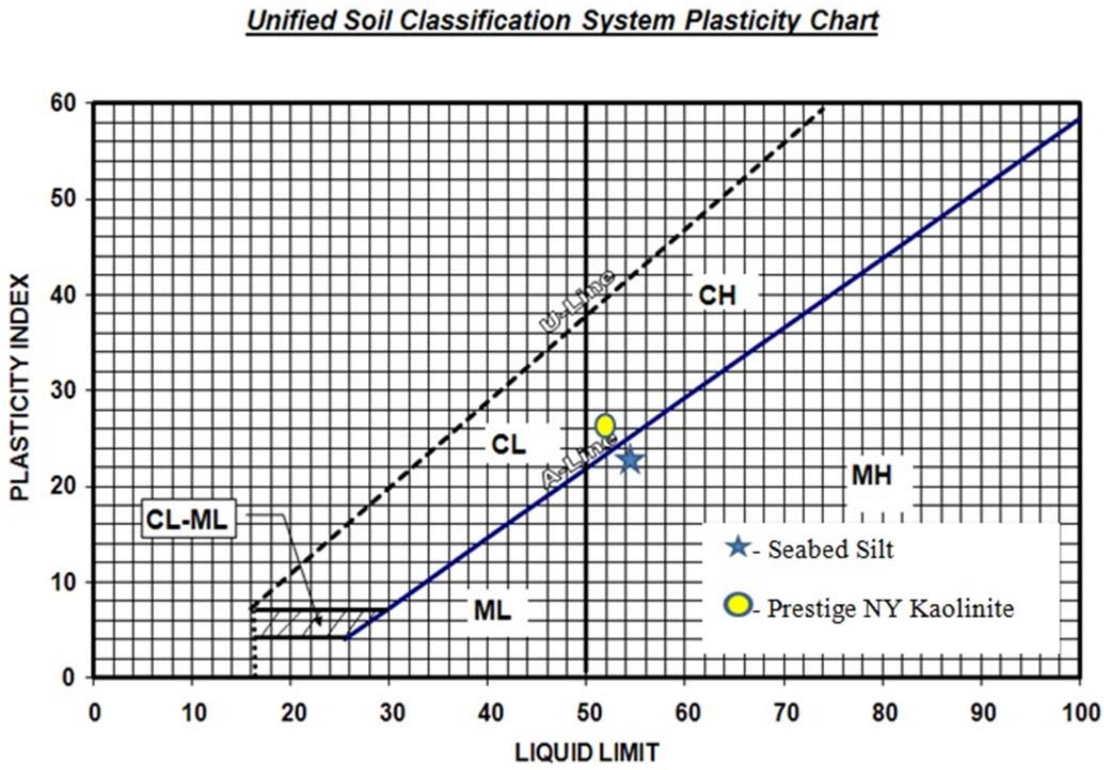

Figure 3.3 USGS Charts (Senthilkumar, 2013, Shannon, 2013)

3.1.5 Oedometer analysis

Oedometer tests were performed to determine the consolidation parameters of the two soils. The soils were prepared with a gravimetric water content of approximately twice the liquid limit and one-dimensional consolidation was implemented. The void ratio versus consolidation pressure curve is shown in Figure 3.4 and the consolidation parameters are given in Table 3.3.

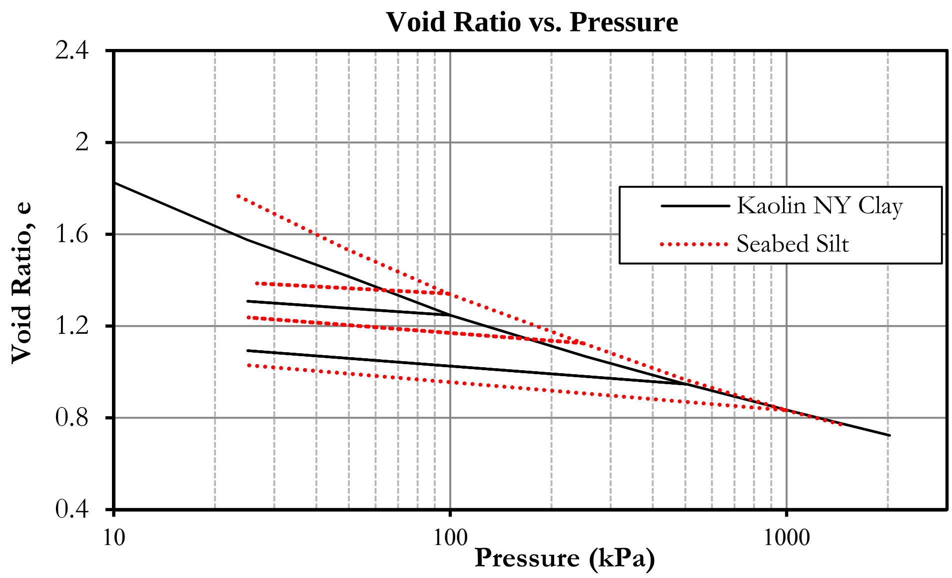

Figure 3.4 Consolidation and re-consolidation curves of oedometer tests (Senthilkumar, 2013, Shannon, 2013)

Table 3.3 Consolidation parameters from oedometer tests (Senthilkumar, 2013, Shannon, 2013)

	Seabed silt	**Prestige NY**
Initial Gravimetric Water Content (%)	120 ≈2×LL	100 ≈2×LL
Average Compression Index, c_c	0.46	0.40
Compressibility Parameter, λ	0.199	0.173
Average Swelling index, c_s	0.12	0.11
Unload/Reload Parameter, κ	0.053	0.046
Average Coefficient of Consolidation, c_v (m^2/sec)	1.2×10^{-7}	2.89×10^{-7}
Average Permeability (m/s)	1.8×10^{-9}	3.6×10^{-9}
Coefficient of Compressibility, m_v (kPa^{-1}) at 50-100 kPa step	0.0016	0.0012
Secondary Compression, c_α	0.0058	0.0057

3.1.6 Triaxial tests

The main purpose of conducting the triaxial tests was to determine the undrained/drained friction angle and other relevant properties that can be applied in numerical modelling of soil behaviour. Table 3.4 below gives the parameters applied and the properties determined in the triaxial tests.

Table 3.4 Parameters and properties in triaxial tests (Senthilkumar, 2013, Shannon, 2013)

	Seabed silt	**Prestige NY**
Initial Gravimetric Water Content (%)	120 ≈ 2×LL	100 ≈ 2×LL
Drained/Undrained Friction Angle, φ' (°)	19.65	21.9
Critical State Line, M	0.80	0.89
Average Coefficient of Consolidation, c_v (m^2/sec)	1.2×10^{-7}	2.19×10^{-7}

3.1.7 Summary

A summary of the average geotechnical properties of the seabed silt and the Prestige NY kaolinite is presented in Table 3.5. The closeness of the properties of both soils justifies the selection of Prestige NY kaolinite as the soil used in the experimental program.

Table 3.5 Geotechnical properties of Seabed silt and Prestige NY kaolinite (Senthilkumar, 2013, Shannon, 2013)

	Seabed silt	**Prestige NY**
Specific Gravity	2.63	2.61
Liquid Limit (%)	55	52
Average Compression Index, c_c	0.46	0.40
Compressibility Parameter, λ	0.199	0.173
Average Swelling Index, c_s	0.12	0.11
Unload/Reload Parameter, κ	0.053	0.046
Average Coefficient of Consolidation, c_v (m^2/sec)	1.2×10^{-7}	2.9×10^{-7}
Average Permeability (m/s)	1.8×10^{-9}	3.6×10^{-9}
Secondary Compression, c_α	0.0058	0.0057
Critical State Friction Angle, φ' (°)	19.7	21.9
Critical State Line, M	0.8	0.85

3.2 Experimental set-up

3.2.1 GDS Direct Simple Shear Testing System

In the experimental program of the current research, cyclic direct simple shear tests were performed on Prestige NY kaolinite clay at low normal stress, using the GDS Standard Simple Shear System (GDS-STDSS), as shown in Figure 3.5. The GDS-STDSS system is an electro-mechanical shear testing device which is designed to meet and exceed the requirements of ASTM-D6528 (2007), 'Standard Test Method for Consolidated Undrained Direct Simple Shear Testing of Cohesive Soils'.

Figure 3.5 GDS Standard Simple Shear System (GDS-STDSS)

The apparatus is a fully self-contained system with no requirements for compressed air or hanging weights. Normal (axial) and shear forces are applied using GDS electro-mechanical force actuators. Each axis (normal or shear) can be controlled in displacement (strain or velocity) mode as well as load or stress mode, which means that both constant-volume and constant-load tests can be performed. As the system is capable of performing cyclic shearing, it meets the needs of the research program. Axial and shear load readings are controlled under closed-loop feedback. Top cap fixity is assured through a system of crossed roller linear guides to minimise top cap rocking during shearing.

3.2.2 Specimen preparation

The Prestige NY kaolinite was first mixed from the powder state to a slurry using a soil mixer, achieving a 70% initial moisture content. The specimens tested in the GDS simple shear system are cylindrical specimens 50mm in diameter. The specimen is laterally confined by Teflon-coated low friction retaining rings, as shown in Figure 3.6(a), ensuring a constant cross-sectional area during shearing. The initial height of the specimen can be varied by adjusting the number of rings. During soil specimen preparation and insertion, the friction rings are first constrained by supporting forms and the reconstituted soil is inserted into the sample preparation apparatus, as shown in Figure 3.6(b). The assembly is then placed in the system as shown in Figure 3.6(c) and the supporting forms are removed. The top cap makes contact with the specimen and the hold-down assemblies are secured into place as shown in Figure 3.6(d).

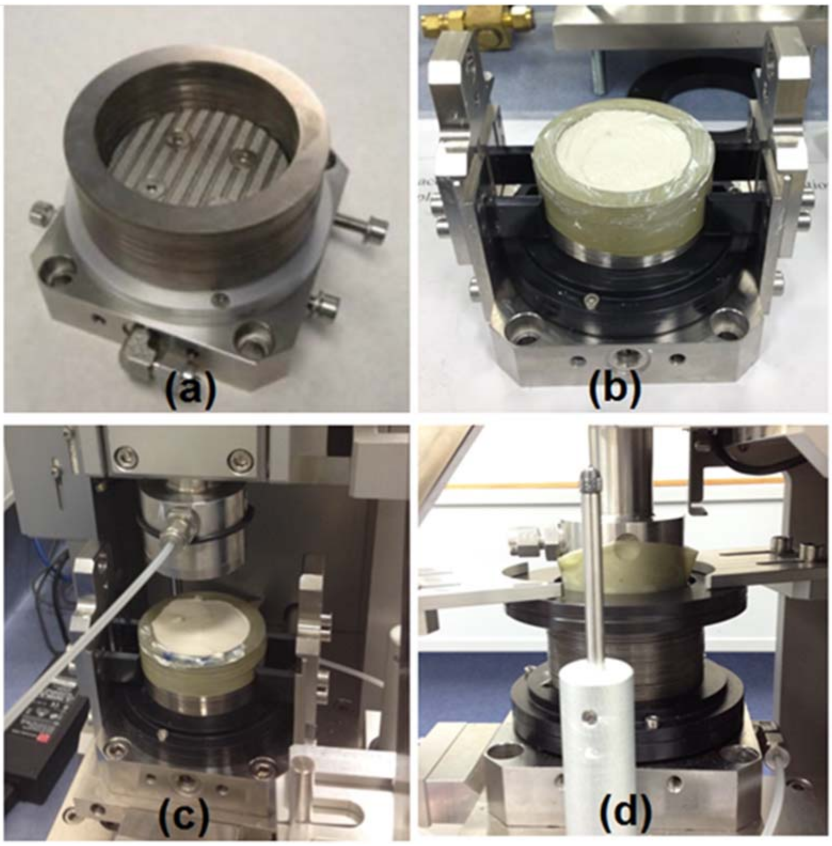

Figure 3.6 Specimen preparation and insertion

3.2.3 Pore pressure measurement

It is difficult to achieve truly undrained conditions in direct simple shear testing, unless a pressurised chamber is installed inside the system to host the sample. The GDS-STDSS system was not originally designed to be capable of doing truly undrained tests and to be equipped with pore pressure measurement capacity. ASTM-D6528 (2007) specifies that constant-volume undrained-equivalent direct simple shear testing can be conducted to determine undrained soil properties in such systems. As presented previously, Bjerrum and Landva (1966) argued that in constant volume testing, the change in applied normal stress equals the change in pore water pressure which would have occurred in truly undrained direct simple shear testing. This argument was verified by Dyvik et al. (1987) for normally consolidated clay.

The intention of the current research program was not to establish truly undrained conditions in direct simple shear tests. The drainage was kept open at the consolidation stage as well as during cyclic shearing. However, when the applied shearing rate/velocity is not slow enough and consequently the soil response is not fully drained, some amount of excess pore pressure builds up, since dissipation of excess pore pressure is not fast enough. Therefore, pore pressure measurement capacity is still required to better interpret and analyse the test results.

Modification to the original GDS-STDSS system was carried out to equip the device with pore pressure measurement capacity. The base pedestal of the specimen set-up, where the bottom porous stone is attached, is connected to a pore pressure transducer (PPT) through the bottom drainage port as shown in Figure 3.7. When the base pedestal is saturated and the bottom drainage valve is closed, the reading from the PPT gives an estimation of the pore pressure level at the bottom of the specimen.

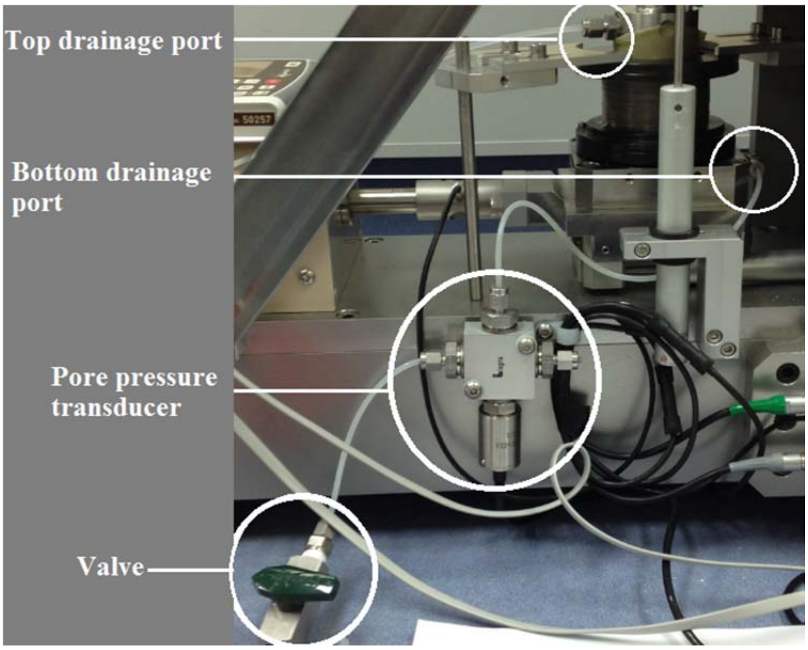

Figure 3.7 Pore pressure measurement configuration

The pore pressure transducer installed is the P620GDS-1MPa-C2.5 transducer produced by GDS Instruments. The transducer was connected to the GDS RS232 Data interface. Connecting the transducer to the data interface enables the transducer to work with the GDS-STDSS system under the same platform of GDSLAB, thus achieving simultaneous data recordings in the test.

Deionised water was used to saturate the transducer and the base pedestal. The water was first de-aired using a pump as illustrated in Figure 3.8(a). The base pedestal was immersed in water for 24 hours to make sure that it is fully saturated prior to sample insertion. The de-aired water was injected into the transducer through the bottom valve using a syringe, as shown in Figure 3.8(b). The readings of the PPT were closely monitored throughout the process to ensure that excess pore pressure was not built up.

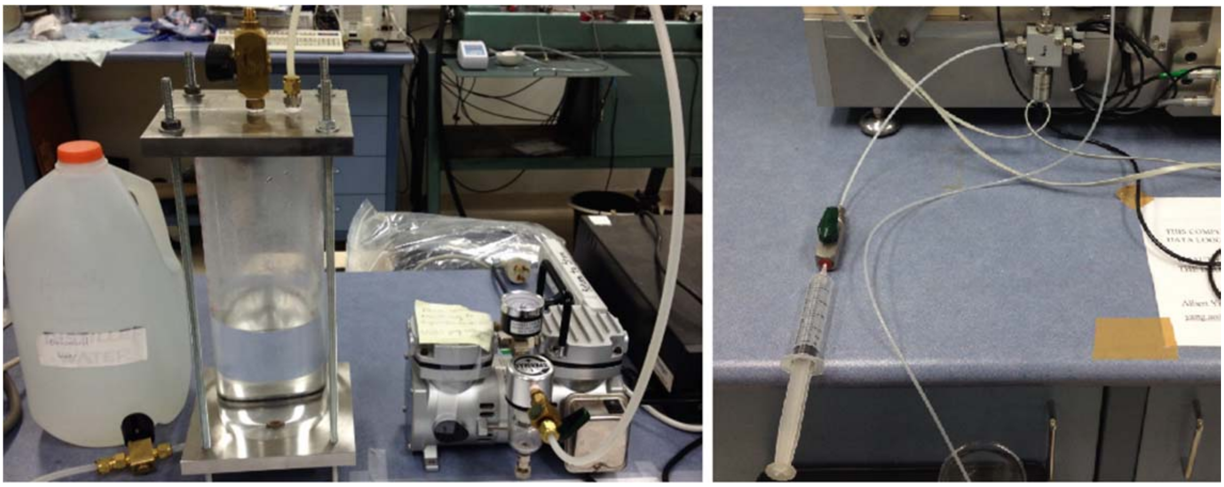

(a) (b)

Figure 3.8 (a) De-airing water apparatus (b) Water injection

The bottom valve was closed when saturation was completed. The top drainage port was kept open during consolidation as well as the shearing stages, and the water coming out from the top drainage port was recorded using a measuring cylinder, as shown in Figure 3.9.

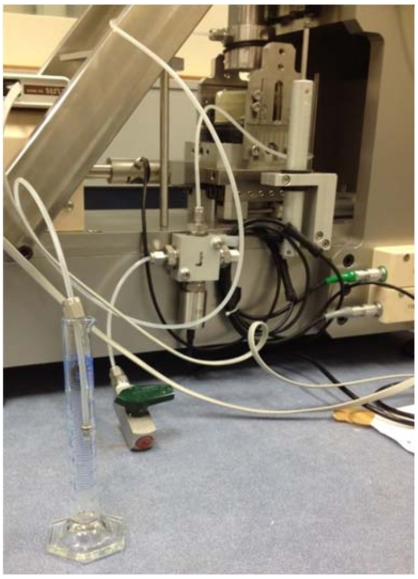

Figure 3.9 Measuring cylinder connecting to the top drainage port

3.3 Test methodology

3.3.1 Consolidation and normal stress

In the current experimental program, ideally the soft clay (Prestige NY kaolinite) would be normally consolidated one-dimensionally to an appropriate vertical/normal stress in the GDS-STDSS system. When the consolidation stage is completed, cyclic direct simple shear testing on the soil specimen would commence under the same normal stress.

As discussed previously, normally the magnitude of effective normal stress imposed on the soil underneath the pipe is relatively low in pipe axial walking problems. The effective normal stress (σ'_n) equals the total normal stress (σ_n) minus the pore water pressure (u). In drained cases, total normal stress (σ_n) may not be equal to the effective normal stress (σ'_n) since the pore water pressure can be very high due to the depth of the seabed, which can be in the order of kilometres. Based on the available literature (Bruton et al., 2007) , the effective normal stress imposed in pipe axial walking is in the range of 2kPa to 10kPa.

However, it was observed and confirmed in the tests that the friction from the horizontal motor rail of the GDS-STDSS system produced undesired variations in the horizontal/shear load readings, as demonstrated in Figure 3.10. In the tests presented in Figure 3.10, the horizontal motor moves back and forth in a sinusoidal function with an amplitude of 2mm, without a soil specimen in place. Vertical stresses of 0kPa, 20kPa and 40kPa were applied on top of the horizontal motor and the readings of the horizontal load cell were recorded.

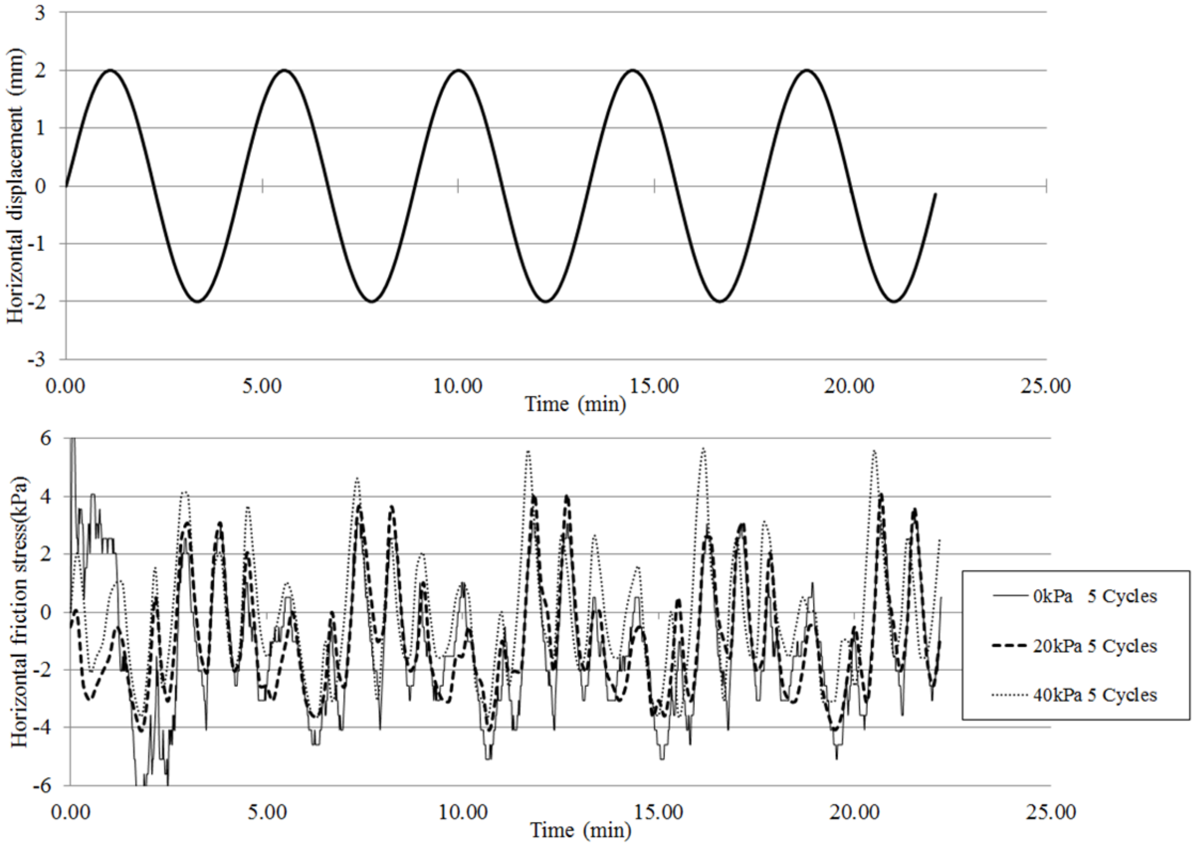

Figure 3.10 Variations in horizontal load readings due to rail friction

As Figure 3.10 shows, the magnitude of variations in horizontal/shear stress readings due to friction is between 2kPa and 5kPa, given the specimen diameter of 50mm. Several attempts were made to eliminate the variations in load readings due to rail friction, including correcting the raw horizontal load readings by offsetting the variations due to friction. However, due to the randomness of the variations, the outcome of the correction was deemed unsatisfactory. It is therefore concluded that the current testing system cannot produce satisfactory horizontal load readings under very low normal stress. The test results also show that the magnitude of the friction does not rise significantly with increasing applied vertical stress. As a result, a higher consolidation and normal stress of 60kPa was applied in the experimental program to minimise the effect of the rail friction.

3.3.2 Shearing velocities and shearing amplitude

The selection of shearing velocities in the current research program was intended to cover the undrained, partially drained and drained conditions in pipe axial walking.

Regarding the shearing amplitude, analysis of field data (White et al., 2011b) suggests that the mobilisation of axial resistance is a time-related process instead of being linked to the distance of shearing. This suggestion is consistent with the excess pore pressure development in the sweeps. In other words, full pipe-soil resistance is only mobilised when steady pore pressures are reached. Combining this with the guidance from ASTM-D6528 (2007), a single shearing amplitude of 10% of specimen height was used in cyclic direct simple shearing. It is worth noting that the value of height in this case should be taken as the specimen height when the consolidation stage is completed.

3.3.3 Summary of test methodology

The Prestige NY kaolinite was first mixed from the powder state to a slurry using a soil mixer, achieving a 70% initial moisture content. The initial specimen height before consolidation was approximately 26mm. All soil specimens were first normally consolidated one-dimensionally in the GDS-STDSS system before shearing took place. Cyclic direct simple shear tests were performed on the normally consolidated specimens under a constant normal stress. The cyclic shearing followed a sinusoidal horizontal displacement function and the shearing amplitude was 10% of the specimen height. Various shearing velocities were applied, to cover the undrained, partially drained and fully drained responses.

3.4 Test results

3.4.1 Consolidation stage

The consolidation stages for all tests reported here were performed identically. The Prestige NY kaolinite was first mixed from the powder state to a slurry using a soil mixer, and staged consolidation was carried out within the GDS STDSS system. First, a consolidation stress of 20kPa was applied and the consolidation stress was increased to 40kPa and 60kPa subsequently. Table 3.6 outlines the key soil properties and test parameters at the consolidation stage.

Table 3.6 Soil properties and test parameters at consolidation stage

Average initial soil moisture content	71.13%	
Average initial soil wet density	1.42g/cm^3	
Initial soil specimen height	26.36mm	
	Consolidation Stress (kPa)	Consolidation Time (min)
Staged Consolidation	20kPa	120
	40kPa	120
	60kPa	until pore water pressure level stabilised

The consolidation displacement vs. time curves are presented in Figure 3.11 . Figure 3.11(a) is the plot of consolidation displacement in mm versus elapsed time in minutes. Figure 3.11(b) is the plot of consolidation displacement as a percentage of final displacement versus normalised time $c_v t/H^2$, where

c_v is the average coefficient of consolidation, taken as $2.9\times10^{-7}m^2/sec$;

t is the elapsed time in seconds;

H is the initial soil specimen height in meters, taken as 0.02636m. The bottom drainage port was closed during consolidation as one-way drainage is considered.

As demonstrated in Figure 3.11, due to the relatively small specimen size in the GDS-STDSS system, the consolidation stage can be completed within a normalised time of $c_v t/H^2 = 12$ (12 hours).

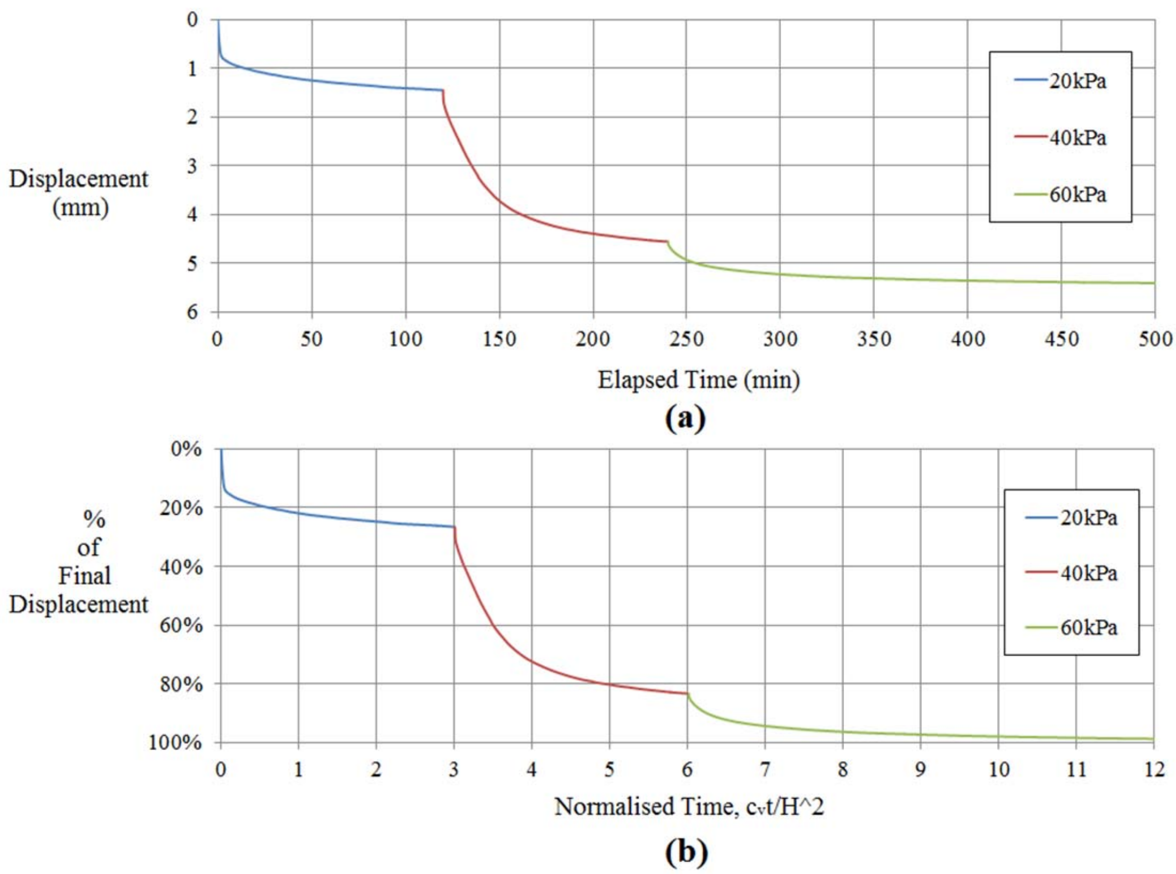

Figure 3.11 Consolidation displacement vs. (a) Elapsed time (b) Normalised time

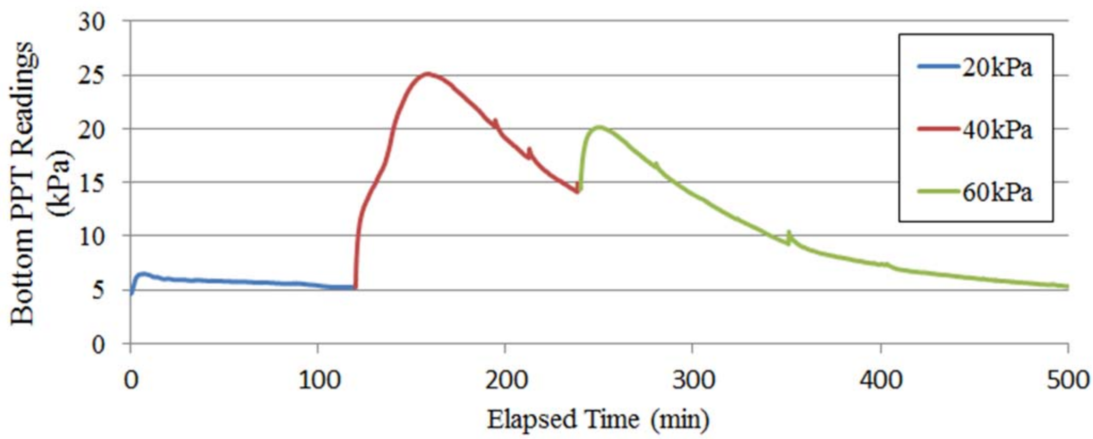

Figure 3.12 PPT Readings at consolidation stage

The readings of the pore pressure transducer (PPT) at the consolidation stage are plotted in Figure 3.12. The readings show that there is a delayed response from the PPT readings. To be more specific, when the consolidation stress increases, the PPT readings do not rise immediately to a peak. Instead, a gradual increase or delayed response is observed from the readings. Further, the change in PPT reading is not equal to the actual excess pore pressure that builds up in the specimen. As introduced earlier, due to the limitations of the experimental set-up, the PPT was connected to the bottom drainage port instead of within the specimen. Therefore, the PPT can only provide an estimation of the pore pressure level at the bottom drainage port. Nevertheless, the PPT readings can provide some useful data when analysing the excess pore pressure development in the specimen at both consolidation and cyclic direct simple shearing stages.

3.4.2 Cyclic shearing stage

Cyclic direct simple shear tests were performed on the normally consolidated specimens under a constant normal stress applied. Table 3.7 summarises the test parameters at the cyclic shearing stage.

Table 3.7 Test parameters at the cyclic shearing stage

Applied normal stress during shearing	Average specimen height before shearing	Shearing amplitude	Shearing velocities	No. of cycles
60kPa	19.50mm	10% of specimen height	0.3mm/s 0.03mm/s 0.005mm/s 0.0005mm/s	10-30

The application of a constant normal stress is consistent with the vertical loading condition of the soil underneath the pipe in pipe axial walking, where the vertical load is due to the pipe's weight. Similar to the drainage path of the soil underneath the pipe where there is free drainage at the soil surface, the top drainage port was kept open at the shearing stage. The shearing amplitude was 10% of the specimen height. Various shearing velocities were applied, to cover the undrained, partially drained and fully drained responses. The period of one cycle ranges from approximately 26 seconds for fast shearing to 1560 seconds for slow shearing.

The specimen was sheared by mobilising the horizontal load motor, as shown in Figure 3.13, and the horizontal displacement followed a sinusoidal function.

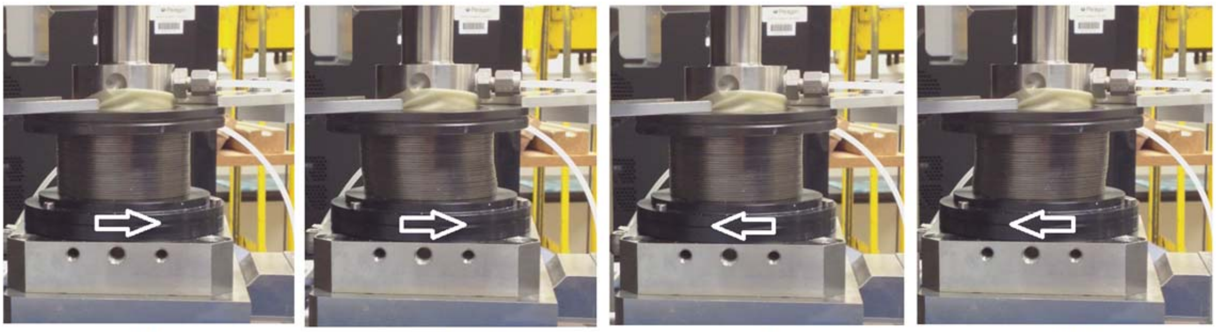

Figure 3.13 Cyclic shearing of the soil specimen

Pore pressure development

Shearing velocities significantly affect the level of the excess pore pressure that builds up during cyclic shearing, and therefore dominate whether the soil response in the shear zone is undrained, partially drained or fully drained in pipe axial walking. The readings of the pore pressure transducer were recorded and Figure 3.14 presents the PPT readings versus time plots. The shearing velocities, from fastest to slowest, are (a) 0.3mm/s, (b)0.03mm/s, (c) 0.005mm/s and (d) 0.0005mm/s.

The shear strain versus time curves are also plotted on the same figure for each shearing velocity. The plots show that for high shearing velocities like those shown in Figures 3.14(a) & (b), excess pore pressure continuously builds up as cyclic shearing progresses, and higher velocity induces higher levels of excess pore pressure. The fast shearing cases can be characterised as undrained shearing. If the shearing velocity is moderate, like that shown in Figure 3.14(c) , excess pore pressure is generated and plateaus after reaching a moderate level. As cyclic shearing continues, excess pore pressure dissipates eventually. The moderate shearing cases can be characterised as partially drained. For very slow shearing like that shown in Figure 3.14(d) , the level of the excess pore pressure that builds up during shearing is negligible compared with faster cases. Therefore, the slow shearing cases can be characterised as drained.

Continuous consolidation

Continuous consolidation of the specimens was observed as the cyclic shearing progressed. This is due to the fact that free drainage at the top of the soil is permitted during cyclic shearing. This drainage path is similar to the drainage path of the soil in the shear zone underneath the axially-walking pipe, where water is free to drain from the soil surface. Figure

3.15 illustrates the vertical displacement (as a percentage of specimen height H) versus shear strain plots at the cyclic shearing stage. The shearing velocities, from fastest to slowest, are (a) 0.3mm/s, (b) 0.03mm/s, (c) 0.005mm/s and (d) 0.0005mm/s.

When the shearing velocity is 0.3mm/s, the specimen consolidates continuously without a clear tendency towards convergence. However, the increase of vertical displacement is relatively small, only passing 5% of specimen height H after 30 cycles. Under a shearing velocity of 0.03mm/s, the vertical displacement increases to 5% of H after 5 cycles and there is a clear tendency towards convergence. The vertical displacement converges to 12% of H after 20 cycles. For the slow shearing cases of 0.005mm/s and 0.0005mm/s, the vertical displacement increases to 5% of H after 2 cycles and 1 cycle respectively. There are clear tendencies towards convergence and the vertical displacements converge to 13% of H for 0.005mm/s and 17% of H for 0.0005mm/s.

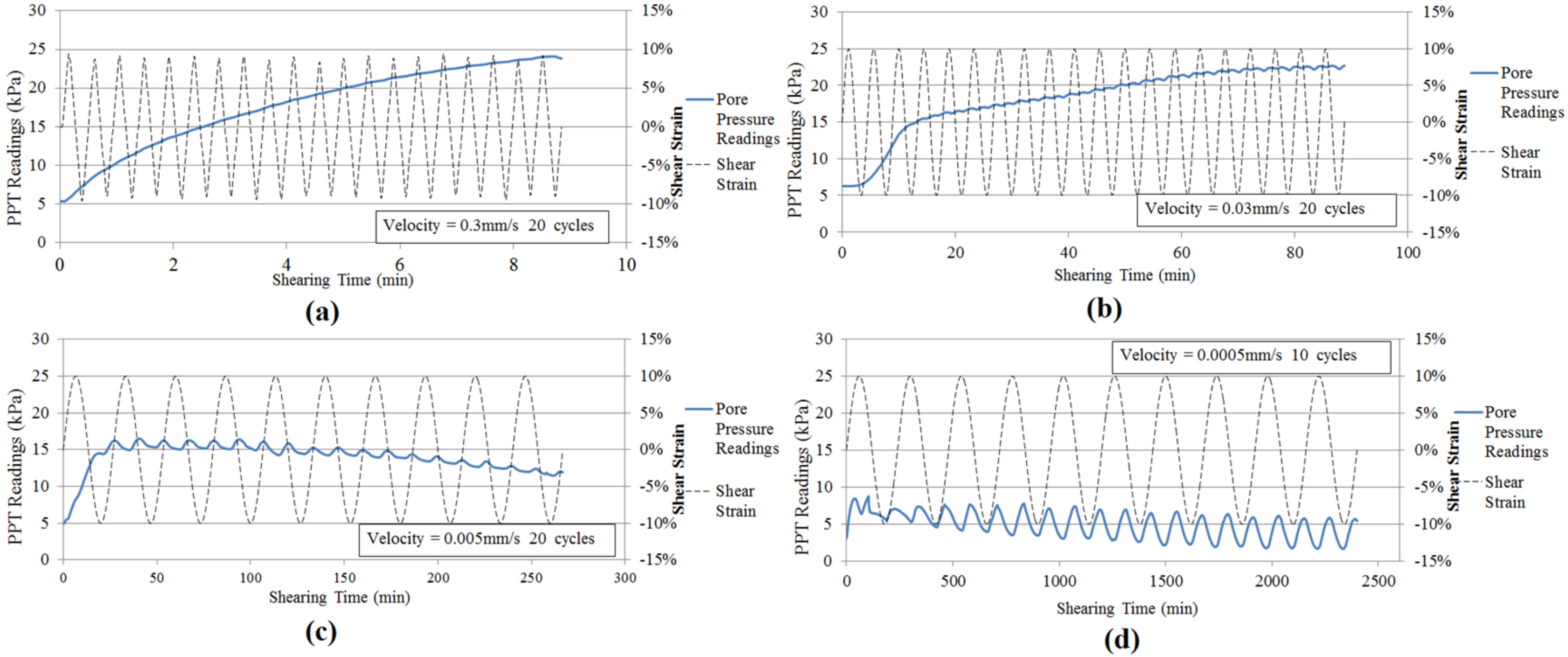

Figure 3.14 Excess pore pressure development at shearing stage

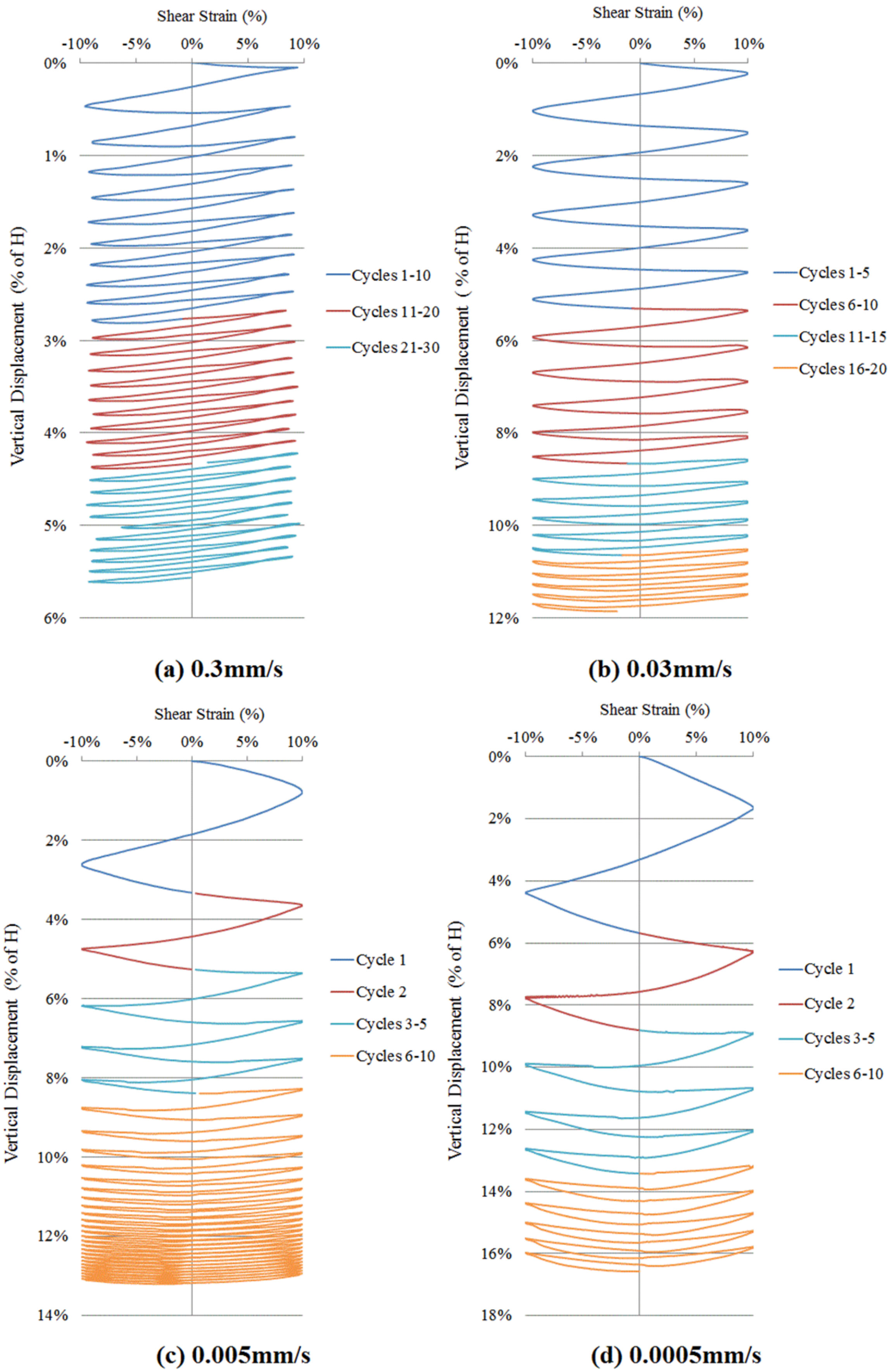

Figure 3.15 Continuous consolidation at shearing stage

Shear stress-strain relationship

The shear stress-strain relationships at the cyclic shearing stage are plotted on Figure 3.16 for shearing velocities (a) 0.3mm/s;(b) 0.03mm/s and Figure 3.17 for shearing velocities (a) 0.005mm/s; (b) 0.0005mm/s. The level of shear resistance is presented as τ/σ_{total}, where τ is the shear/horizontal stress and σ_{total} is the total normal stress applied.

At a high shearing velocity of 0.3mm/s as shown in Figure 3.16(a), a peak or breakout shear resistance is observed when the specimen is sheared for the first time, reaching a peak of just over τ/σ_{total}=0.4. The shear resistance gradually reduces to a residual level of τ/σ_{total} =0.17 after 5 cycles and the shear stress-strain relationship remains stable for the subsequent cycles, representing a ductile response.

At a moderate shearing velocity of 0.03mm/s as shown in Figure 3.16(b), a peak shear resistance takes place when the specimen is first loaded, reaching a peak of approximately τ/σ_{total} =0.25. The shear resistance reduces to a residual level and shows ductile response in cycle 2. The response stays ductile for subsequent cycles. However, the level of residual shear resistance increases gradually as cyclic shearing continues. This is due to the fact that excess pore pressure dissipates and effective stress rises as shearing continues, resulting in higher shear resistance. The residual shear resistance is close to τ/σ_{total} =0.2 in cycles 2-5 but gradually grows to τ/σ_{total} =0.32 in cycles 6-20.

At low shearing velocities of 0.005mm/s and 0.0005mm/s as shown in Figure 3.17 (a) and (b) respectively, only ductile response is observed when the specimen is first sheared, and the shear resistance is always residual. The level of residual shear resistance increases gradually as excess pore pressure dissipates and effective stress rises, and the shear resistance converges to τ/σ_{total} =0.46 for 0.005mm/s and to τ/σ_{total} =0.52 for 0.0005mm/s.

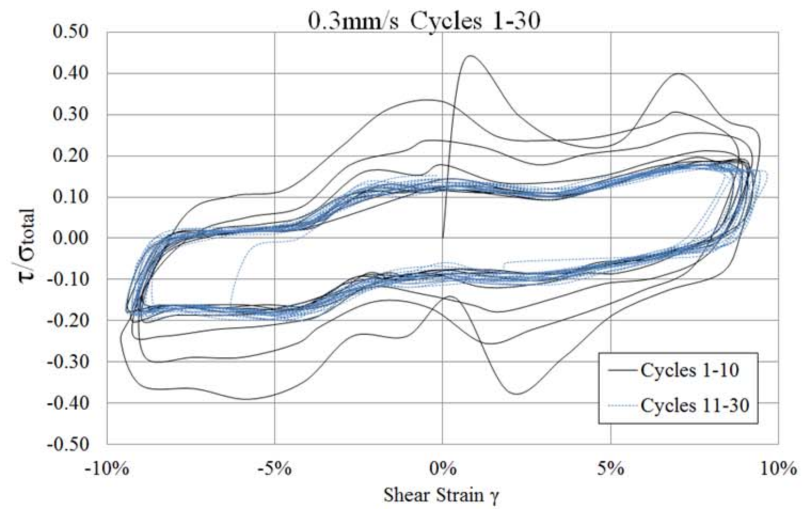

(a) 0.3mm/s

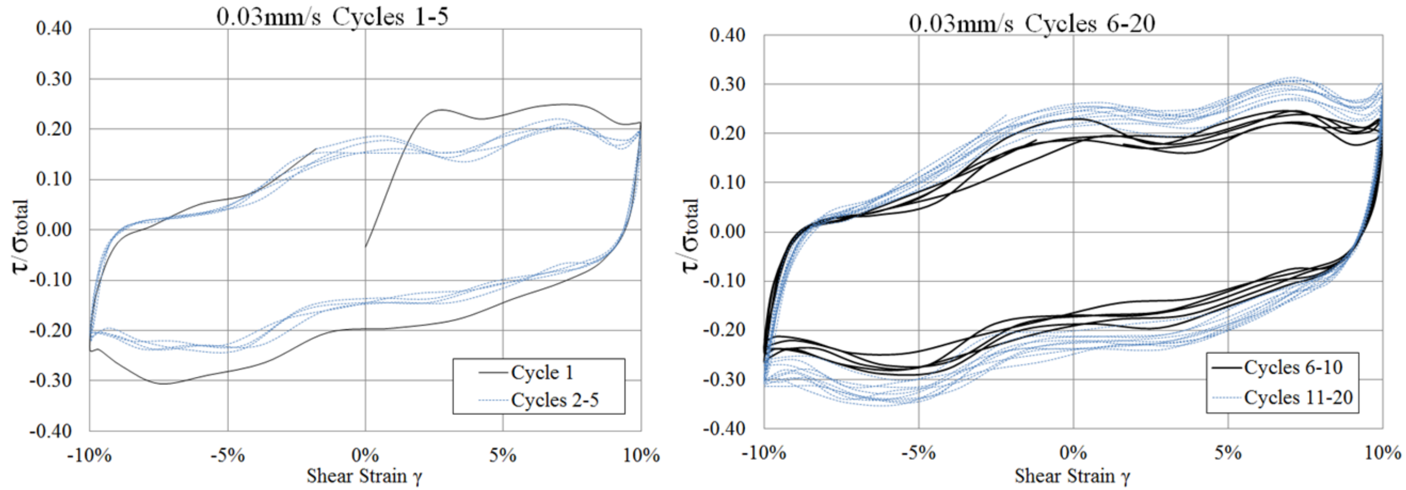

(b) 0.03mm/s

Figure 3.16 Shear stress-strain relationship for (a) 0.3mm/s and (b) 0.03mm/s

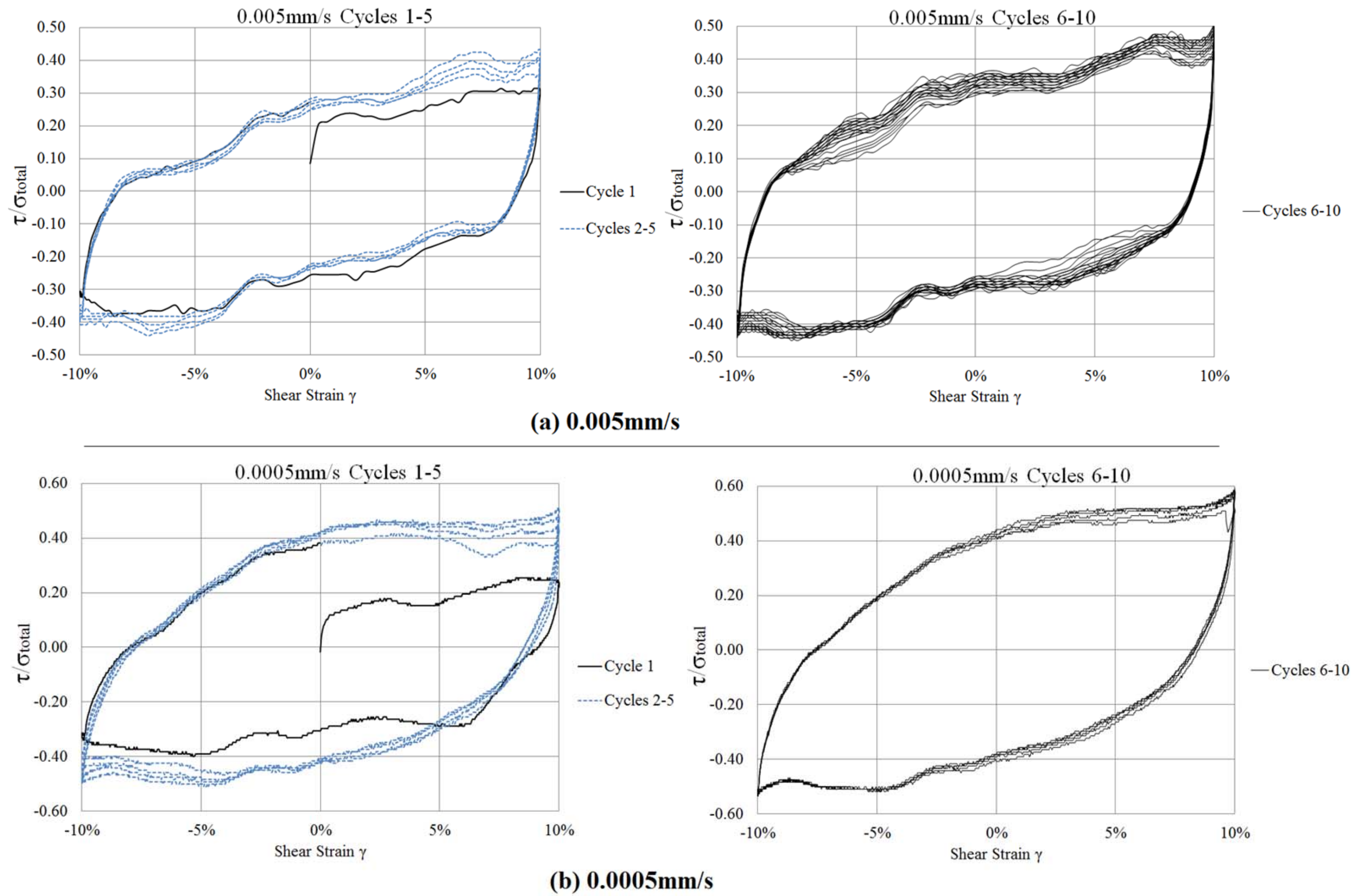

Figure 3.17 Shear stress-strain relationship for (a) 0.005mm/s and (b) 0.0005mm/s

3.5 Concluding remarks

Shearing velocities significantly affect the level of the excess pore pressure that builds up during cyclic shearing, and therefore dominate whether the soil response in the shear zone is undrained, partially drained or fully drained in pipe axial walking. At a high shearing velocity, excess pore pressure builds up continuously and the shearing is undrained. At a moderate shearing velocity, excess pore pressure builds up and dissipates and effective stress rises eventually, resulting in higher shear resistance. At a low shearing velocity, no excess pore pressure builds up and the shearing is drained.

Continuous consolidation of the specimens was observed as the cyclic shearing progressed. This is due to the fact that free drainage at the top of the soil is permitted during cyclic shearing. This drainage path is similar to the drainage path of the soil in the shear zone underneath the axially-walking pipe, where water is free to drain from the soil surface.

The residual shear resistance in cyclic shearing indicates the level of axial soil resistance in the shear zone when offshore pipeline axial walking occurs. Figure 3.18 shows the residual shear resistance versus velocity plot for the cyclic direct simple shear tests performed. The level of shear resistance is presented as τ/σ_{total}, where τ is the shear/horizontal stress and σ_{total} is the total normal stress applied. The shearing velocity is normalised as $\upsilon H/c_v$, where

υ is the shearing velocity in m/sec;
H is the soil specimen height before shearing, taken as 0.0195m.
c_v is the average coefficient of consolidation, taken as 2.9×10^{-7} m^2/sec ;

The residual resistance levels versus axial displacement rate plots in MAPS tests are also presented in Figure 3.18(Senthilkumar, 2013). The results are from the tests with smooth pipe surface at various pipe embedment depths. The axial pipe residual resistance is normalised by the maximum recorded vertical load V_{max} and the axial displacement rate is normalised by the effective pipe diameter D' and the coefficient of consolidation C_v.

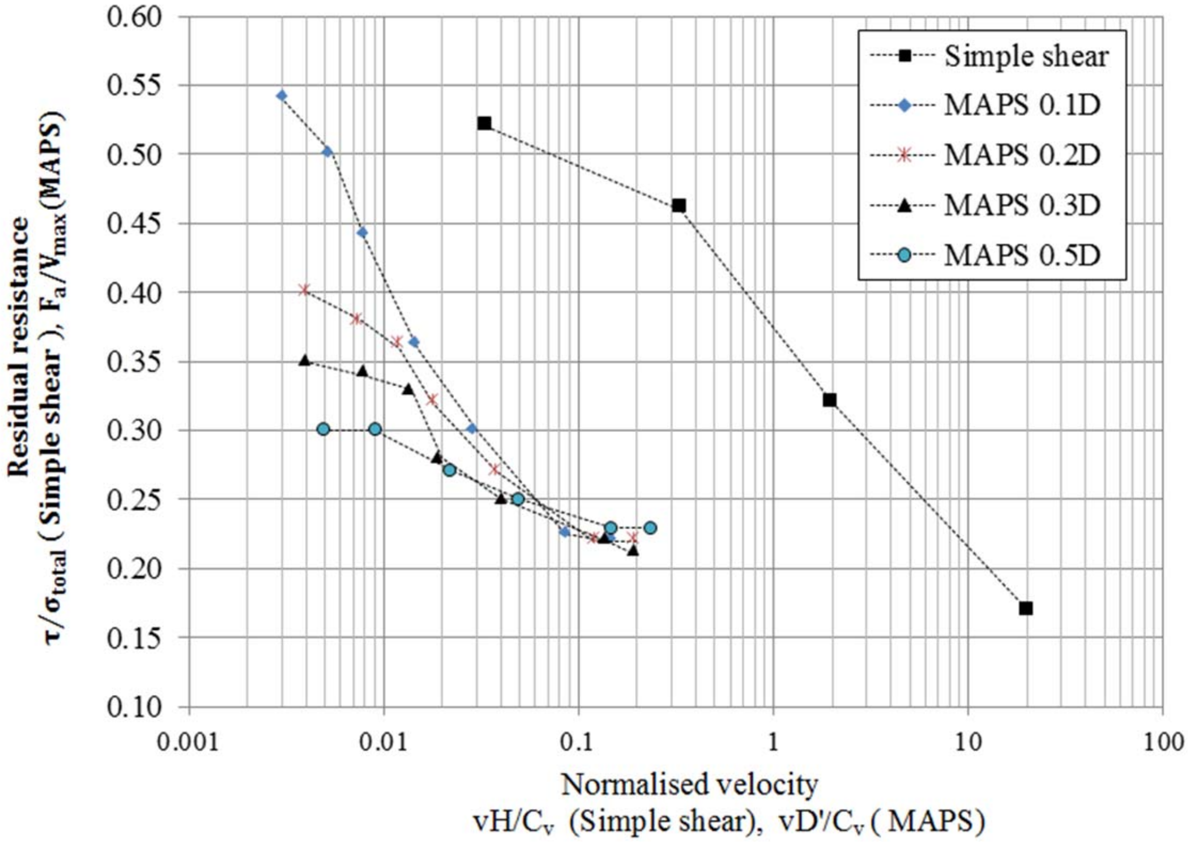

Figure 3.18 Residual resistance versus normalised velocity

The residual resistance in cyclic direct simple shear tests indicates the level of shear resistance of the soil in the shear zone, while the residual resistance in MAPS tests represents the pipe-soil interface resistance in the axial direction. The velocity in the direct simple shear tests is normalised by the specimen height, whereas the velocity in the MAPS tests is normalised by the effective pipe diameter. The above facts mean that the relationships between residual shear resistance and shearing velocity in direct simple shear tests and in MAPS tests do not match exactly with each other. Nevertheless, Figure 3.18 suggests that some shifting factors or transferring equations may be developed to relate the residual resistance as well as the undrained/drained limit in direct simple shear tests to those in pipe-soil interface interaction in the axial direction. If standard test methods such as the current direct simple shear test can be applied in practical design taking offshore pipeline axial walking into consideration, the process would be significantly simplified in terms of time and cost.

More results for cyclic direct simple shear tests can be obtained from finite element analysis and a set of data can be established which can be applied in the calibration of large-scale pipe axial walking modelling, and provide guidance on the design practice of offshore pipelines when considering on-bottom stability in axial direction.

Chapter 4 – Numerical Modelling

The numerical modelling work of the current research program is presented in this chapter. Finite element analyses were conducted to capture the behaviour of soil within the shear zone, using the Abaqus Standard finite element analysis software package. Abaqus is a suite of powerful engineering simulation programs based on the finite element method and it is capable of solving a wide range of problems from simple linear analysis to complicated nonlinear behaviour. In particular, for this research program, the soil constitutive model is capable of incorporating shear-induced pore water pressure generation. This requires an advanced constitutive soil model such as Modified Cam-clay model, which is included in the Abaqus standard package.

The critical state soil theory, upon which the Modified Cam-clay model is based, and the model itself are introduced in this chapter, followed by the two-dimensional finite element analysis (FEA) of cyclic direct simple shearing on soft clay, and the results of the analyses are presented.

4.1 Finite element model

4.1.1 Critical state soil theory and modified Cam-clay model

The specific model implemented in Abaqus Standard is an extension of the Modified Cam-clay model (Abaqus 6.13 Online Documentation). The model is based on the critical state soil theory developed by researchers at Cambridge University (Roscoe et al., 1958, Burland and Roscoe, 1969, Schofield and Wroth, 1968). The model is capable of describing the stress-strain behaviour of soft soils. In particular, the model can predict pressure-dependent soil strength and the compression and dilatancy (volume change) caused by shearing. Because the model is based on critical state theory, it predicts unlimited soil deformations without changes in stress or volume when the critical state is reached.

Detailed elaborations of the critical state soil theory and the modified Cam-clay model are provided in Appendix A.

4.1.2 Two-dimensional finite element model

A two-dimensional finite element model has been developed in Abaqus to simulate cyclic direct simple shearing on soft clay (Prestige NY kaolinite). The dimensions of the 2-D model are consistent with the dimensions of the soil specimen in the experimental program, as shown in Figure 4.1. The initial height of the model (H) is 18.67mm and the length of the model (L) is 50mm. The soil specimen in the experimental program is a cylinder of 50mm diameter and an average initial height of 26.36mm. The soil is represented by 4-node bilinear displacement and pore pressure element (CPE4P).

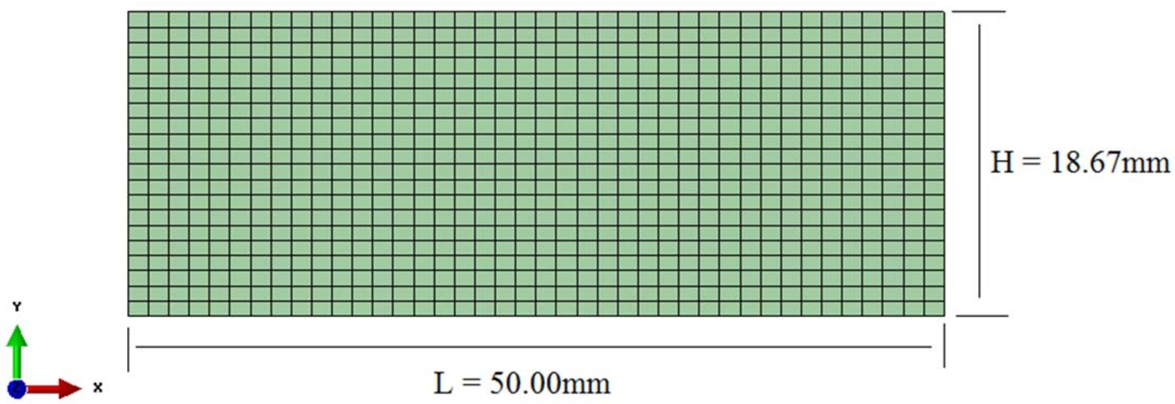

Figure 4.1 Two-dimensional finite element model

4.1.3 Material properties

Table 4.1 presents the soil properties in the modified Cam-clay model that was applied to simulate the elastic and plastic behaviour of the soft clay (Prestige NY kaolinite) in finite element analysis. The soil properties of the Prestige NY kaolinite are based on the various tests conducted previously at Monash University, Australia (Shannon, 2013, Senthilkumar, 2013) and the initial soil conditions are consistent with the initial soil conditions in the experimental program. It was assumed that the soil is fully saturated (i.e. S=1) and the initial water content (ω_0) was equal to 70%.

Table 4.1 Material inputs for the finite element modelling

Initial conditions		
Specific gravity, G_s	2.61	
Degree of saturation, S	1	
Initial water content, ω_0	70%	
Initial void ratio, e_0	1.827	
Initial saturate density, ρ_{sat}	1.57g/cm^3	
Modified Cam-clay inputs		
Porous Elastic	Shear = Poisson	
	Logarithmic elastic bulk modulus, κ	0.040
	Poisson's ratio, υ	0.3
Clay Plasticity	Intercept, N	2.10
	Logarithmic plastic bulk modulus, λ	0.174
	Stress ratio at critical state, M	0.85

In the 'Porous Elastic' Modified Cam-clay inputs, the 'Shear=Poisson' option was chosen to compute the instantaneous shear modulus G from the bulk modulus and Poisson's ratio. The Poisson's ratio was assumed to be a constant of 0.3 under drained conditions.

To properly simulate the pore pressure development in the soil, the vertical permeability at different void ratio levels was defined as given in Table 4.2. The permeability input was based on the experimental investigation of the vertical and horizontal permeability of kaolin clay by Al-Tabbaa and Wood (1987) as well as on the tests performed at Monash University, Australia (Shannon, 2013, Senthilkumar, 2013)

Table 4.2 Vertical permeability for different void ratio levels

Void ratio, *e*	Vertical permeability, k_v in m/s
0.8	2.6184E-10
0.9	3.7991E-10
1.0	5.3000E-10
1.1	7.1627E-10
1.2	9.4295E-10
1.3	1.2143E-09
1.4	1.5348E-09
1.5	1.9086E-09
1.6	2.3404E-09
1.7	2.8346E-09
1.8	3.3958E-09
1.9	4.0284E-09
2.0	4.7373E-09
2.1	5.5270E-09
2.2	6.4022E-09
2.3	7.3678E-09
2.4	8.4284E-09
2.5	9.5888E-09

4.1.4 Load and boundary conditions

Consolidation stage

At the consolidation stage, the soil is normally consolidated and a constant consolidation stress is applied uniformly on the top surface of the soil model. Pore water is free to drain from the top surface and drainage is not allowed at the bottom, as in the experimental set-up. The model is constrained on both the left and right vertical sides and no displacement is allowed in the horizontal direction (x-direction). The model can be compressed one-dimensionally in the vertical direction (y-direction) at the consolidation stage.

Cyclic shearing stage

At the cyclic shearing stage, the soil is subjected to a constant vertical stress applied uniformly on the top surface of the soil model. Pore water is free to drain from the top surface and drainage is not allowed at the bottom. The constraints on the vertical sides are released and displacement is allowed in both the horizontal direction (x-direction) and the vertical direction (y-direction).

Cyclic shearing is implemented by specifying the horizontal displacement of the element nodes along the vertical sides. The horizontal displacements of the nodes along the vertical sides are linearly distributed and the two nodes at the same height level (i.e. y coordinates are the same) have the same horizontal displacement, as demonstrated in Figure 4.2(a). This implementation of cyclic shearing closely simulates the horizontal displacement of the soil specimen in the experimental program, where the specimen is constrained by a stack of retaining rings, as shown in Figure 4.2(b). As in the experimental program, the cyclic horizontal displacement also follows a sinusoidal function.

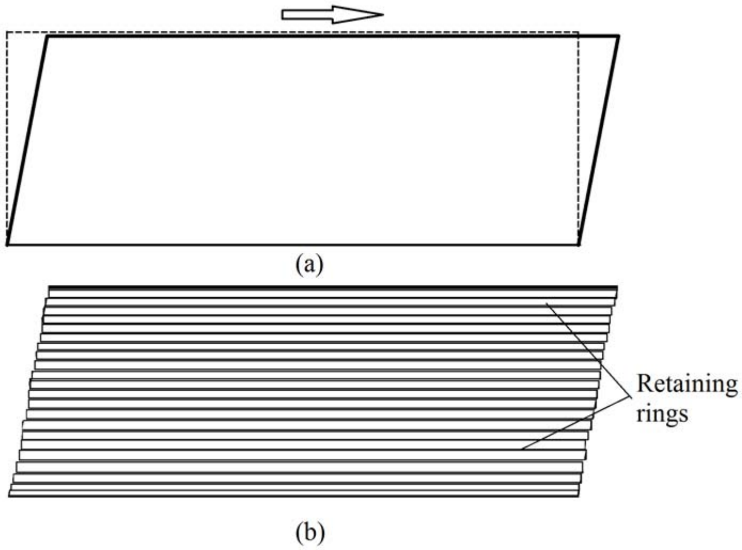

Figure 4.2 Implementation of deformation pattern in cyclic shearing in FEA model

4.1.5 Validation of the finite element model

The results of the finite element analysis with the use of actual soil properties were compared with the experimental data to validate the model. As discussed in Chapter 3, the pore pressure transducer (PPT) in the experimental program is not capable of recording real-time pore pressure level within the soil specimen and can only give an estimation of the pore pressure level at the bottom of the specimen. As a result, it is not feasible to compare the pore pressure level in the FEA with that in the experimental program to validate the model. Nevertheless, the shear stress-strain relationships in FEA and experimental results can be compared.

Figure 4.3 shows a comparison of shear stress-strain curves between the experimental and finite element analysis results. In the results presented the vertical stress is 60kPa, the shear amplitude is 10%, the shearing velocity is 0.005mm/s. Therefore, it is fully drained shearing.

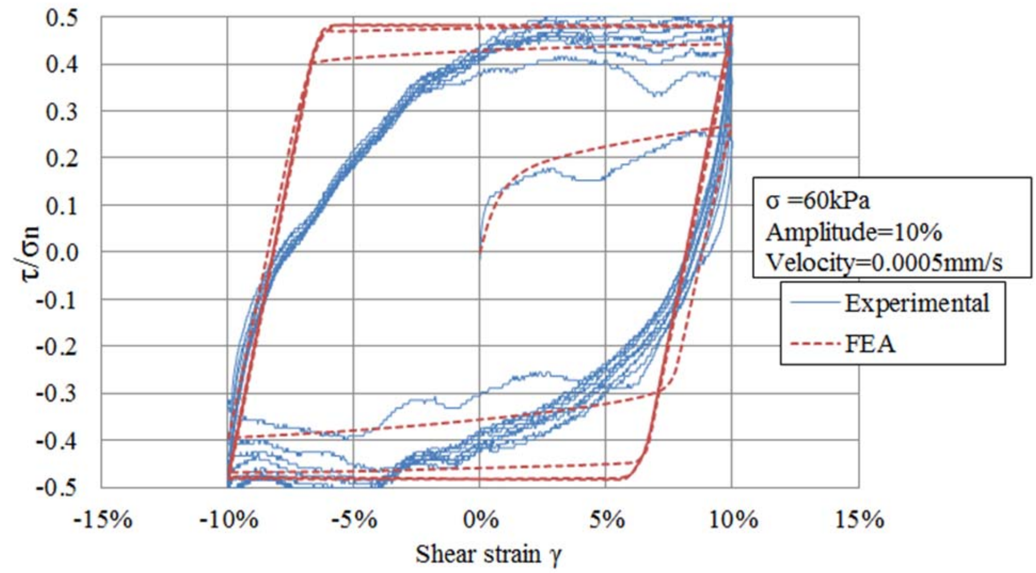

Figure 4.3 Comparison between experimental and FEA shear stress-strain curves

The peak shear stress prediction of the finite element analysis matches the experimental data closely, but there is some difference between the experimental curve and the FEA curve. While the initial portion of the shear stress-strain responses of the experimental and FEA results are close, the experimental results indicate that the slope of the curve changes continuously in subsequent shearing cycles and the curve forms an overall shape close to an ellipse, as shown in Figure 4.3. In contrast, the slope of the FEA curve remains constant before reaching the peak shear stress level, and the curve forms an overall shape close to a parallelogram. This difference can be explained by the yielding function of the modified Cam-clay model. In this model, the soil behaviour is elastic until the stress state of the soil specimen (p', q) hits the yield surface. The shear modulus G remains unchanged after the soil reaches critical state and the slope of the FEA curve therefore remains constant for subsequent shearing cycles.

4.2 Finite element analysis results

4.2.1 Scope of the analyses

Using the finite element model developed, a parametric study was conducted to investigate the influence of vertical stress, shearing velocity and shearing amplitude on the soil behaviour in the shear zone. Table 4.3 summarises the variables in the finite element analyses (FEA). Unlike in the experimental program, where the testing equipment could not produce satisfactory horizontal load readings under very low vertical stress, a very low consolidation/vertical stress can be applied in the finite element analysis. Five shearing velocities were applied in the FEA, covering the undrained, partially drained and drained responses in cyclic shearing. Shearing amplitudes of 5% and 10% of specimen height were applied in FEA, and the height was taken as the specimen height when the consolidation stage was completed.

Table 4.3 Variables in finite element analyses

Consolidation/Vertical Stress	Shearing Velocity	Shearing Amplitude
10kPa 20kPa 40kPa 60kPa	1.0mm/s 0.3mm/s 0.03mm/s 0.005mm/s 0.0005mm/s	5% of H 10% of H

4.2.2 Consolidation stage

Vertical displacement

A constant vertical stress is applied at the consolidation stage and the analysis enters the cyclic shearing stage when excess pore pressure dissipation is completed. The vertical displacement vs. time and void ratio vs. time plots at the consolidation stage are presented in Figures 4.4(a) and (b) respectively. The time is normalised as $c_v t/H^2$, where

c_v is the average coefficient of consolidation, taken as 2.9×10^{-7}m^2/sec ;

t is the elapsed time in seconds;

H is the initial soil height in meters, taken as 0.01867m. The bottom drainage port was closed during consolidation, as such one-way drainage is considered.

The results show that higher consolidation stress results in larger vertical displacement and further compression of the soil skeleton. The void ratio decreases from the initial void ratio of 1.827 to 1.5 under an applied vertical stress of 10kPa, whereas the void ratio drops from 1.827 to 1.4 under an applied vertical stress of 60kPa.

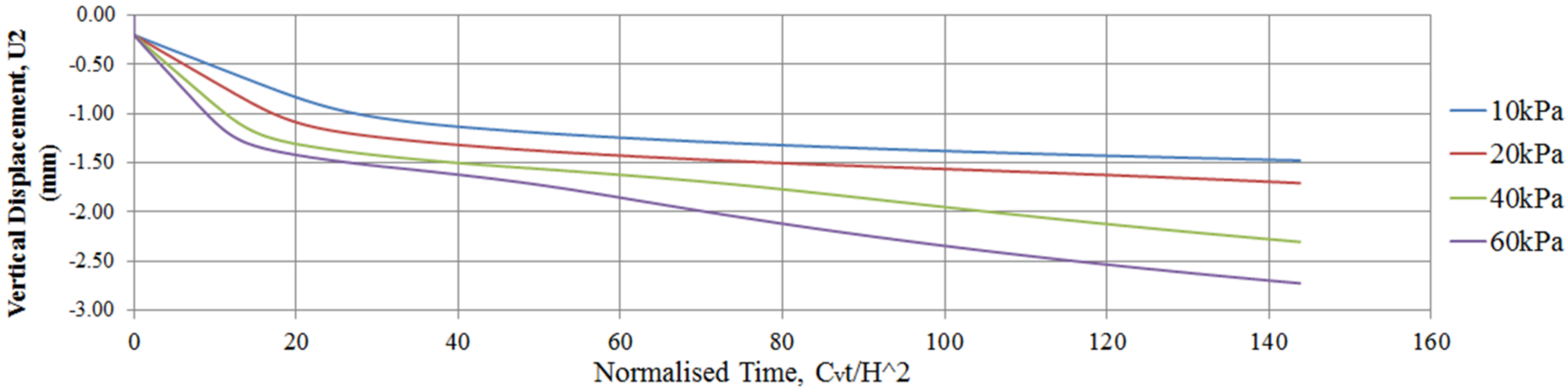

(a)

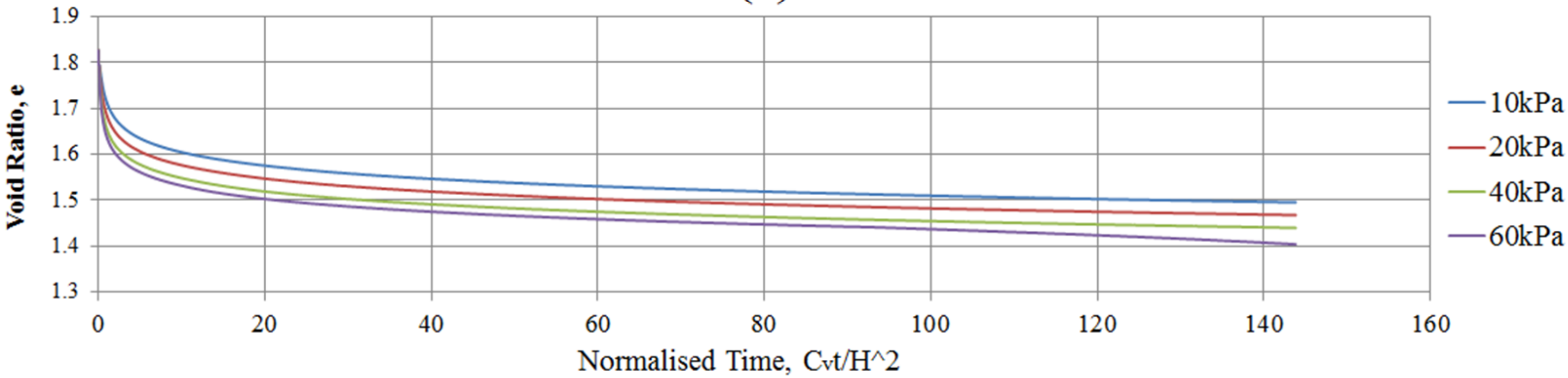

(b)

Figure 4.4 (a) Vertical displacement vs. normalised time and (b) void ratio vs. normalised time plots at consolidation stage

Excess pore pressure development

The excess pore pressure level is measured in the centre-bottom element, which is Element 20 of the model as shown in Figure 4.5 . Figure 4.6 (a) is the excess pore pressure Δu vs. normalised time plot and Figure 4.6(b) is the $\Delta u/\sigma_n$ vs. normalised time plot at consolidation stage, where σ_n is the vertical stress applied at the top surface of the soil.

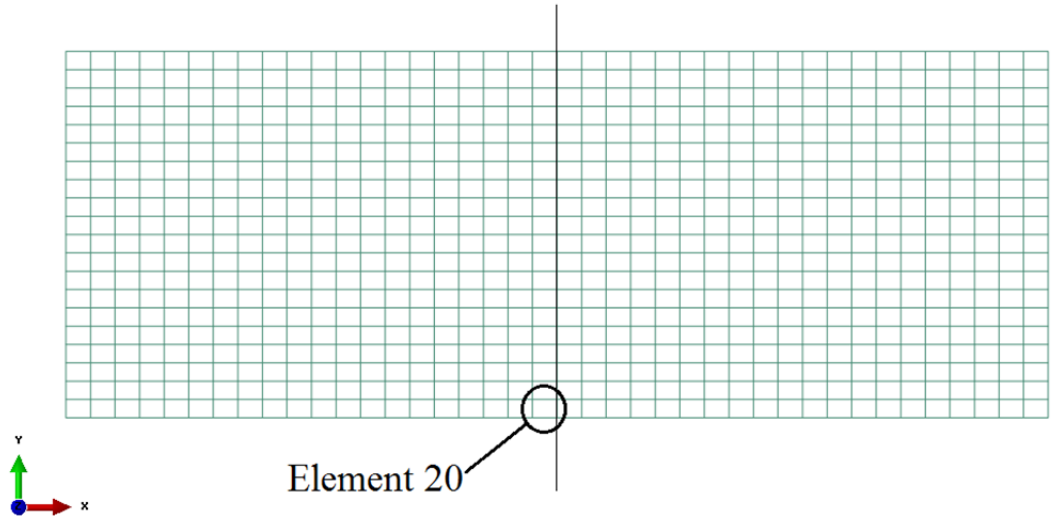

Figure 4.5 Excess pore pressure reference element

Figure 4.6 demonstrates that the excess pore pressure responses at the consolidation stage can be simulated appropriately and recorded simultaneously in the finite element analysis. As predicted, the applied vertical stress is first taken entirely by the excess pore pressure such that $\Delta u/\sigma_n = 1$. The soil skeleton gradually takes the vertical pressure and the excess pore pressure dissipates until dissipation is completed such that $\Delta u/\sigma_n = 0$.

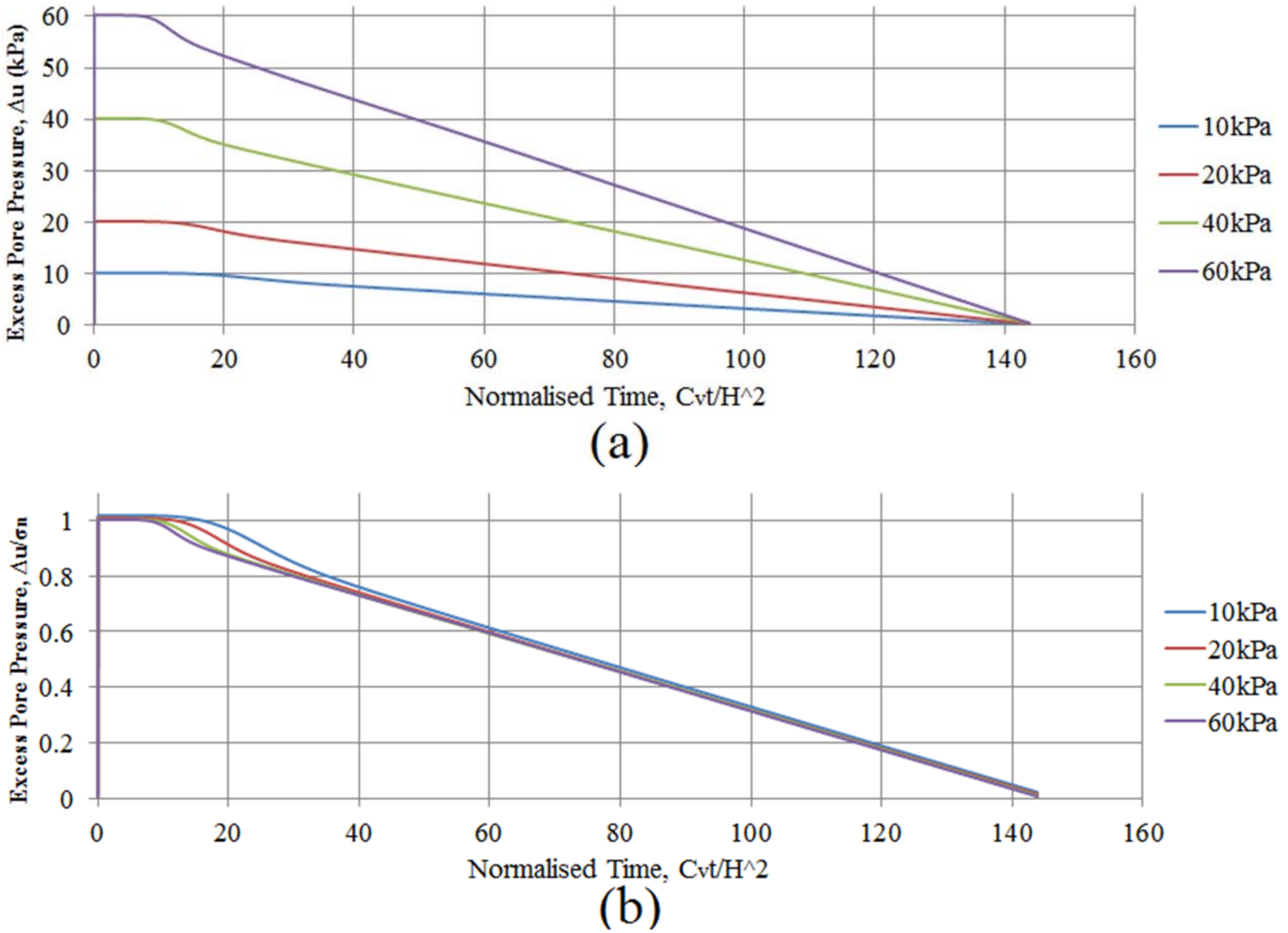

Figure 4.6 (a) Excess pore pressure Δu vs. normalised time and (b) $\Delta u/\sigma_n$ vs. normalised time plots at consolidation stage

4.2.3 Cyclic shearing stage

As in the experimental program, the horizontal displacement follows a sinusoidal function at the cyclic shearing stage as demonstrated in Figure 4.7(a) . The shear strain γ is defined as

$$\gamma = \frac{\delta}{H_{ps}} \times 100\% \tag{4.1}$$

where δ is the horizontal displacement of the top nodes in the FEA model, and H_{ps} is the height of the soil model before shearing starts, as shown in Figure 4.7(b).

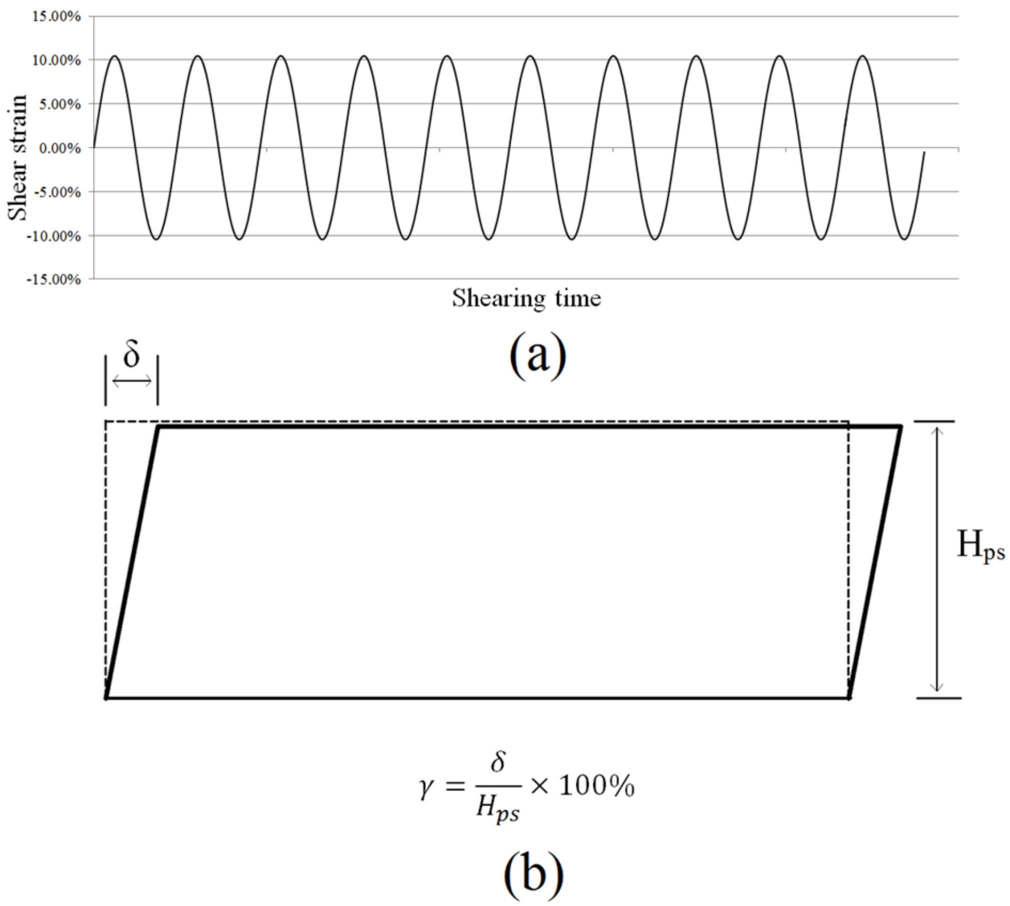

Figure 4.7 (a) horizontal displacement function and (b) shear strain definition

Pore pressure development

The pore pressure development in the soil at cyclic shearing stage was analysed and an example contour of pore pressure distribution within the soil model is shown in Figure 4.8 . In this example presented, the applied vertical stress is 60kPa, the shearing velocity is 0.3mm/s and the shearing amplitude is 5% of H.

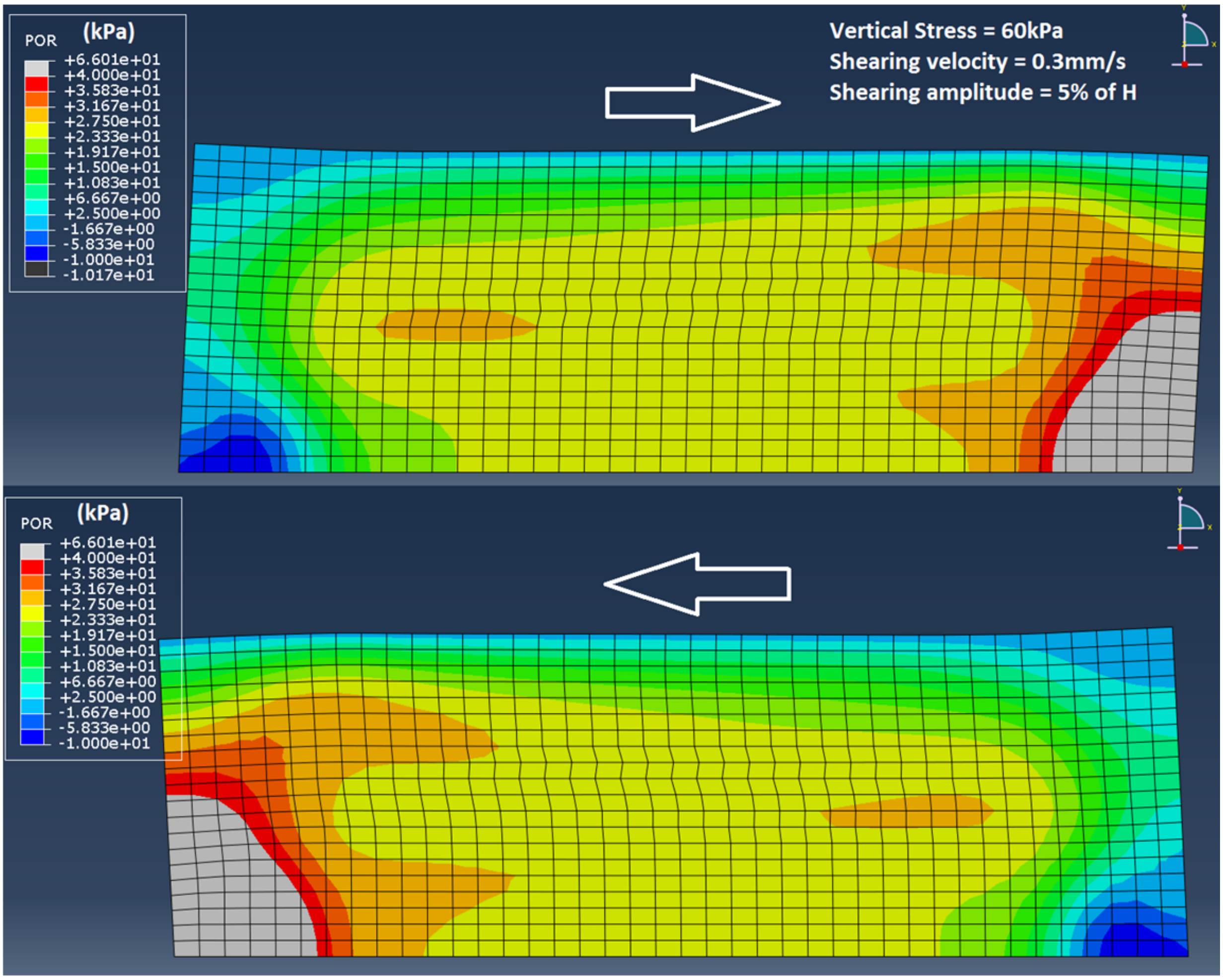

Figure 4.8 Pore pressure distribution at cyclic shearing stage

Figure 4.8 shows that the shear-induced pore pressure can be simulated in the current finite element model and the pore pressure in the soil is not uniformly distributed. Local maxima and minima are observed close to the boundaries of the soil, including the vertical sides and the corners. It is also observed that pore pressure distribution within the core of the model (middle 1/3) is relatively uniform and the excess pore pressure level is again measured in the centre-bottom element, which is Element 20 of the model, as shown in Figure 4.5 .

The pore pressure versus time plots are presented in Figures 4.9 and 4.10 for applied vertical stresses of 10kPa and 60kPa respectively. The shear strain versus time curves are also plotted on the same figures. The pore pressure versus time plots for applied vertical stresses of 20kPa and 40kPa are included in Appendix B.

As elaborated in Chapter 3, the pore pressure transducer readings in the experimental program can only provide an estimation of the pore pressure level in the soil specimen, whereas the exact pore pressure within the soil can be obtained using finite element analysis. Nevertheless, the pore pressure development in the finite element analyses is consistent with the pore pressure development in the experimental results.

At high shearing velocities (1mm/s & 0.3mm/s), excess pore pressure continuously builds up as cyclic shearing progresses, and induces a higher level of excess pore pressure. Therefore it is undrained shearing.

At moderate shearing velocities (0.03mm/s & 0.005mm/s), excess pore pressure is generated and peaks after reaching a moderate level. As cyclic shearing continues, excess pore pressure dissipates eventually. Therefore it is partially drained shearing.

At very low shearing velocities (0.0005mm/s & 0.0001mm/s), excess pore pressure does not build up and therefore it is drained shearing.

For an applied vertical stress σ_n of 10kPa, the maximum excess pore pressure Δu generated is close to 2kPa, which gives $\Delta u/\sigma_n$ close to 0.2. However, for applied vertical stresses σ_n of 20kPa, 40kPa and 60kPa, the maximum excess pore pressure Δu generated is close to $\Delta u/\sigma_n = 0.5$.

In Figures 4.9 and 4.10 , when comparing the excess pore pressure development of analyses that have the same vertical stress and shearing velocities but vary in amplitude (5%, 10%), it is clear that shear amplitude has little or no effect on the generation of excess pore pressure during cyclic shearing. This finding is consistent with the suggestion made by White et al. (2011b), who argue that the mobilisation of axial resistance in offshore pipelines is a time-related process rather than being linked to the distance of shearing.

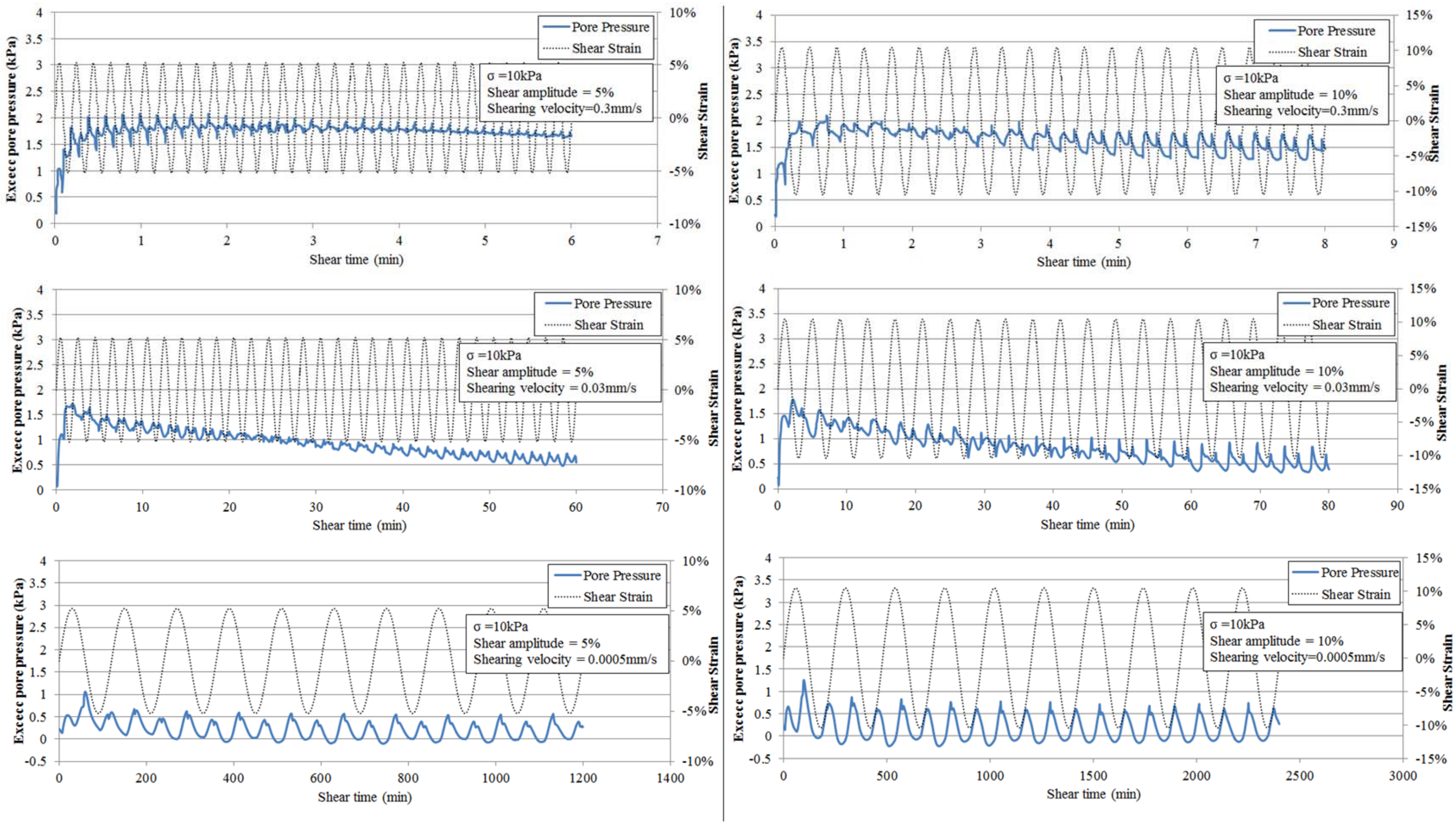

Figure 4.9 Excess pore pressure development at cyclic shearing stage for applied vertical stress of 10kPa

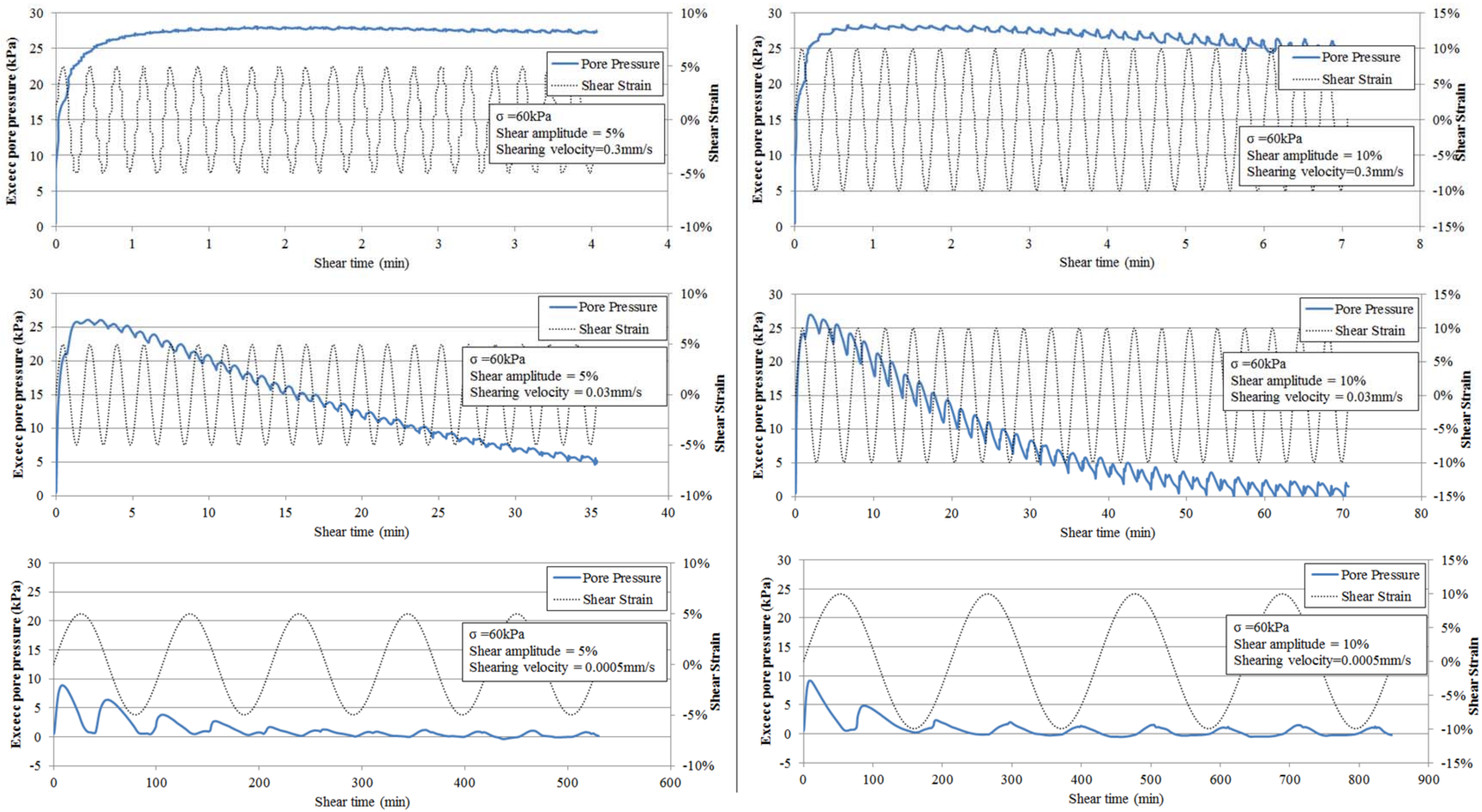

Figure 4.10 Excess pore pressure development at cyclic shearing stage for applied vertical stress of 60kPa

Continuous consolidation

Since the pore water is free to drain from the top surface of the soil model, continuous consolidation takes place at the cyclic shearing stage in the finite element analyses. This is consistent with what was observed in the experimental results. The void ratios versus shear strain plots at the cyclic shearing stage are presented in Figures 4.11 and 4.12 for applied vertical stresses of 10kPa and 60kPa respectively. The void ratios versus shear strain plots at the cyclic shearing stage for applied vertical stresses of 20kPa and 40kPa are included in Appendix B. The void ratio is measured from Element 20 of the model as shown in Figure 4.5 and the analysis results with a shear amplitude of 10% of H are presented.

At high shearing velocities (1mm/s & 0.3mm/s), the decrease in void ratio is minimal because excess pore pressure continuously builds up and it is undrained shearing. At moderate shearing velocities (0.03mm/s & 0.005mm/s), the void ratio drops continuously as excess pore pressure dissipates and the soil skeleton compresses further. As cyclic shearing progresses, the void ratio converges as the dissipation of excess pore pressure is completed and there is no further compression. At very slow shearing velocity (0.0005mm/s & 0.0001mm/s), most of the compression of the soil skeleton and the decrease in void ratio occur in the first two cycles, and there is no further change in void ratio in subsequent cycles.

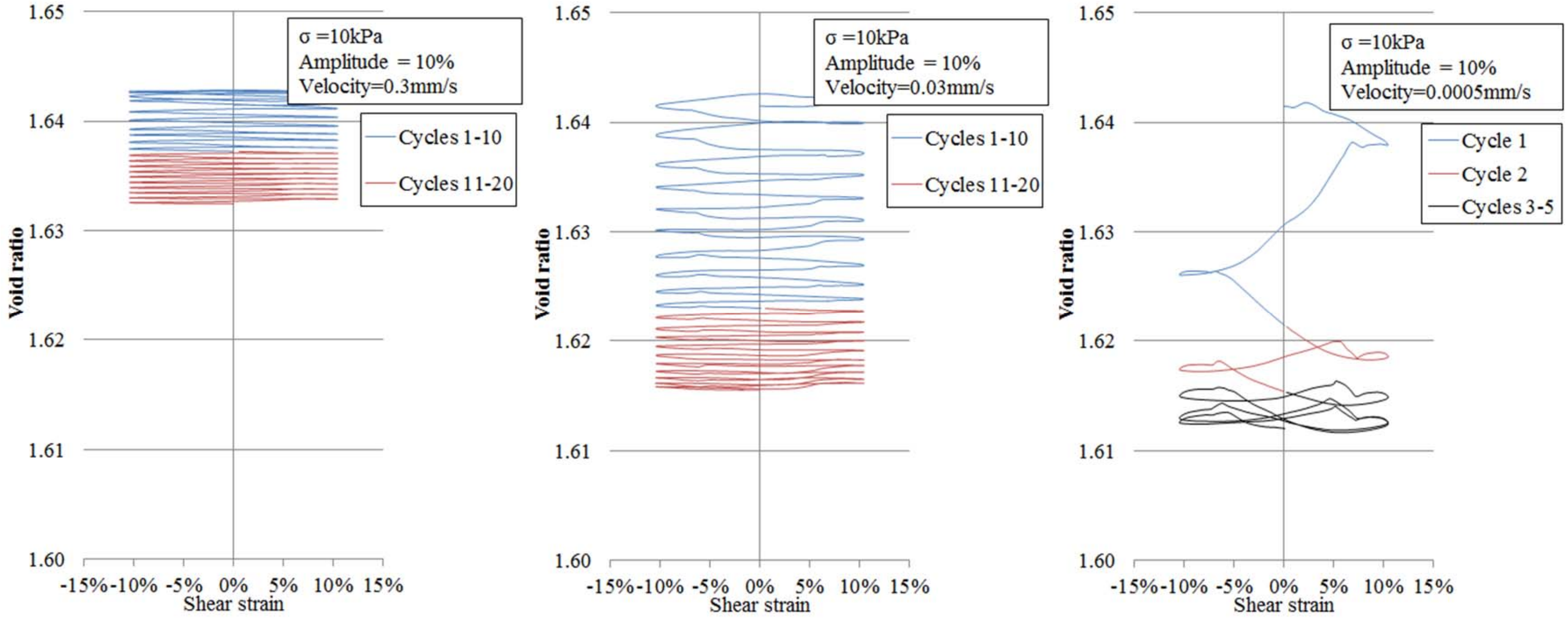

Figure 4.11 Void ratio versus shear strain plots for applied vertical stress of 10kPa and shear amplitude of 10% of H

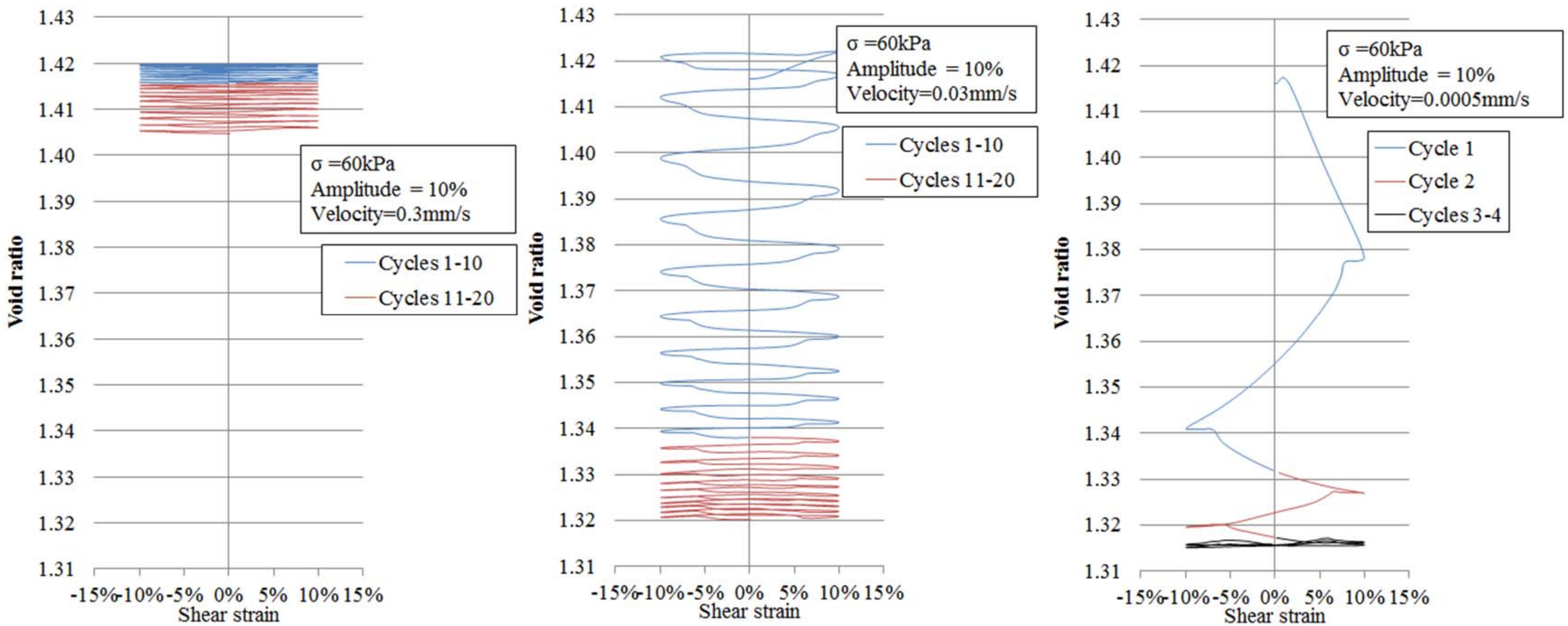

Figure 4.12 Void ratio versus shear strain plots for applied vertical stress of 60kPa and shear amplitude of 10% of H

Shear stress-strain relationship

The shear stress-strain curves at the cyclic shearing stage are plotted on Figures 4.13 and 4.14 for applied vertical stresses of 10kPa and 60kPa respectively. The shear stress-strain curves at the cyclic shearing stage curves for applied vertical stresses of 20kPa and 40kPa are provided in Appendix B. The level of shear stress is normalised as τ/σ_n, where τ is the shear stress and σ_n is the applied vertical stress at the top surface.

At high shearing velocities (1mm/s & 0.3mm/s), the shearing is undrained and τ/σ_n remains unchanged as cyclic shearing progresses. For a very low applied vertical stress of 10kPa, the undrained shear resistance equals τ/σ_n=0.4, while for applied vertical stresses of 20kPa, 40kPa and 60kPa, the undrained shear resistance gives τ/σ_n=0.25. This difference can be explained by the level of excess pore pressure generated under a vertical stress of 10kPa. For an applied vertical stress σ_n of 10kPa, the maximum excess pore pressure Δu generated is close to 2kPa, which gives $\Delta u/\sigma_n$ close to 0.2. However, for applied vertical stresses σ_n of 20kPa, 40kPa and 60kPa, the maximum excess pore pressure Δu generated is close to $\Delta u/\sigma_n$ = 0.5.

At moderate shearing velocities of 0.03mm/s and 0.005mm/s, the shearing is partially drained and τ/σ_n increases as cyclic shearing progresses. This is because excess pore pressure dissipates and effective stress increases, resulting in higher shear resistance. The initial shear resistance is close to the undrained shear resistance (τ/σ_n=0.4 for σ_n=10kPa and τ/σ_n=0.25 for σ_n=20,40,60kPa). As cyclic shearing continues, the shear resistance eventually reaches a peak level close to τ/σ_n=0.45. Shearing amplitude has no effect on the peak resistance level.

At low shearing velocities of 0.0005mm/s and 0.0001mm/s, the shearing is drained and fully drained shear resistance is reached within 4 cycles for 5% shear amplitude and 2 cycles for 10% shear amplitude. The fully drained shear resistance is at a level close to τ/σ_n=0.48.

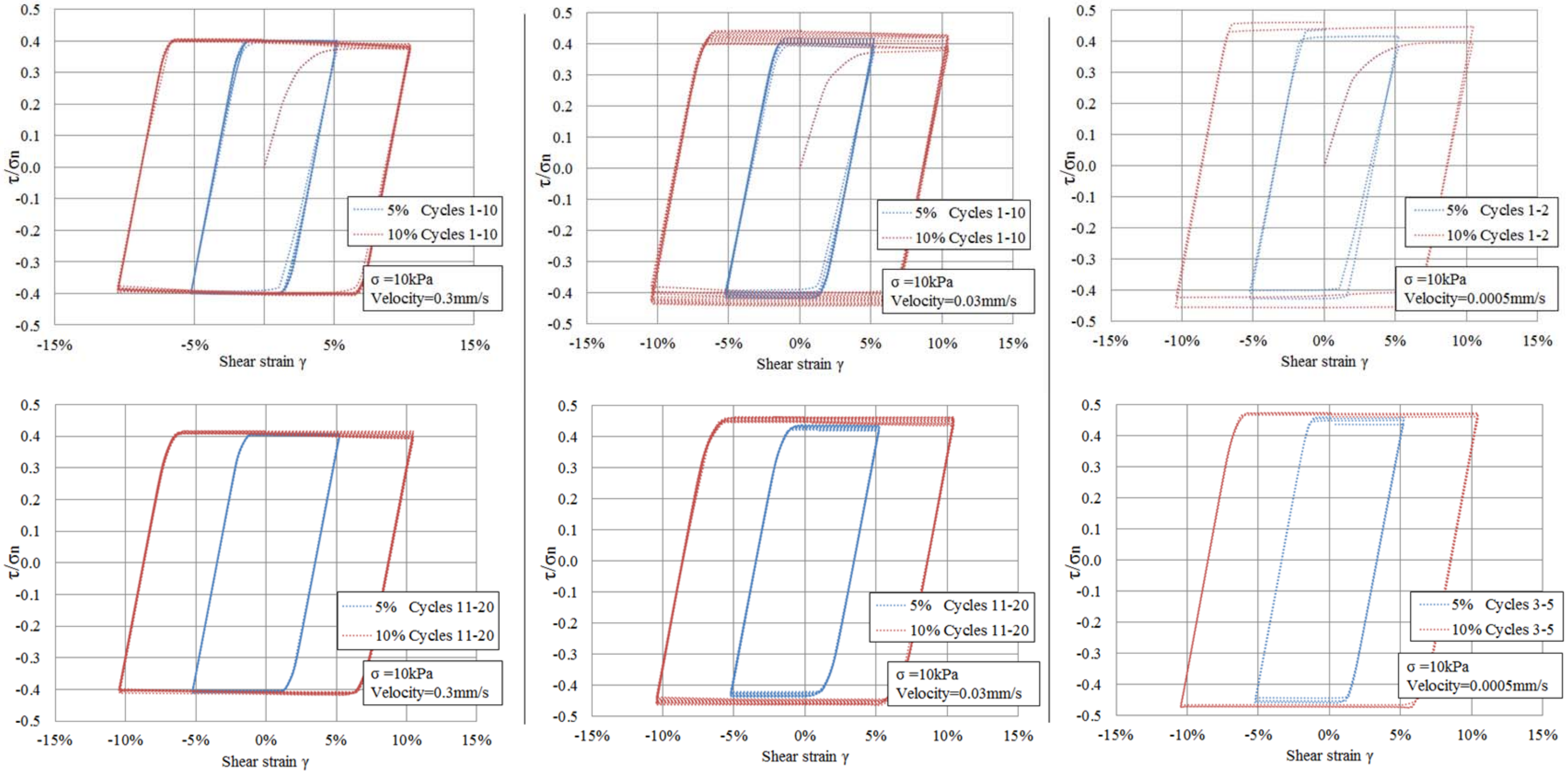

Figure 4.13 Shear stress-strain curves for applied vertical stress of 10kPa

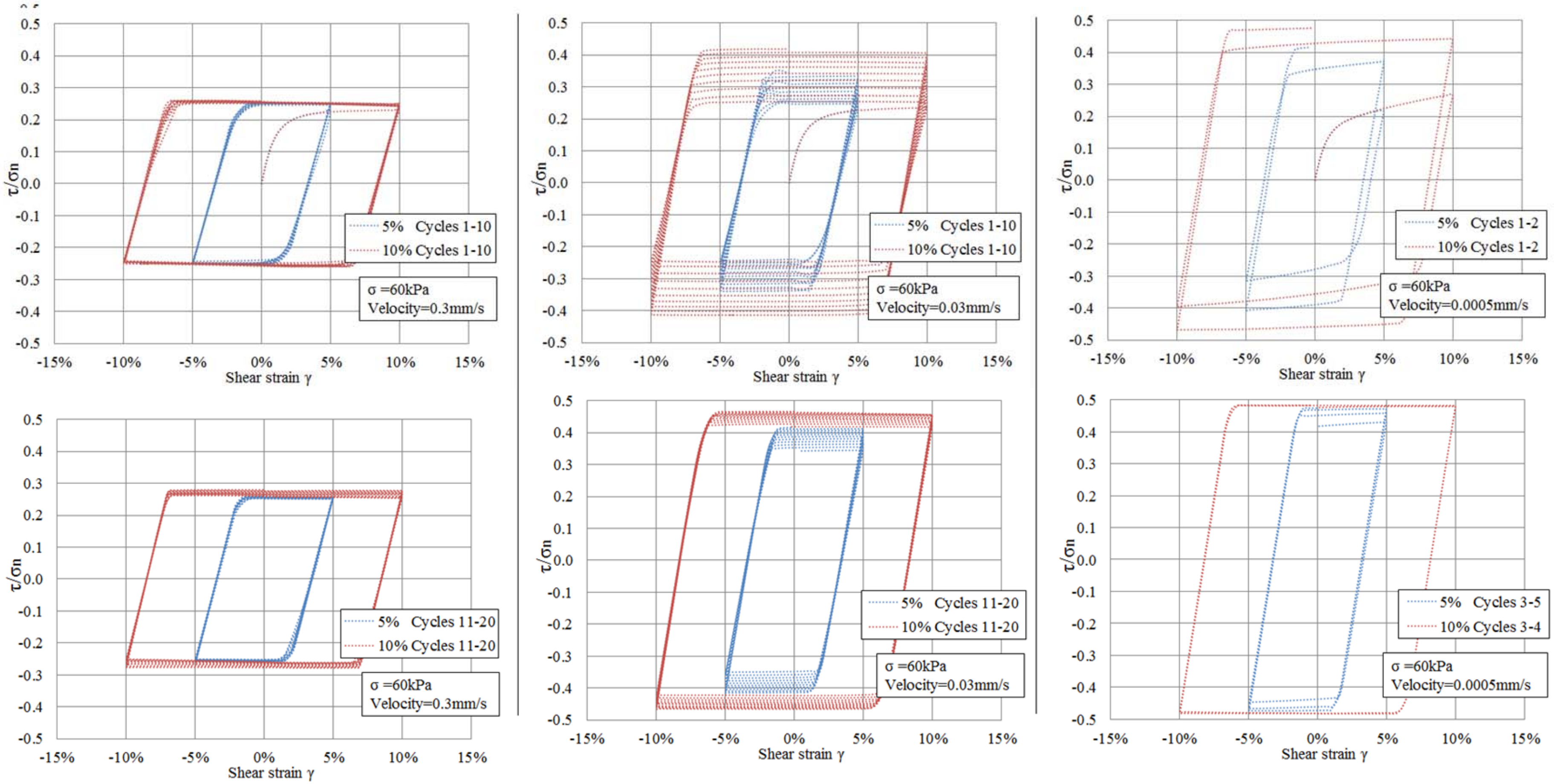

Figure 4.14 Shear stress-strain curves for applied vertical stress of 60kPa

Effective stress interpretation

Finite element analysis is capable of providing effective stress levels at the cyclic shearing stage and the shear stress-strain relationship can therefore be interpreted in terms of effective stress. Figure 4.15 presents the effective stress interpretation of the shear stress-strain relationship of applied vertical stresses of 10kP and 60kPa with shear amplitude of 10%. τ/σ_n' is plotted against γ, where τ is the shear stress, σ_n' is the effective vertical stress and γ is the shear strain.

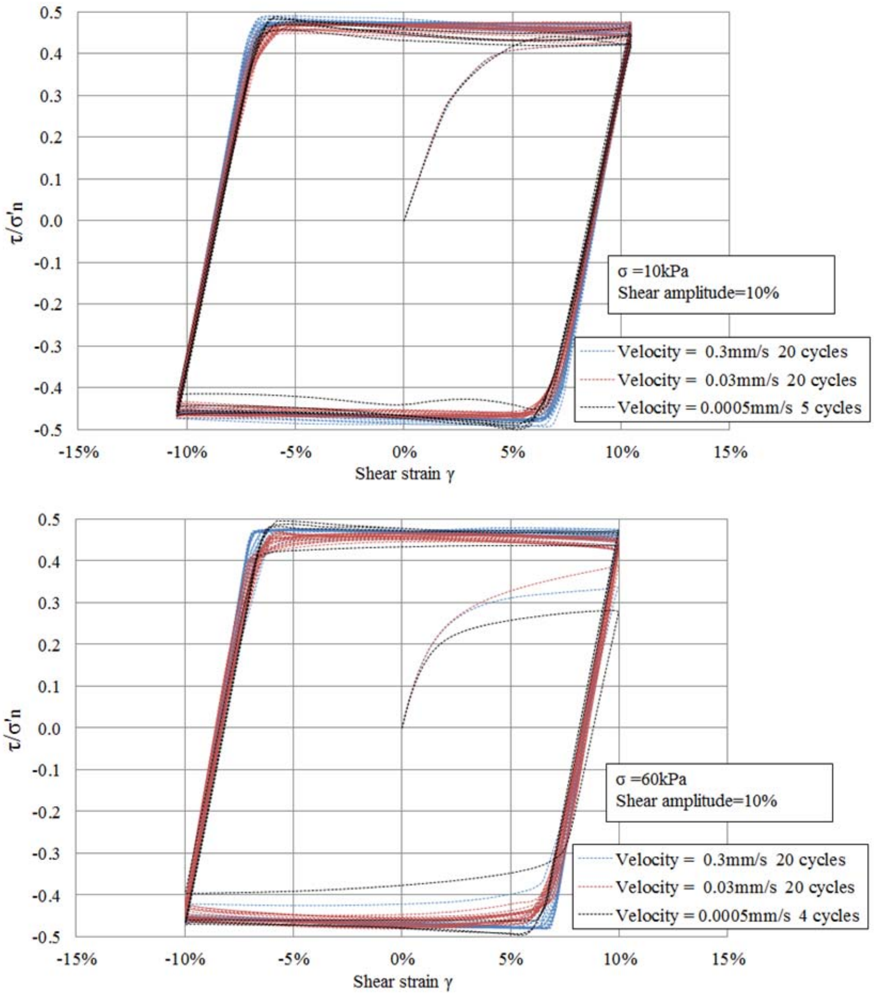

Figure 4.15 Effective stress interpretation of shear stress-strain relationship

In the effective stress interpretation, all shear stress-strain curves overlie each other, except for the initial responses. This is true for both cycles at a particular shearing velocity, and cycles at different shearing velocities. This verifies that the axial shear resistance in the shear zone is dominated by the excess pore pressure levels. The effective stress interpretation also suggests that, despite the fact that the experimental set-up cannot produce satisfactory output at a low vertical stress (i.e.10kPa), the application of a higher vertical stress (i.e. 60kPa) can still capture the appropriate soil behaviour in cyclic shearing.

4.3 Summary of major findings

Finite element analyses were conducted to capture the behaviour of soil within the shear zone, using the modified Cam-clay model. A two-dimensional finite element model has been developed and analyses were performed applying varying vertical stresses, shearing velocities and shearing amplitudes. The soil behaviour in the shear zone, in particular the shear-induced pore pressure, can be simulated using the current finite element model.

For an applied vertical stress σ_n of 10kPa, the maximum excess pore pressure Δu generated is close to 2kPa, which gives $\Delta u/\sigma_n$ close to 0.2. However, for applied vertical stresses σ_n of 20kPa, 40kPa and 60kPa, the maximum excess pore pressure Δu generated is close to $\Delta u/\sigma_n = 0.5$. When comparing the excess pore pressure development of analyses that have the same vertical stress and shearing velocities but vary in amplitude (5%, 10%), it was found that shear amplitude has little or no effect on the generation of excess pore pressure during cyclic shearing. This finding is consistent with the suggestion made by White et al. (2011b), who argue that the mobilisation of axial resistance in offshore pipelines is a time-related process rather than being linked to the distance of shearing.

Since the pore water is free to drain from the top surface of the soil model, continuous consolidation takes place at the cyclic shearing stage in the finite element analyses, which is consistent with what was observed in the experimental results.

Figure 4.16 presents the residual shear resistance versus velocity plot of the finite element analyses completed. The level of shear resistance is presented as τ/σ_{total}, where τ is the shear/horizontal stress and σ_{total} is the total normal stress applied. The shearing velocity is normalised as $\upsilon H/c_v$, where

υ is the shearing velocity in m/sec;

H is the soil specimen height before shearing;

c_v is the average coefficient of consolidation, taken as 2.9×10 -7 m2/sec ;

The residual resistance levels versus velocity plots of the experimental program are also presented in Figure 4.16 .

The undrained shear resistance gives τ/σ_n=0.4 for a very low applied vertical stress of 10kPa, while for applied vertical stresses of 20kPa, 40kPa and 60kPa, the undrained shear resistance level is close to τ/σ_n=0.25. This is because under a very low vertical stress of 10kPa the maximum excess pore pressure Δu generated gives $\Delta u/\sigma_n$ close to 0.2, whereas for vertical stresses σ_n of 20kPa, 40kPa and 60kPa, the maximum excess pore pressure Δu generated is close to $\Delta u/\sigma_n$ = 0.5. In comparison, the experimental results indicate an undrained residual resistance of τ/σ_n=0.17. The level of fully drained shear resistance is consistent under different applied vertical stresses, being close to τ/σ_n=0.48. In comparison, the experimental results indicate a fully drained shear resistance of τ/σ_n=0.52. The difference in shear resistance levels between the finite element analysis and the experimental program may be attributed to the limitations of the experimental equipment and some disparities in the drainage conditions.

Figure 4.16 also identifies the drained and undrained limits of the residual resistance, and the distribution of residual resistance against normalised velocity is uniform.

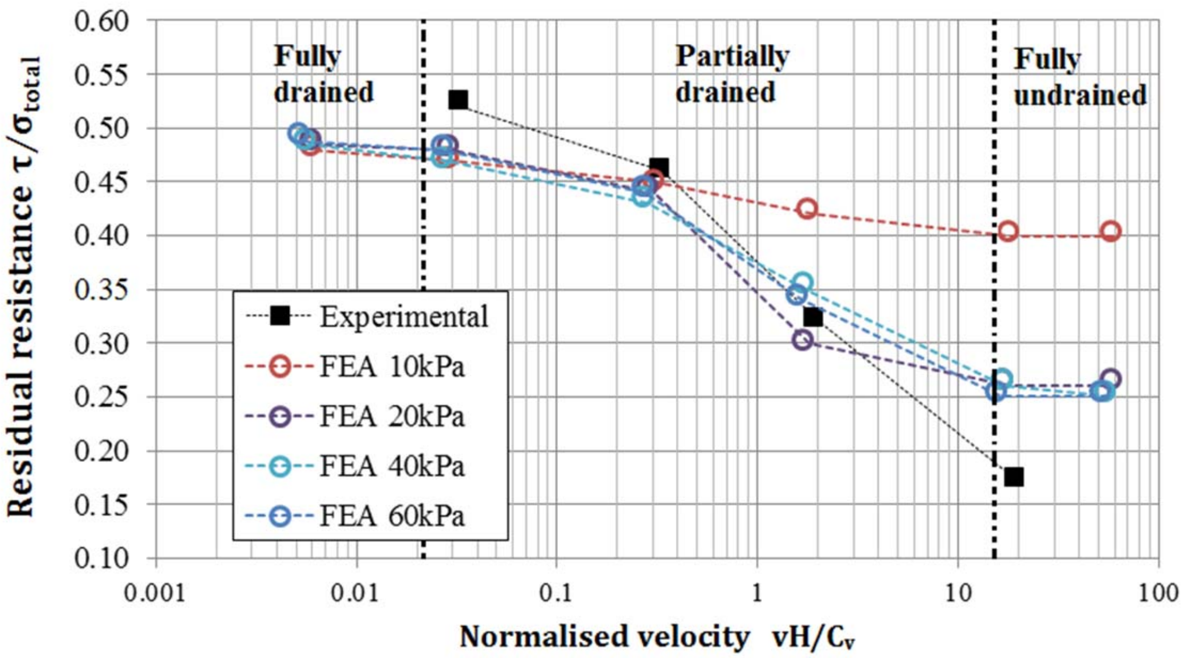

Figure 4.16 Residual resistance versus normalised velocity

In the effective stress interpretation, all shear stress –strain curves overlie each other, except for the initial responses. This is true for both cycles at a particular shearing velocity, and cycles at different shearing velocities. This verifies that the axial shear resistance in the shear zone is dominated by the excess pore pressure levels. The effective stress interpretation also suggests that, despite the fact that the experimental set-up cannot produce satisfactory output at a low vertical stress (i.e.10kPa), the application of a higher vertical stress (i.e. 60kPa) can still capture the appropriate soil behaviour in cyclic shearing.

Chapter 5 – Conclusions and recommendations

This thesis presents the results of research on the behaviour of soil within the shear zone in pipe axial walking problems. Both experimental and numerical modelling studies were undertaken. This chapter summarises the major findings of the present research, and provides recommendations for future research.

5.1 Conclusions

Offshore pipeline axial walking is the undesired accumulation of axial displacement of offshore pipelines during operation cycles. Research indicates that the axial resistance will tend towards the drained values during cycles of pipe movement, regardless of the rate or duration of each movement. A reliable prediction of this mechanism could bring significant design benefits, as drained resistance is usually higher than undrained resistance. Consequently, a higher range of axial resistance can be applied, leading to more cost-effective design. The pipe-soil interaction in pipe axial walking problems is extensively influenced by the soil response. The axial response is significantly influenced by the generation and dissipation of excess pore water pressure which leads to undrained and drained soil behaviour. It is likely that the response is between fully undrained and fully drained in typical field conditions. Analysis of the field data also suggests that the mobilisation of axial resistance is a time-related process instead of being linked to the distance of shearing. This suggestion is consistent with excess pore pressure development in cycles. In other words, the full pipe-soil resistance is only mobilised when steady pore pressures are reached. The residual resistance is the primary component of the load-displacement relationship in pipe axial walking, and it is dominated by the axial displacement rate.

The portion of the soil below the pipe which undergoes shearing, characterised as the *shear zone*, is significant for pipe axial walking assessment. Cyclic direct simple shear testing was selected as the preferred testing method to conduct the investigation owing to its various merits, including its loading pattern, allowing rotation of principle stress axes, the small specimen size required, and its shear failure planes. Furthermore, a finite element model has been developed which can capture the behaviour of soil within the shear zone, utilising an advanced constitutive soil model.

Both experimental and numerical analysis results suggest that at a high shearing velocity, excess pore pressure builds up continuously in the shear zone and the shearing is undrained. At a moderate shearing velocity, excess pore pressure builds up and dissipates, and effective stress drops and rises, eventually resulting in a drained shear resistance. At a low shearing velocity, no excess pore pressure builds up and the shearing is drained.

The relationship between residual shear resistance and shearing velocity has been established and the drained and undrained limits of the residual resistance have been identified in cyclic direct simple shear tests. Some shifting factors or transferring equations may be developed to relate the residual resistance as well as the undrained/drained limits in direct simple shear tests to those in pipe-soil interface interactions in the axial direction. If standard test methods such as the current direct simple shear test can be applied in the practical design, taking offshore pipeline axial walking into consideration, the process would be significantly simplified in terms of time and cost.

5. 2 Recommendations for future research

Some modifications to the standard direct simple shear devices are required if direct simple shear testing is to be widely used in practical design taking offshore pipeline axial walking into account. First and foremost, since the effective stresses in axial walking problems are very low, the device should be capable of providing reliable load readings under very low stress levels (2kPa to 10kPa). In addition, although the truly undrained condition is not required in such tests, it is desirable that the real-time pore water pressure level in the specimen can be accurately measured.

A more complicated three-dimensional finite element model can be developed based on the current two-dimensional model, if convergence issues can be resolved. The data obtained from both experimental work and numerical analysis can be applied in the calibration of large-scale pipe axial walking modelling, and provide guidance on the design of offshore pipelines considering on-bottom stability in axial direction.

References

AIREY, D. & WOOD, D. 1984. Discussion of "Specimen Size Effect in Simple Shear Test" by M. Vucetic and S. Lacasse (December, 1982). *Journal of Geotechnical Engineering,* 110**,** 439-442.

AIREY, D. W. 1984. *Clays in circular simple shear apparatus* Ph.D. thesis University of Cambridge,United Kingdom.

AIREY, D. W. & WOOD, D. M. 1987. Evaluation of direct simple shear tests on clay. *Geotechnique,* 37**,** 25-35.

AL-TABBAA, A. & WOOD, D. M. 1987. Some measurements of the permeability of kaolin. *Geotechnique,* 37**,** 499-503.

ASTM-D6528 2007. Standard Test Method for Consolidated Undrained Direct Simple Shear Testing of Cohesive Soils. *D 6528-07*

BARDET, J.-P. 1997. *Experimental Soil Mechanics* Prentice-Hall, Inc.

BJERRUM, L. 1954. *Theoretical and experimental investigation on the shear strength of soil,* Oslo, Norwegian Geotechnical Institute Publication 5.

BJERRUM, L. & LANDVA, A. 1966. Direct simple-shear tests on a Norwegian quick clay. *Geotechnique,* 16**,** 1-20.

BRUTON, D., CARR, M. & WHITE, D. J. 2007. The influence of pipe-soil interaction on lateral buckling and walking of pipelines - The SAFEBUCK JIP. *The 6th International Offshore Site Investigation and Geotechnics Conference: Confronting New Challegnes and Sharing Knowledge.* London, UK, 133-148.

BRUTON, D., CARR, M. & WHITE, D. J. 2008. Pipe-Soil Interaction during Lateral Buckling and Pipeline Walking — The SAFEBUCK JIP. *Offshore Technology Conference, 5-8 May 2008, Houston, Texas, USA.*

BUDHU, M. 1979. *Simple shear deformation of sands.* Ph.D. Thesis, University of Cambridge, United Kingdom.

BURLAND, J. B. & ROSCOE, K. H. 1969. Local Strains and Pore Pressures in a Normally Consolidated Clay Layer During One-Dimensional Consolidation. *Géotechnique* [Online], 19. Available: http://www.icevirtuallibrary.com/content/article/10.1680/geot.1969.19.3.335.

CARR, M., SINCLAIR, F. & BRUTON, D. 2006. Pipeline Walking - Understanding the Field Layout Challenges, and Analytical Solutions Developed for the SAFEBUCK JIP. *Proc Offshore Tech Conf.*

CASOLA, F., EL-CHAYEB, A., GRECO, S. & CARLUCCI, A. 2011. Characterization of pipe soil interaction and influence on HPHT pipeline design. 21st International Offshore and Polar Engineering Conference, Maui, Hawaii,USA. 111-121.

CHAKKARAPANI, V., NAIR, A., WHOOLEY, A., CHAUVET, C., ELTAHER, A. & JUKES, P. 2011. Vibration assessment methodology for subsea pipework. 30th International Conference on Ocean,Offhosre and Arctic Engineering, Rotterdam, The Netherlands. 737-743.

DASSAULT 2013. Dassault Systèmes. Abaqus Online Documentatio.

DUNCAN, J. M. & CHANG, C. Y. 1970. Nonlinear analysis of stress and strain in soils *ASCE J. Soil Mech. Found,,* Div. 96 No.SM5**,** 1629-1653.

DYVIK, R., BERRE, T., LACASSE, S. & RAADIM, B. 1987. Comparison of truly undrained and constant volume direct simple shear tests. *Geotechnique,* 37**,** 3-10.

FUJIWARA, T., UTO, S. & KANADA, S. 1997. An experimental study of the effects that change the vibration mode of riser VIV. ASME Conference Proceedings. 487-492.

GROGNET, M. 2011. The boundary conditions in direct simple shear tests- *Developments for peat testing at low normal stress.* Master of Science Thesis, Delft University of Technology, The Netherlands.

HELWANY, S. 2007. *Applied Soil Mechanics with Abaqus Applications* John Wiley & Sons, Inc. New Jersey, United States.

KJELLMAN, W. 1951. Testing The Shear Strength of Clay in Sweden. *Géotechnique,* 2**,** 225-232.

LUCKS, A. S., CHRISTIAN, J. T., BRANDOW, G. E. & HOEG, K. 1972. Stress Conditions in NGI simple shear test *Journal of Soil Mechanics, ASCE,* 98,SM1**,** 155-160.

MERIFIELD, R., WHITE, D. J. & RANDOLPH, M. F. 2008. The ultimate undrained resistance of partially embedded pipelines. *Geotechnique,* 58**,** 461-470.

MYRHAUG, D. & ONG, M. C. 2011. Long-and short-crested random wave-induced scour below pipelines. *Proceedings of the Institution of Civil Engineers: Maritime Engineering,* 164**,** 173-184.

OLIPHANT, J. & MACONOCHIE, A. 2006. Axial pipeline-soil interaction. San Francisco, CA, United States: International Society of Offshore and Polar Engineers.

RANDOLPH, M. F. 2011. *Offshore geotechnical engineering* Abingdon, Oxon ; New York :, Spon Press.

RANDOLPH, M. F. Offshore geotechnics - The challenges of deepwater soft sediments. Geotechnical Special Publication, 2012. 241-271.

RANDOLPH, M. F. & HOUSE, A. R. 2001. The complementary roles of physical and computational modelling. *Int. J. of Physical Modelling in Geotechnics,* 1**,** 1-8.

RANDOLPH, M. F., WHITE, D. J. & YAN, Y. 2012. Modelling the axial soil resistance on deep-water pipelines. *Geotechnique,* 62**,** 837-846.

ROSCOE, K. H. An apparatus for the application of simple shear to soil samples Proceedings Third ICSMFE 1953. 186-191.

ROSCOE, K. H., SCHOFIELD, A. N. & WROTH, C. P. 1958. On The Yielding of Soils. *Géotechnique* [Online], 8.

SAADA, A. S. & TOWNSEND, F. C. 1981. STATE OF THE ART - LABORATORY STRENGTH TESTING OF SOILS. *ASTM Special Technical Publication***,** 7-77.

SCHOFIELD, A. N. & WROTH, C. P. 1968. *Critical State Soil Mechanics*, McGraw-Hill, New York.

SENTHILKUMAR, M. 2013. *Offshore pipe-clay seabed interaction in axial direction.* Ph.D. thesis. Monash University, Australia

SHANNON, B. 2013. *Fracture Propagation of Cohesive Soils Under Tensile Loading and Desiccation* Ph.D. thesis. Monash University, Australia.

SHEN, C. K., SADIGH, K. & HERRMANN, L. R. 1978. Analysis of the NGI simple shear apparatus for cyclic soil testing. *ASTM Special Technical Publication***,** 148-162.

STEENFELT, J. S. Sliding resistance for foundations on clay till. Proc. Wroth Memorial Conference, Predictive Soil Mechanics, 1993 Thomas Telford. 664–684.

SYMES, M. J. P. R., GENS, A. & HIGHT, D. W. 1984. Undrained anisotropy and principal stress rotation in saturated sand. *Geotechnique,* 34**,** 11-27.

TERZAGHI, K., PECK, R. B. & MERSI, G. 1996. *Soil Mechanics in Engineering Practice*, Wiley-Interscience

TORNES, K., OSE, B. A., JURY, J. & THOMSON, P. 2000. Axial creeping of high temperature flowlines caused by soil ratcheting. *Proceedings 19 Int. Conf. on Offshore Mechanics and Arctic Eng, OMAEth.*

VUCETIC, M. & LACASSE, S. 1982. Specimen size effect in simple shear test. *Journal of the Geotechnical Engineering Division, ASCE,* 108**,** 1567-1585.

WHITE, D. J. & CATHIE, D. N. Geotechnics for subsea pipelines. 2nd International Symposium on Frontiers in Offshore Geotechnics, ISFOG 2010, November 8, 2010 - November 10, 2010, 2011 Perth, WA, Australia. Taylor & Francis - Balkema, 87-123.

WHITE, D. J., GANESAN, S. A., BOLTON, M. D., BRUTON, D. A. S. & LANGFORD, D. 2011a. SAFEBUCK JIP - Observations of Axial Pipe-soil Interaction from Testing on

Soft Natural Clays. *Proceedings of the Offshore Technology Conference.* Houston, Texas, USA.

WHITE, D. J., HILL, A. J., WESTGATE, Z. J. & BALLARD, J. C. 2011b. Observations of pipe-soil response from the first deep water deployment of the SMARTPIPE®. *Frontiers in Offshore Geotechnics II.* 851-856.

WRIGHT, D. K., GILBERT, P. A. & SAADA, A. S. Shear devices for determing dynamic soil properties. Specialty Conference, Earthquake Engineering and Soil Dynamics 1978 Pasadena 1056-1075.

ZEKKOS, D., ATHANASOPOULOS, G. A., BRAY, J. D., GRIZI, A. & THEODORATOS, A. 2010. Large-scale direct shear testing of municipal solid waste. *Waste Management,* 30**,** 1544-1555.

ZHOU, H., WHITE, D. J. & RANDOLPH, M. F. 2008. Physical and numerical simulation of shallow penetration of a cylindrical object into soft clay. GeoCongress, New Orleans, United States. 108-117.

Appendices

Appendix A Critical state soil theory and modified Cam-clay model

Introduction

The specific model implemented in Abaqus Standard is an extension of the Modified Cam-clay model (Abaqus 6.13 Online Documentation). The model is based on the critical sate soil theory developed by researchers at Cambridge University (Roscoe et al., 1958, Burland and Roscoe, 1969, Schofield and Wroth, 1968). The model is capable of describing the stress-strain behaviour of soft soils. In particular, the model can predict the pressure-dependent soil strength and the compression and dilatancy (volume change) caused by shearing. Because the model is based on critical state theory, it predicts unlimited soil deformations without changes in stress or volume when the critical state is reached.

The Cam-clay model assumes that the soil is fully saturated. When the soil is loaded, significant irreversible (plastic) volume changes occur, due to the water that is expelled from the voids. In critical state soil theory, the state of a soil specimen is characterised by three parameters: mean effective stress p', deviator stress (shear stress) q, and void ratio e. The mean effective stress can be defined in terms of the principal effective stresses σ_1', σ_2', σ_3' as

$$p' = \frac{1}{3}(\sigma_1' + \sigma_2' + \sigma_3') \tag{A.1}$$

and the shear stress is defined as

$$q = \frac{1}{\sqrt{2}}\sqrt{(\sigma_1' - \sigma_2')^2 + (\sigma_2' - \sigma_3')^2 + (\sigma_1' - \sigma_3')^2} \tag{A.2}$$

For the consolidation stage of a consolidated-drained triaxial compression test, $\sigma_1' = \sigma_2' = \sigma_3'$, where σ_3' is the confining pressure, thus

$$p' = \frac{1}{3}(\sigma_1' + \sigma_2' + \sigma_3') = \sigma_3' \tag{A.3}$$

and

$$q = 0 \tag{A.4}$$

For the shearing stage of a triaxial compression test $\sigma'_1 \neq \sigma'_2 = \sigma'_3$, therefore

$$p' = \frac{1}{3}(\sigma'_1 + \sigma'_2 + \sigma'_3) = \frac{1}{3}(\sigma'_1 + 2\sigma'_3) \tag{A.5}$$

And

$$q = \frac{1}{\sqrt{2}}\sqrt{2(\sigma'_1 - \sigma'_3)^2} = \sigma'_1 - \sigma'_3 \tag{A.6}$$

The effective stress path of a triaxial test represents the locus of the effective stress state in the p'- q plane. For a consolidated-drained triaxial test, the effective stress path is a straight line and the slope of the line is defined as $\Delta q/\Delta p'$.

Because σ'_3 is constant and from Equation A.6

$$\Delta q = \Delta\sigma'_1 - \Delta\sigma'_3 = \Delta\sigma'_1 - 0 = \Delta\sigma'_1$$

And from Equation A.5

$$\Delta p' = \frac{1}{3}(\Delta\sigma'_1 + \Delta 2\sigma'_3) = \frac{1}{3}(\Delta\sigma'_1 + 0) = \frac{\Delta\sigma'_1}{3}$$

Therefore

$$slope = \frac{\Delta\sigma'_1}{\Delta\sigma'_1 /3} = 3$$

Normal consolidation line and Unloading-reloading lines

A typical *e*-log *p'* curve of an isotropic consolidation test is shown in Figure A.1(a) . The maximum past pressure exerted on the clay specimen is defined as the pre-consolidation pressure p'_c , and a normally consolidated (NC) clay is defined as a clay that has a present vertical effective stress p'_0 equal to its pre-consolidation pressure p'_c . An over-consolidated (OC) clay is defined as a clay that has a present vertical effective stress less than its pre-consolidation pressure. The over-consolidation ratio is the ratio of the pre-consolidation pressure to the present vertical effective stress ($\mathrm{OCR} = \mathrm{p}'_c / \mathrm{p}'_0$).

The pre-consolidation pressure is located near the point where the *e*-log *p'* curve changes its slope. The compression index (C_c) and swelling index (C_s) can also be obtained from the *e*-

log *p'* curve. The compression index is the slope of the loading portion in the *e*-log *p'* plane, and the swelling index is the slope of the unloading portion.

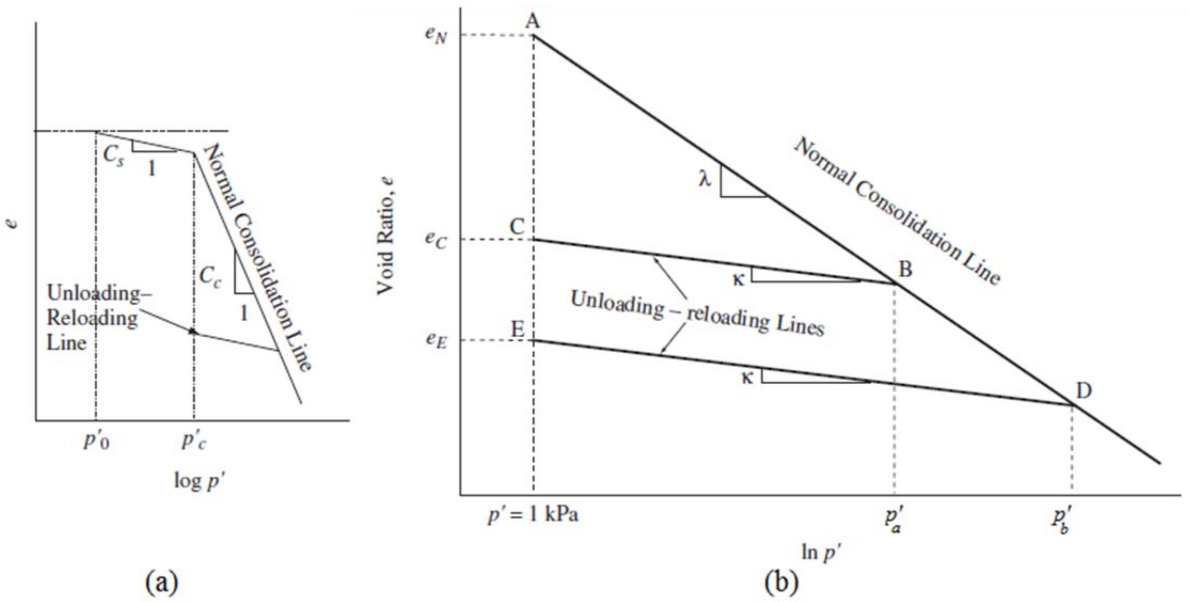

Figure A.1 (a) *e*-log *p'* curve of an isotropic consolidation test and (b) consolidation curve in the *e*-ln *p'* plane (Helwany, 2007)

In the derivation of the modified Cam-clay model, it is assumed that when a soil sample is consolidated under isotropic stress conditions ($p' = \sigma_1' = \sigma_2' = \sigma_3'$), the relationship between its void ratio (*e)* and ln *p'* is a straight line. This line is the normal consolidation line shown in Figure A.1(b) . In addition, there exists a set of straight unloading-reloading (swelling) lines that describe the unloading-reloading behaviour of the soft soil in the *e*-ln *p'* plane. The plane λ is the slope of the normal consolidation line and κ is the slope of the unloading-reloading line.

In the *e*-ln *p'* plane, the normal consolidation line is defined by the equation

$$e = e_N - \lambda \ln p' \tag{A.7}$$

and the equation for an unloading-reloading line has the form

$$e = e_c - \kappa \ln p' \tag{A.8}$$

The material parameters λ, κ, and e_N are unique for a particular soil, and e_N is the void ratio on the normal consolidation line at unit mean effective stress (point A in Figure A.1b).

Slopes λ and κ of the normal consolidation and unloading-reloading lines in the *e-ln p'* plane are related to the compression index (C_c) and swelling index (C_s):

$$\lambda = \frac{C_c}{\ln 10} = \frac{C_c}{2.3} \tag{A.9}$$

and

$$\kappa = \frac{C_s}{\ln 10} = \frac{C_s}{2.3} \tag{A.10}$$

Critical state line

Increasing the shear stress on a soil specimen, will eventually lead to a state in which further shearing can occur without changes in volume, as shown in Figure A.2, known as Critical state condition. The critical state line (CSL) (Figures A.3a and b) is a representation of the critical state condition. The critical state line in *e-p'-q* space is shown in Figure A.4 .

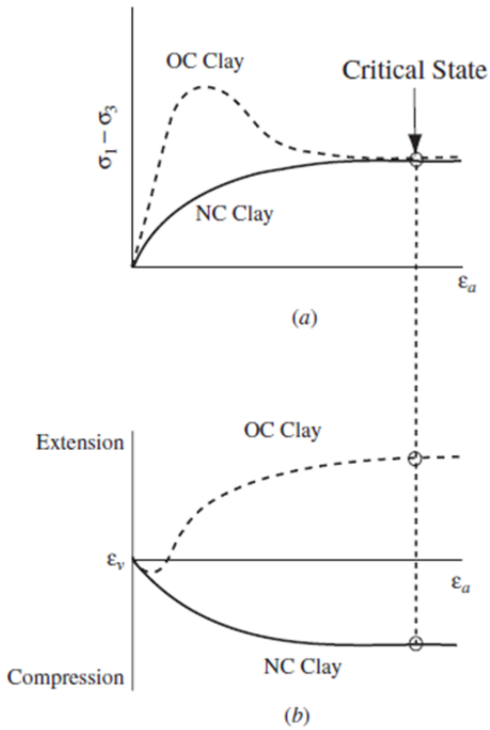

Figure A.2 Critical state definition (Helwany, 2007)

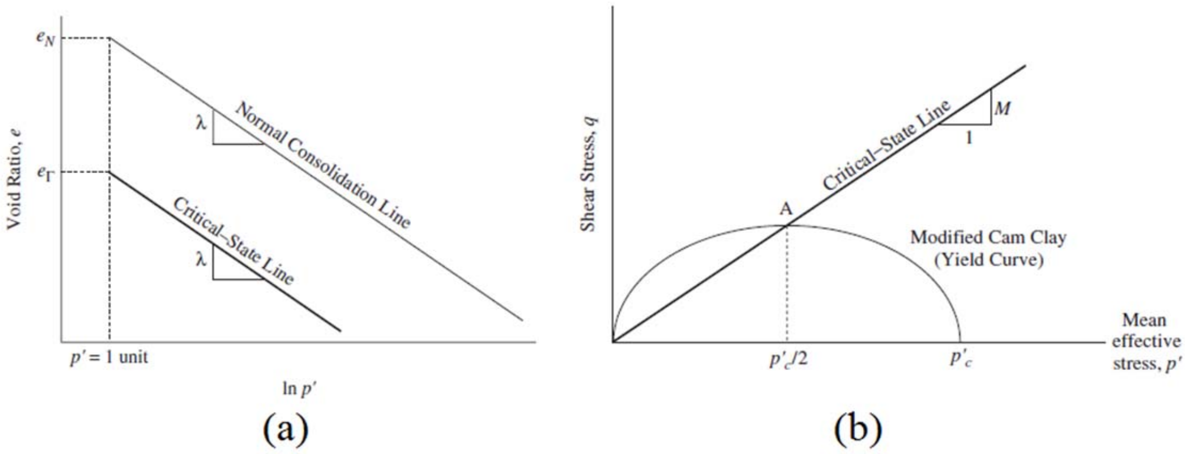

Figure A.3 (a) Normal consolidation and critical state lines in the *e*-ln *p'* plane (b) yield surface of a Cam-clay model in the *q*-*p'* plane (Helwany, 2007)

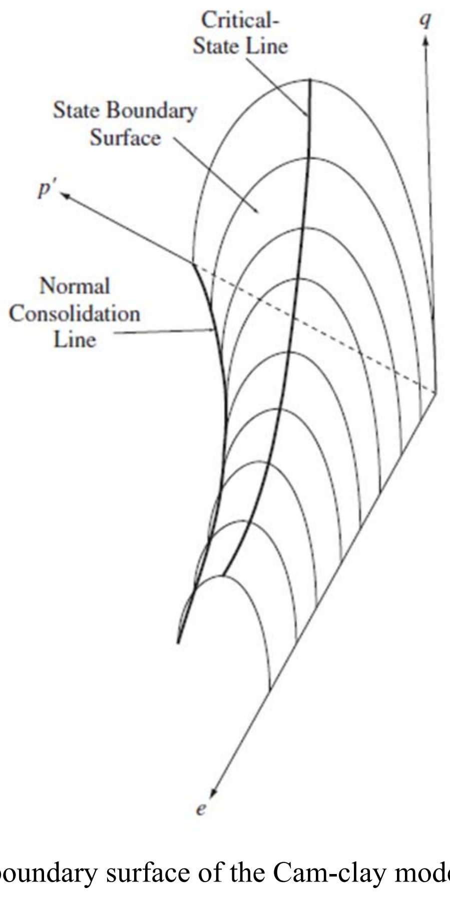

Figure A.4 State boundary surface of the Cam-clay model (Helwany, 2007)

Consolidated-drained (CD) or consolidated-undrained (CU) triaxial tests on representative soil specimens need to be conducted to obtain the critical state line. The critical state friction angle of the soil can be obtained from triaxial tests, by drawing the effective stress Mohr's circle that represents a critical state condition. A straight-line tangent to the effective-stress Mohr's circle is drawn, which represents the effective-stress Mohr-Coulomb failure criterion. The slope of this line is the critical state friction angle ϕ'. The slope of the critical state line in the *p'*- *q* plane, M (Figure A.3b), can be calculated as

$$M = \frac{6 \sin \phi'}{3 - \sin \phi'} \tag{A.11}$$

In reference to Figure A.3(b), the critical state line has the following equation in the *p'*- *q* plane:

$$q_f = M p'_f \tag{A.12}$$

where p'_f is the mean effective stress at failure and q_f is the shear stress at failure. This failure criterion bears the same meaning as the Mohr-Coulomb failure criterion

$$\tau_f = c' + \sigma' \tan \phi' \tag{A.13}$$

where τ_f is the shear stress at failure and σ' is the effective normal stress, and c' is the cohesion.

The critical state line is parallel to the normal consolidation line in the *e*-ln *p'* plane, as shown in Figure A.3(a) . The equation of the critical state line in this plane is given as

$$e_f = e_\Gamma - \lambda \ln p' \tag{A.14}$$

where e_f is the void ratio at failure and e_Γ is the void ratio of the critical state line at $p' = 1kPa$. The parameters e_N and e_Γ are related by the equation

$$e_\Gamma = e_N - (\lambda - \kappa) \ln 2 \tag{A.15}$$

Yield function

In the p'- q plane, the modified Cam-clay yield surface is an ellipse given by

$$\frac{q^2}{p'^2} + M^2 \left(1 - \frac{p'_c}{p'}\right) = 0 \tag{A.16}$$

Figure A.3(b) shows an elliptical yield surface corresponding to a pre-consolidation pressure p'_c. The parameter p'_c controls the size of the yield surface and is different for each unloading-reloading line. The parameter p'_c is used to define the hardening behaviour of the soil. The soil behaviour is elastic until the stress state of the soil specimen (p', q) hits the yield surface. The soil behaves in a plastic manner after reaching the yield surface. Figure A.4 presents the yield surface in *e-p'-q* space, termed the state boundary surface.

Elastic response

The elastic response of the Modified Cam-clay model is defined by Young's modules *E*, shear modulus *G*, Poisson's ratio υ, and bulk modulus *K*. These parameters are related by

$$E = 3K(1 - 2\upsilon) \tag{A.17}$$

and

$$G = \frac{3K(1-2\upsilon)}{2(1+\upsilon)} \tag{A.18}$$

The elastic behaviour of soil is nonlinear and stress-dependent. Therefore, the elastic moduli need be presented in incremental form.

For soils modelled by the Modified Cam-clay model, the bulk modulus *K* is stress-dependent. The bulk modulus depends on the mean effective stress p', void ratio e_0, and unloading-reloading line slope κ. The elastic behaviour is described by

$$K = \frac{(1+e_0)p'}{\kappa} \tag{A.19}$$

Substituting Equation 39 into Equation 37 and 38 yields

$$E = \frac{3(1-2\upsilon)(1+e_o)p'}{\kappa} \tag{A.20}$$

and

$$G = \frac{3(1-2\upsilon)(1+e_o)p'}{2(1+\upsilon)\kappa} \tag{A.21}$$

Young's modules E and shear modulus G are not constants. They are a function of the mean effective stress p', void ratio e_0 , unloading-reloading line slope κ and Poisson's ratio υ. For simplicity, Poisson's ratio υ is commonly assumed to be constant.

Appendix B Additional FEA results

Additional results of the finite element analyses are presented in this appendix, including the pore pressure development, consolidation and shear stress-strain curves.

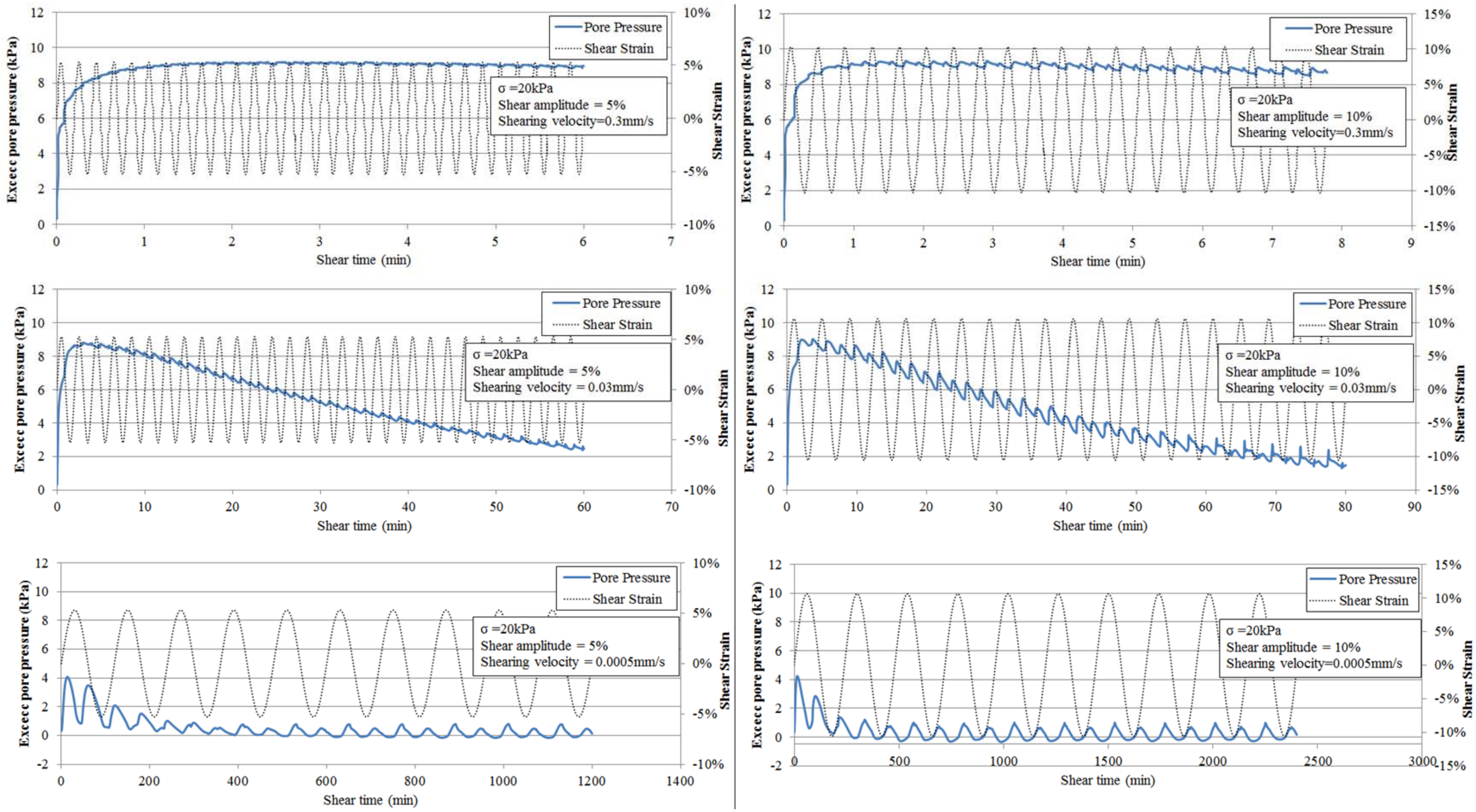

Figure A.5 Excess pore pressure development at cyclic shearing stage for applied vertical stress of 20kPa

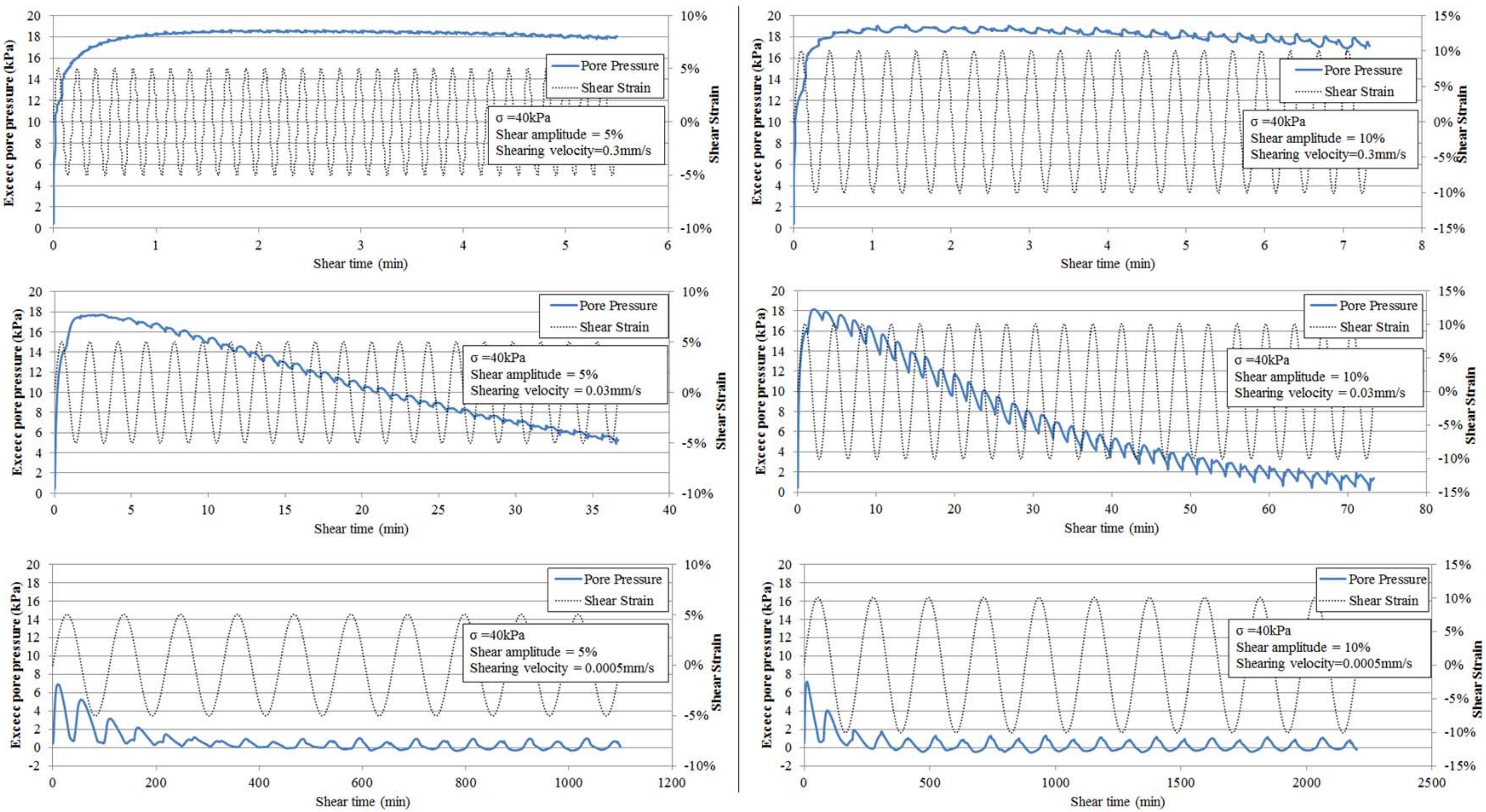

Figure A.6 Excess pore pressure development at cyclic shearing stage for applied vertical stress of 40kPa

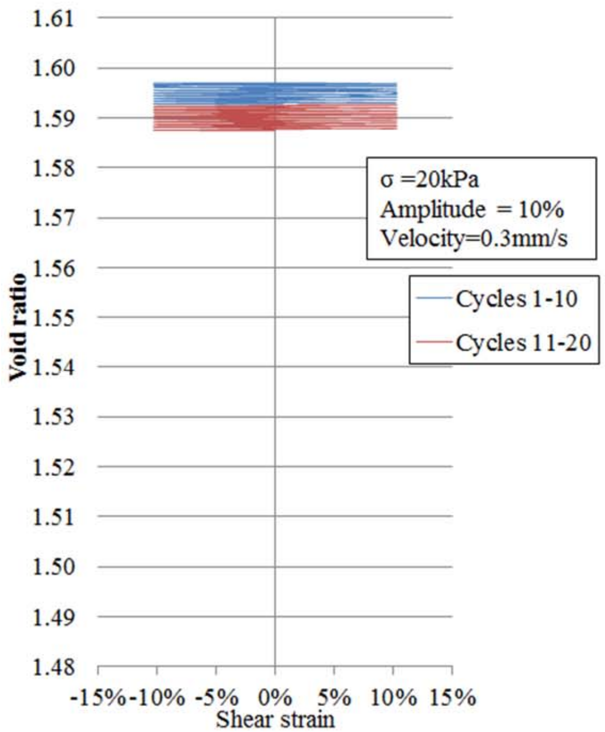

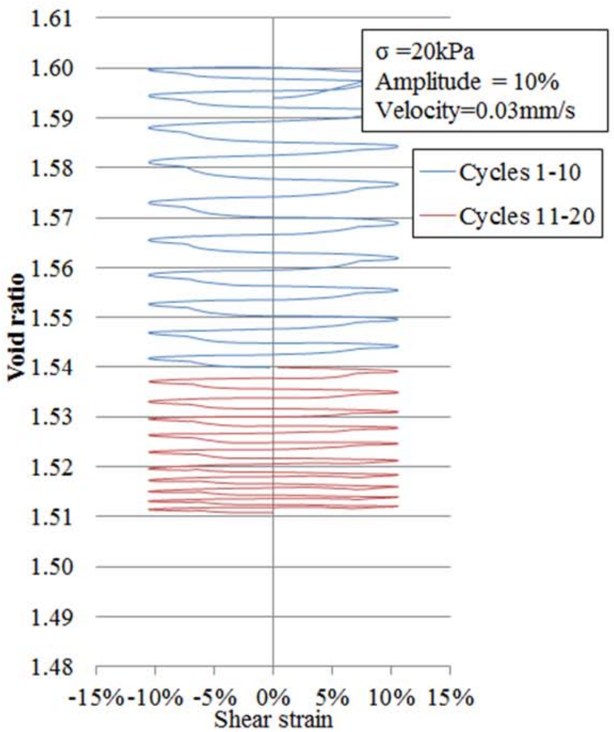

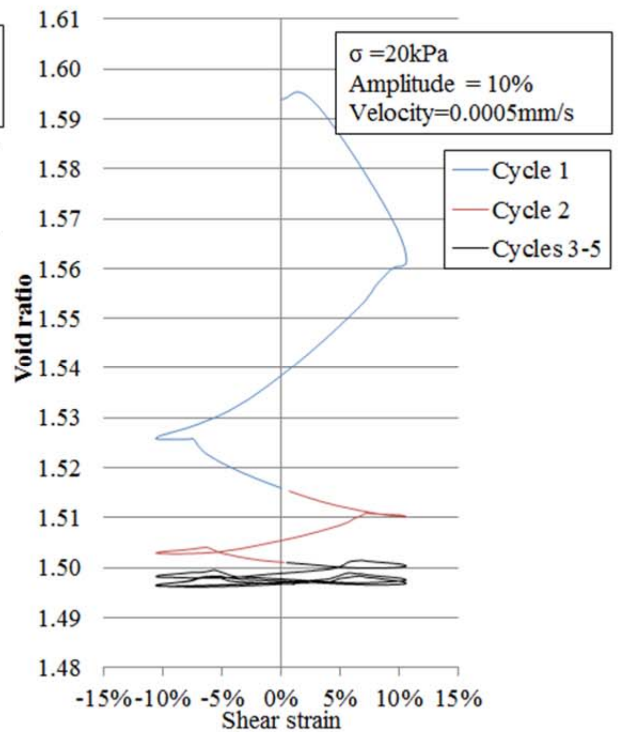

Figure A.7 Void ratio versus shear strain plots for applied vertical stress of 20kPa and shear amplitude of 10% of H

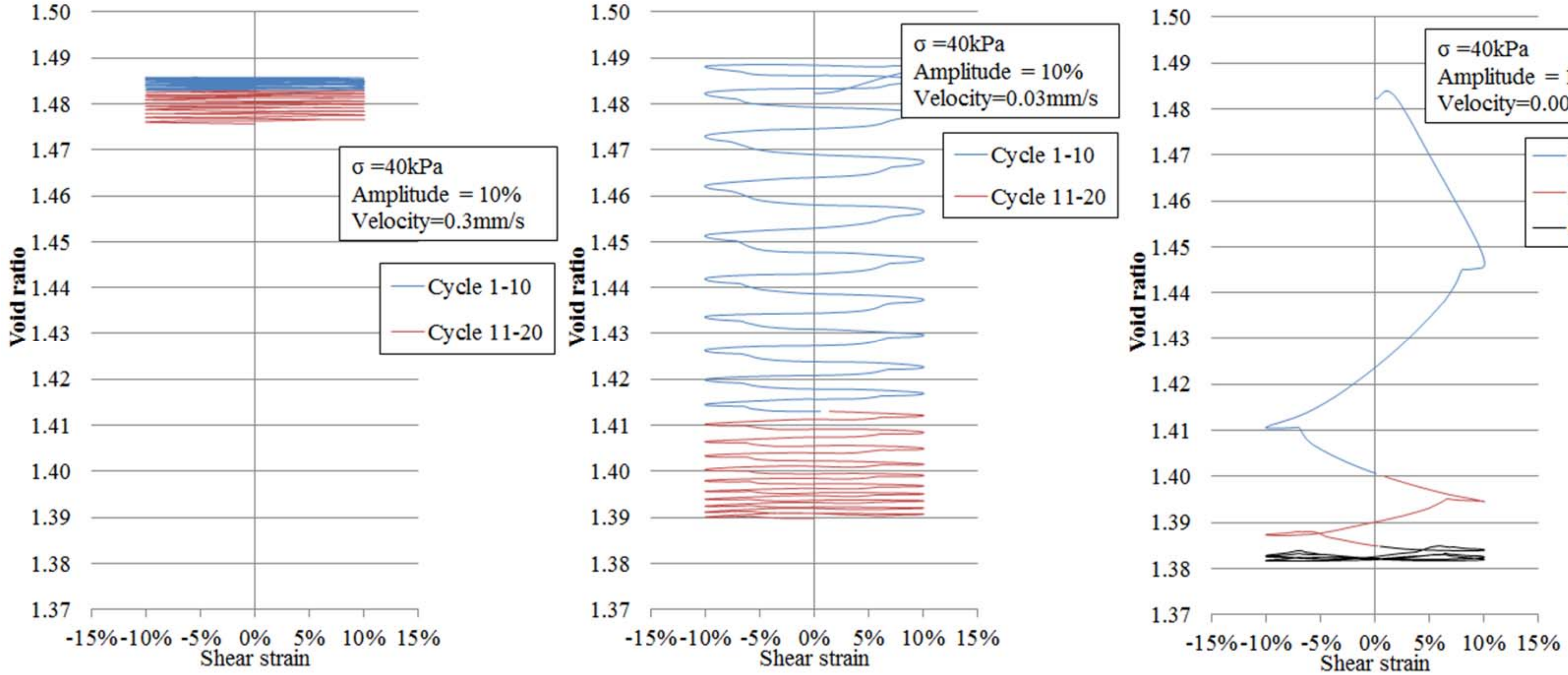

Figure A.8 Void ratio versus shear strain plots for applied vertical stress of 40kPa and shear amplitude of 10% of H

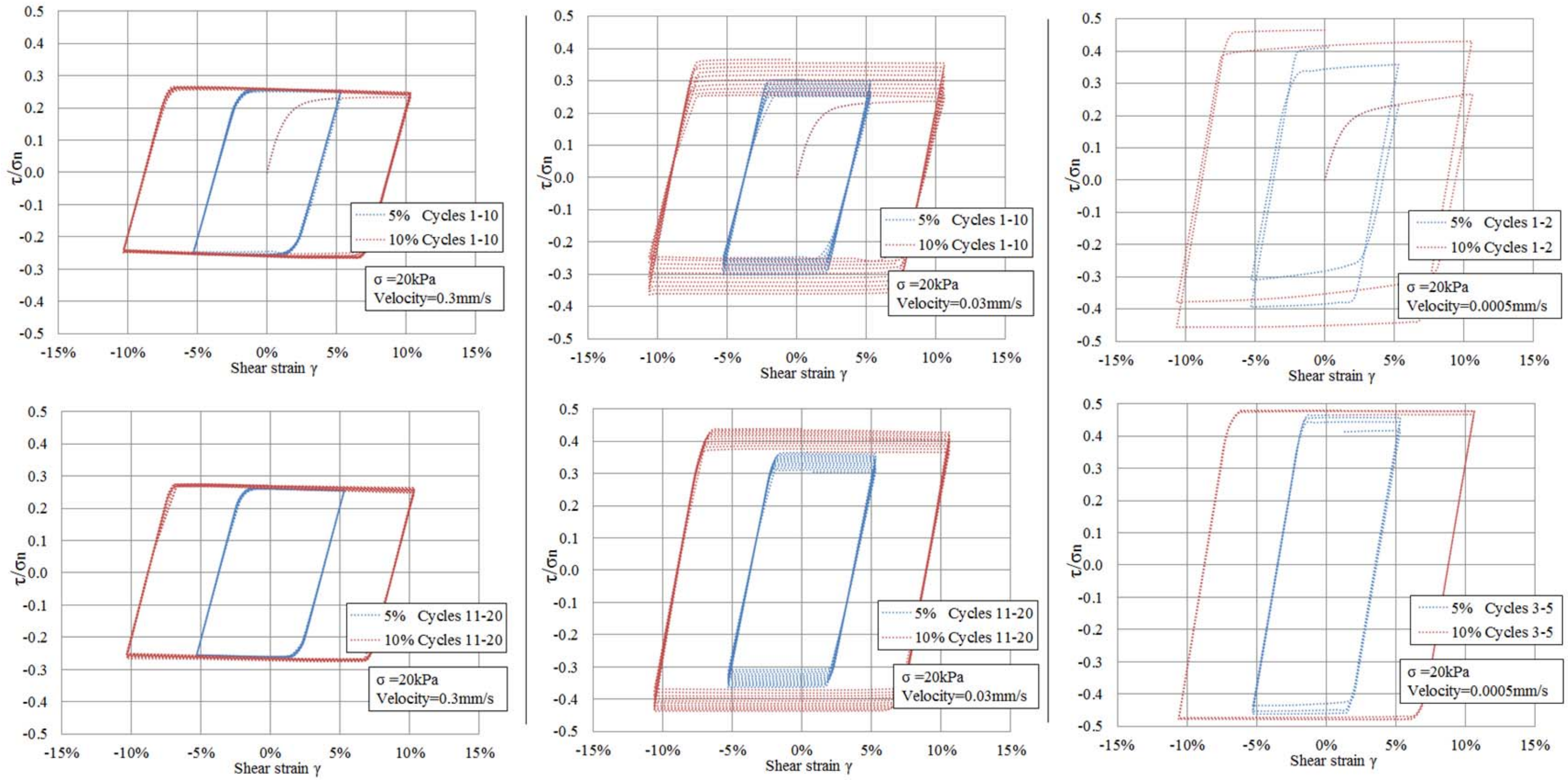

Figure A.9 Shear stress-strain curves for applied vertical stress of 20kPa

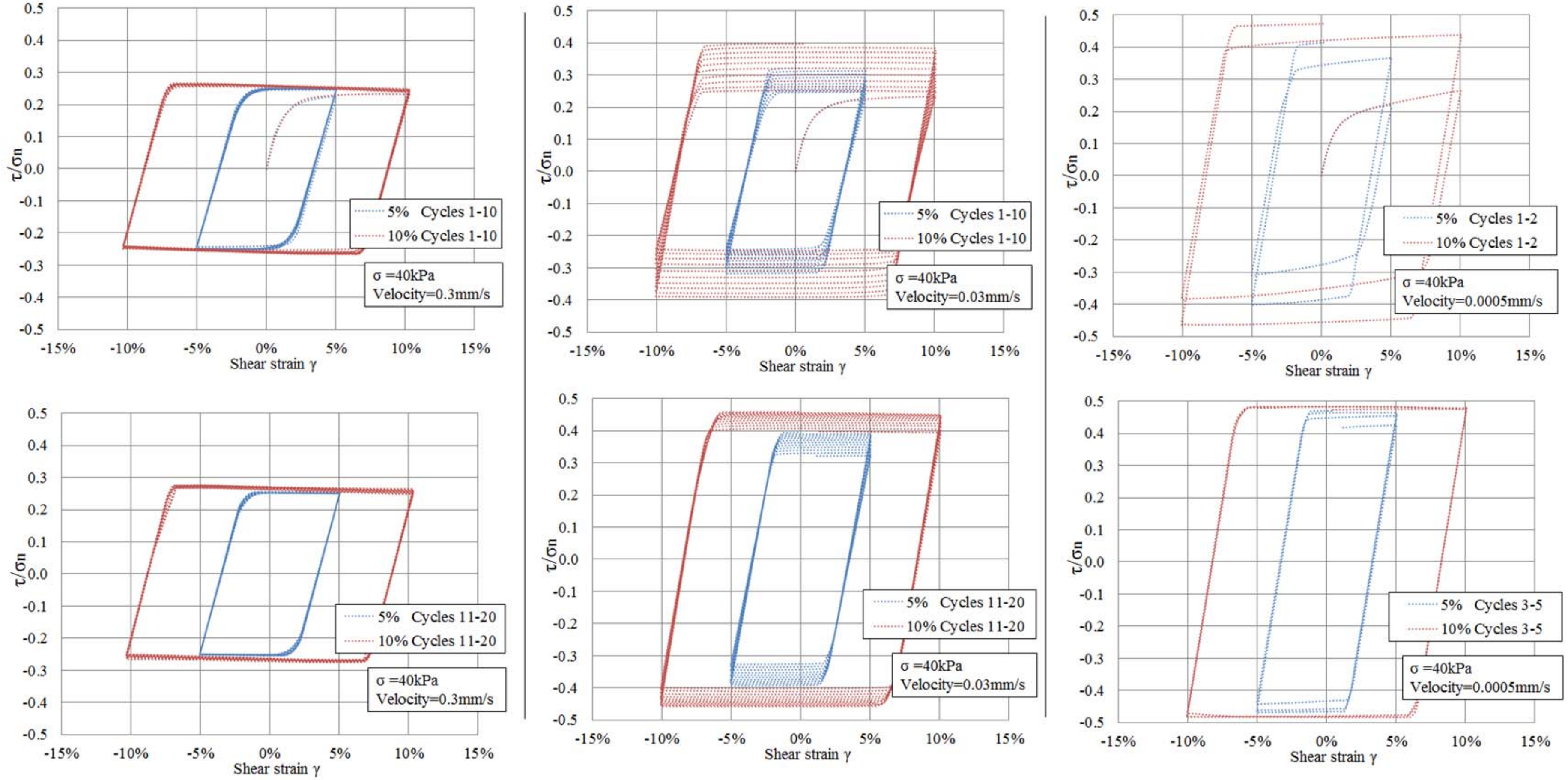

Figure A.10 Shear stress-strain curves for applied vertical stress of 40kPa

Appendix C sample .inp file of the finite element model

An example .inp file for the two dimensional finite element soil model developed is provided in this appendix. This .inp file is for an analysis with an applied vertical stress of 60kPa, shearing velocity of 0.03mm/s and shear amplitude of 10%. This file outlines how the model is constructed, how the soil properties are defined and how the loadings and boundary conditions are implemented.

```
** Job name: 2D FEA soil model
** Applied vertical stress = 60kPa
** Shearing velocity = 0.03mm/s
** Shearing amplitude = 10%
** Generated by: Abaqus/CAE 6.11-1
*Preprint, echo=NO, model=NO, history=NO, contact=NO
**
** PARTS
**
*Part, name=soil
*End Part
**
**
** ASSEMBLY
**
*Assembly, name=Assembly
**
*Instance, name=soil-1, part=soil
*Node
      1,           0.,           0.
      2, 0.00124999997,           0.
      3, 0.00249999994,           0.
      4, 0.00374999992,           0.
      5, 0.00499999989,           0.
      6, 0.00625000009,           0.
      7, 0.00749999983,           0.
      8, 0.00875000004,           0.
      9, 0.00999999978,           0.
     10, 0.0112500004,           0.
     11, 0.0125000002,           0.
     12, 0.0137499999,           0.
     13, 0.0149999997,           0.
     14, 0.0162499994,           0.
     15, 0.0175000001,           0.
     16, 0.0187500007,           0.
     17, 0.0199999996,           0.
     18, 0.0212500002,           0.
     19, 0.0225000009,           0.
     20, 0.0237499997,           0.
     21, 0.0250000004,           0.
     22, 0.0262499992,           0.
     23, 0.0274999999,           0.
     24, 0.0287500005,           0.
     25, 0.0299999993,           0.
     26,      0.03125,           0.
     27, 0.0324999988,           0.
     28, 0.0337500013,           0.
     29, 0.0350000001,           0.
     30,  0.036249999,           0.
     31, 0.0375000015,           0.
     32, 0.0387500003,           0.
     33, 0.0399999991,           0.
     34, 0.0412500016,           0.
     35, 0.0425000004,           0.
     36, 0.0437499993,           0.
     37, 0.0450000018,           0.
     38, 0.0462500006,           0.
     39, 0.0474999994,           0.
     40, 0.0487499982,           0.
     41, 0.0500000007,           0.
     42,           0., 0.000933500007
     43, 0.00124999997, 0.000933500007
     44, 0.00249999994, 0.000933500007
     45, 0.00374999992, 0.000933500007
     46, 0.00499999989, 0.000933500007
     47, 0.00625000009, 0.000933500007
     48, 0.00749999983, 0.000933500007
     49, 0.00875000004, 0.000933500007
     50, 0.00999999978, 0.000933500007
     51, 0.0112500004, 0.000933500007
     52, 0.0125000002, 0.000933500007
     53, 0.0137499999, 0.000933500007
     54, 0.0149999997, 0.000933500007
     55, 0.0162499994, 0.000933500007
     56, 0.0175000001, 0.000933500007
     57, 0.0187500007, 0.000933500007
     58, 0.0199999996, 0.000933500007
     59, 0.0212500002, 0.000933500007
     60, 0.0225000009, 0.000933500007
     61, 0.0237499997, 0.000933500007
     62, 0.0250000004, 0.000933500007
     63, 0.0262499992, 0.000933500007
     64, 0.0274999999, 0.000933500007
     65, 0.0287500005, 0.000933500007
     66, 0.0299999993, 0.000933500007
     67,      0.03125, 0.000933500007
     68, 0.0324999988, 0.000933500007
     69, 0.0337500013, 0.000933500007
     70, 0.0350000001, 0.000933500007
     71,  0.036249999, 0.000933500007
     72, 0.0375000015, 0.000933500007
     73, 0.0387500003, 0.000933500007
     74, 0.0399999991, 0.000933500007
     75, 0.0412500016, 0.000933500007
     76, 0.0425000004, 0.000933500007
     77, 0.0437499993, 0.000933500007
     78, 0.0450000018, 0.000933500007
     79, 0.0462500006, 0.000933500007
     80, 0.0474999994, 0.000933500007
     81, 0.0487499982, 0.000933500007
     82, 0.0500000007, 0.000933500007
     83,           0., 0.00186700001
     84, 0.00124999997, 0.00186700001
     85, 0.00249999994, 0.00186700001
     86, 0.00374999992, 0.00186700001
     87, 0.00499999989, 0.00186700001
     88, 0.00625000009, 0.00186700001
     89, 0.00749999983, 0.00186700001
     90, 0.00875000004, 0.00186700001
     91, 0.00999999978, 0.00186700001
     92, 0.0112500004, 0.00186700001
     93, 0.0125000002, 0.00186700001
     94, 0.0137499999, 0.00186700001
     95, 0.0149999997, 0.00186700001
     96, 0.0162499994, 0.00186700001
     97, 0.0175000001, 0.00186700001
```

98, 0.0187500007, 0.00186700001
99, 0.0199999996, 0.00186700001
100, 0.0212500002, 0.00186700001
101, 0.0225000009, 0.00186700001
102, 0.0237499997, 0.00186700001
103, 0.0250000004, 0.00186700001
104, 0.0262499992, 0.00186700001
105, 0.0274999999, 0.00186700001
106, 0.0287500005, 0.00186700001
107, 0.0299999993, 0.00186700001
108, 0.03125, 0.00186700001
109, 0.0324999988, 0.00186700001
110, 0.0337500013, 0.00186700001
111, 0.0350000001, 0.00186700001
112, 0.036249999, 0.00186700001
113, 0.0375000015, 0.00186700001
114, 0.0387500003, 0.00186700001
115, 0.0399999991, 0.00186700001
116, 0.0412500016, 0.00186700001
117, 0.0425000004, 0.00186700001
118, 0.0437499993, 0.00186700001
119, 0.0450000018, 0.00186700001
120, 0.0462500006, 0.00186700001
121, 0.0474999994, 0.00186700001
122, 0.0487499982, 0.00186700001
123, 0.0500000007, 0.00186700001
124, 0., 0.00280050002
125, 0.00124999997, 0.00280050002
126, 0.00249999994, 0.00280050002
127, 0.00374999992, 0.00280050002
128, 0.00499999989, 0.00280050002
129, 0.00625000009, 0.00280050002
130, 0.00749999983, 0.00280050002
131, 0.00875000004, 0.00280050002
132, 0.00999999978, 0.00280050002
133, 0.0112500004, 0.00280050002
134, 0.0125000002, 0.00280050002
135, 0.0137499999, 0.00280050002
136, 0.0149999997, 0.00280050002
137, 0.0162499994, 0.00280050002
138, 0.0175000001, 0.00280050002
139, 0.0187500007, 0.00280050002
140, 0.0199999996, 0.00280050002
141, 0.0212500002, 0.00280050002
142, 0.0225000009, 0.00280050002
143, 0.0237499997, 0.00280050002
144, 0.0250000004, 0.00280050002
145, 0.0262499992, 0.00280050002
146, 0.0274999999, 0.00280050002
147, 0.0287500005, 0.00280050002
148, 0.0299999993, 0.00280050002
149, 0.03125, 0.00280050002
150, 0.0324999988, 0.00280050002
151, 0.0337500013, 0.00280050002
152, 0.0350000001, 0.00280050002
153, 0.036249999, 0.00280050002
154, 0.0375000015, 0.00280050002
155, 0.0387500003, 0.00280050002
156, 0.0399999991, 0.00280050002
157, 0.0412500016, 0.00280050002
158, 0.0425000004, 0.00280050002
159, 0.0437499993, 0.00280050002
160, 0.0450000018, 0.00280050002
161, 0.0462500006, 0.00280050002
162, 0.0474999994, 0.00280050002
163, 0.0487499982, 0.00280050002
164, 0.0500000007, 0.00280050002
165, 0., 0.00373400003
166, 0.00124999997, 0.00373400003
167, 0.00249999994, 0.00373400003
168, 0.00374999992, 0.00373400003
169, 0.00499999989, 0.00373400003
170, 0.00625000009, 0.00373400003
171, 0.00749999983, 0.00373400003
172, 0.00875000004, 0.00373400003
173, 0.00999999978, 0.00373400003
174, 0.0112500004, 0.00373400003
175, 0.0125000002, 0.00373400003
176, 0.0137499999, 0.00373400003
177, 0.0149999997, 0.00373400003
178, 0.0162499994, 0.00373400003
179, 0.0175000001, 0.00373400003
180, 0.0187500007, 0.00373400003
181, 0.0199999996, 0.00373400003
182, 0.0212500002, 0.00373400003
183, 0.0225000009, 0.00373400003
184, 0.0237499997, 0.00373400003
185, 0.0250000004, 0.00373400003
186, 0.0262499992, 0.00373400003
187, 0.0274999999, 0.00373400003
188, 0.0287500005, 0.00373400003
189, 0.0299999993, 0.00373400003
190, 0.03125, 0.00373400003
191, 0.0324999988, 0.00373400003
192, 0.0337500013, 0.00373400003
193, 0.0350000001, 0.00373400003
194, 0.036249999, 0.00373400003
195, 0.0375000015, 0.00373400003
196, 0.0387500003, 0.00373400003
197, 0.0399999991, 0.00373400003
198, 0.0412500016, 0.00373400003
199, 0.0425000004, 0.00373400003
200, 0.0437499993, 0.00373400003
201, 0.0450000018, 0.00373400003
202, 0.0462500006, 0.00373400003
203, 0.0474999994, 0.00373400003
204, 0.0487499982, 0.00373400003
205, 0.0500000007, 0.00373400003
206, 0., 0.00466750003
207, 0.00124999997, 0.00466750003
208, 0.00249999994, 0.00466750003
209, 0.00374999992, 0.00466750003
210, 0.00499999989, 0.00466750003
211, 0.00625000009, 0.00466750003
212, 0.00749999983, 0.00466750003
213, 0.00875000004, 0.00466750003
214, 0.00999999978, 0.00466750003
215, 0.0112500004, 0.00466750003
216, 0.0125000002, 0.00466750003
217, 0.0137499999, 0.00466750003
218, 0.0149999997, 0.00466750003
219, 0.0162499994, 0.00466750003
220, 0.0175000001, 0.00466750003
221, 0.0187500007, 0.00466750003
222, 0.0199999996, 0.00466750003
223, 0.0212500002, 0.00466750003
224, 0.0225000009, 0.00466750003
225, 0.0237499997, 0.00466750003
226, 0.0250000004, 0.00466750003
227, 0.0262499992, 0.00466750003
228, 0.0274999999, 0.00466750003
229, 0.0287500005, 0.00466750003
230, 0.0299999993, 0.00466750003
231, 0.03125, 0.00466750003
232, 0.0324999988, 0.00466750003
233, 0.0337500013, 0.00466750003
234, 0.0350000001, 0.00466750003
235, 0.036249999, 0.00466750003
236, 0.0375000015, 0.00466750003
237, 0.0387500003, 0.00466750003
238, 0.0399999991, 0.00466750003
239, 0.0412500016, 0.00466750003
240, 0.0425000004, 0.00466750003
241, 0.0437499993, 0.00466750003
242, 0.0450000018, 0.00466750003
243, 0.0462500006, 0.00466750003
244, 0.0474999994, 0.00466750003
245, 0.0487499982, 0.00466750003
246, 0.0500000007, 0.00466750003
247, 0., 0.00560100004

248, 0.00124999997, 0.00560100004
249, 0.00249999994, 0.00560100004
250, 0.00374999992, 0.00560100004
251, 0.00499999989, 0.00560100004
252, 0.00625000009, 0.00560100004
253, 0.00749999983, 0.00560100004
254, 0.00875000004, 0.00560100004
255, 0.00999999978, 0.00560100004
256, 0.0112500004, 0.00560100004
257, 0.0125000002, 0.00560100004
258, 0.0137499999, 0.00560100004
259, 0.0149999997, 0.00560100004
260, 0.0162499994, 0.00560100004
261, 0.0175000001, 0.00560100004
262, 0.0187500007, 0.00560100004
263, 0.0199999996, 0.00560100004
264, 0.0212500002, 0.00560100004
265, 0.0225000009, 0.00560100004
266, 0.0237499997, 0.00560100004
267, 0.0250000004, 0.00560100004
268, 0.0262499992, 0.00560100004
269, 0.0274999999, 0.00560100004
270, 0.0287500005, 0.00560100004
271, 0.0299999993, 0.00560100004
272, 0.03125, 0.00560100004
273, 0.0324999988, 0.00560100004
274, 0.0337500013, 0.00560100004
275, 0.0350000001, 0.00560100004
276, 0.036249999, 0.00560100004
277, 0.0375000015, 0.00560100004
278, 0.0387500003, 0.00560100004
279, 0.0399999991, 0.00560100004
280, 0.0412500016, 0.00560100004
281, 0.0425000004, 0.00560100004
282, 0.0437499993, 0.00560100004
283, 0.0450000018, 0.00560100004
284, 0.0462500006, 0.00560100004
285, 0.0474999994, 0.00560100004
286, 0.0487499982, 0.00560100004
287, 0.0500000007, 0.00560100004
288, 0., 0.00653450005
289, 0.00124999997, 0.00653450005
290, 0.00249999994, 0.00653450005
291, 0.00374999992, 0.00653450005
292, 0.00499999989, 0.00653450005
293, 0.00625000009, 0.00653450005
294, 0.00749999983, 0.00653450005
295, 0.00875000004, 0.00653450005
296, 0.00999999978, 0.00653450005
297, 0.0112500004, 0.00653450005
298, 0.0125000002, 0.00653450005
299, 0.0137499999, 0.00653450005
300, 0.0149999997, 0.00653450005
301, 0.0162499994, 0.00653450005
302, 0.0175000001, 0.00653450005
303, 0.0187500007, 0.00653450005
304, 0.0199999996, 0.00653450005
305, 0.0212500002, 0.00653450005
306, 0.0225000009, 0.00653450005
307, 0.0237499997, 0.00653450005
308, 0.0250000004, 0.00653450005
309, 0.0262499992, 0.00653450005
310, 0.0274999999, 0.00653450005
311, 0.0287500005, 0.00653450005
312, 0.0299999993, 0.00653450005
313, 0.03125, 0.00653450005
314, 0.0324999988, 0.00653450005
315, 0.0337500013, 0.00653450005
316, 0.0350000001, 0.00653450005
317, 0.036249999, 0.00653450005
318, 0.0375000015, 0.00653450005
319, 0.0387500003, 0.00653450005
320, 0.0399999991, 0.00653450005
321, 0.0412500016, 0.00653450005
322, 0.0425000004, 0.00653450005
323, 0.0437499993, 0.00653450005
324, 0.0450000018, 0.00653450005
325, 0.0462500006, 0.00653450005
326, 0.0474999994, 0.00653450005
327, 0.0487499982, 0.00653450005
328, 0.0500000007, 0.00653450005
329, 0., 0.00746800005
330, 0.00124999997, 0.00746800005
331, 0.00249999994, 0.00746800005
332, 0.00374999992, 0.00746800005
333, 0.00499999989, 0.00746800005
334, 0.00625000009, 0.00746800005
335, 0.00749999983, 0.00746800005
336, 0.00875000004, 0.00746800005
337, 0.00999999978, 0.00746800005
338, 0.0112500004, 0.00746800005
339, 0.0125000002, 0.00746800005
340, 0.0137499999, 0.00746800005
341, 0.0149999997, 0.00746800005
342, 0.0162499994, 0.00746800005
343, 0.0175000001, 0.00746800005
344, 0.0187500007, 0.00746800005
345, 0.0199999996, 0.00746800005
346, 0.0212500002, 0.00746800005
347, 0.0225000009, 0.00746800005
348, 0.0237499997, 0.00746800005
349, 0.0250000004, 0.00746800005
350, 0.0262499992, 0.00746800005
351, 0.0274999999, 0.00746800005
352, 0.0287500005, 0.00746800005
353, 0.0299999993, 0.00746800005
354, 0.03125, 0.00746800005
355, 0.0324999988, 0.00746800005
356, 0.0337500013, 0.00746800005
357, 0.0350000001, 0.00746800005
358, 0.036249999, 0.00746800005
359, 0.0375000015, 0.00746800005
360, 0.0387500003, 0.00746800005
361, 0.0399999991, 0.00746800005
362, 0.0412500016, 0.00746800005
363, 0.0425000004, 0.00746800005
364, 0.0437499993, 0.00746800005
365, 0.0450000018, 0.00746800005
366, 0.0462500006, 0.00746800005
367, 0.0474999994, 0.00746800005
368, 0.0487499982, 0.00746800005
369, 0.0500000007, 0.00746800005
370, 0., 0.00840150006
371, 0.00124999997, 0.00840150006
372, 0.00249999994, 0.00840150006
373, 0.00374999992, 0.00840150006
374, 0.00499999989, 0.00840150006
375, 0.00625000009, 0.00840150006
376, 0.00749999983, 0.00840150006
377, 0.00875000004, 0.00840150006
378, 0.00999999978, 0.00840150006
379, 0.0112500004, 0.00840150006
380, 0.0125000002, 0.00840150006
381, 0.0137499999, 0.00840150006
382, 0.0149999997, 0.00840150006
383, 0.0162499994, 0.00840150006
384, 0.0175000001, 0.00840150006
385, 0.0187500007, 0.00840150006
386, 0.0199999996, 0.00840150006
387, 0.0212500002, 0.00840150006
388, 0.0225000009, 0.00840150006
389, 0.0237499997, 0.00840150006
390, 0.0250000004, 0.00840150006
391, 0.0262499992, 0.00840150006
392, 0.0274999999, 0.00840150006
393, 0.0287500005, 0.00840150006
394, 0.0299999993, 0.00840150006
395, 0.03125, 0.00840150006
396, 0.0324999988, 0.00840150006
397, 0.0337500013, 0.00840150006

398, 0.0350000001, 0.00840150006
399, 0.036249999, 0.00840150006
400, 0.0375000015, 0.00840150006
401, 0.0387500003, 0.00840150006
402, 0.0399999991, 0.00840150006
403, 0.0412500016, 0.00840150006
404, 0.0425000004, 0.00840150006
405, 0.0437499993, 0.00840150006
406, 0.0450000018, 0.00840150006
407, 0.0462500006, 0.00840150006
408, 0.0474999994, 0.00840150006
409, 0.0487499982, 0.00840150006
410, 0.0500000007, 0.00840150006
411, 0., 0.00933500007
412, 0.00124999997, 0.00933500007
413, 0.00249999994, 0.00933500007
414, 0.00374999992, 0.00933500007
415, 0.00499999989, 0.00933500007
416, 0.00625000009, 0.00933500007
417, 0.00749999983, 0.00933500007
418, 0.00875000004, 0.00933500007
419, 0.00999999978, 0.00933500007
420, 0.0112500004, 0.00933500007
421, 0.0125000002, 0.00933500007
422, 0.0137499999, 0.00933500007
423, 0.0149999997, 0.00933500007
424, 0.0162499994, 0.00933500007
425, 0.0175000001, 0.00933500007
426, 0.0187500007, 0.00933500007
427, 0.0199999996, 0.00933500007
428, 0.0212500002, 0.00933500007
429, 0.0225000009, 0.00933500007
430, 0.0237499997, 0.00933500007
431, 0.0250000004, 0.00933500007
432, 0.0262499992, 0.00933500007
433, 0.0274999999, 0.00933500007
434, 0.0287500005, 0.00933500007
435, 0.0299999993, 0.00933500007
436, 0.03125, 0.00933500007
437, 0.0324999988, 0.00933500007
438, 0.0337500013, 0.00933500007
439, 0.0350000001, 0.00933500007
440, 0.036249999, 0.00933500007
441, 0.0375000015, 0.00933500007
442, 0.0387500003, 0.00933500007
443, 0.0399999991, 0.00933500007
444, 0.0412500016, 0.00933500007
445, 0.0425000004, 0.00933500007
446, 0.0437499993, 0.00933500007
447, 0.0450000018, 0.00933500007
448, 0.0462500006, 0.00933500007
449, 0.0474999994, 0.00933500007
450, 0.0487499982, 0.00933500007
451, 0.0500000007, 0.00933500007
452, 0., 0.0102685001
453, 0.00124999997, 0.0102685001
454, 0.00249999994, 0.0102685001
455, 0.00374999992, 0.0102685001
456, 0.00499999989, 0.0102685001
457, 0.00625000009, 0.0102685001
458, 0.00749999983, 0.0102685001
459, 0.00875000004, 0.0102685001
460, 0.00999999978, 0.0102685001
461, 0.0112500004, 0.0102685001
462, 0.0125000002, 0.0102685001
463, 0.0137499999, 0.0102685001
464, 0.0149999997, 0.0102685001
465, 0.0162499994, 0.0102685001
466, 0.0175000001, 0.0102685001
467, 0.0187500007, 0.0102685001
468, 0.0199999996, 0.0102685001
469, 0.0212500002, 0.0102685001
470, 0.0225000009, 0.0102685001
471, 0.0237499997, 0.0102685001
472, 0.0250000004, 0.0102685001
473, 0.0262499992, 0.0102685001
474, 0.0274999999, 0.0102685001
475, 0.0287500005, 0.0102685001
476, 0.0299999993, 0.0102685001
477, 0.03125, 0.0102685001
478, 0.0324999988, 0.0102685001
479, 0.0337500013, 0.0102685001
480, 0.0350000001, 0.0102685001
481, 0.036249999, 0.0102685001
482, 0.0375000015, 0.0102685001
483, 0.0387500003, 0.0102685001
484, 0.0399999991, 0.0102685001
485, 0.0412500016, 0.0102685001
486, 0.0425000004, 0.0102685001
487, 0.0437499993, 0.0102685001
488, 0.0450000018, 0.0102685001
489, 0.0462500006, 0.0102685001
490, 0.0474999994, 0.0102685001
491, 0.0487499982, 0.0102685001
492, 0.0500000007, 0.0102685001
493, 0., 0.0112020001
494, 0.00124999997, 0.0112020001
495, 0.00249999994, 0.0112020001
496, 0.00374999992, 0.0112020001
497, 0.00499999989, 0.0112020001
498, 0.00625000009, 0.0112020001
499, 0.00749999983, 0.0112020001
500, 0.00875000004, 0.0112020001
501, 0.00999999978, 0.0112020001
502, 0.0112500004, 0.0112020001
503, 0.0125000002, 0.0112020001
504, 0.0137499999, 0.0112020001
505, 0.0149999997, 0.0112020001
506, 0.0162499994, 0.0112020001
507, 0.0175000001, 0.0112020001
508, 0.0187500007, 0.0112020001
509, 0.0199999996, 0.0112020001
510, 0.0212500002, 0.0112020001
511, 0.0225000009, 0.0112020001
512, 0.0237499997, 0.0112020001
513, 0.0250000004, 0.0112020001
514, 0.0262499992, 0.0112020001
515, 0.0274999999, 0.0112020001
516, 0.0287500005, 0.0112020001
517, 0.0299999993, 0.0112020001
518, 0.03125, 0.0112020001
519, 0.0324999988, 0.0112020001
520, 0.0337500013, 0.0112020001
521, 0.0350000001, 0.0112020001
522, 0.036249999, 0.0112020001
523, 0.0375000015, 0.0112020001
524, 0.0387500003, 0.0112020001
525, 0.0399999991, 0.0112020001
526, 0.0412500016, 0.0112020001
527, 0.0425000004, 0.0112020001
528, 0.0437499993, 0.0112020001
529, 0.0450000018, 0.0112020001
530, 0.0462500006, 0.0112020001
531, 0.0474999994, 0.0112020001
532, 0.0487499982, 0.0112020001
533, 0.0500000007, 0.0112020001
534, 0., 0.0121355001
535, 0.00124999997, 0.0121355001
536, 0.00249999994, 0.0121355001
537, 0.00374999992, 0.0121355001
538, 0.00499999989, 0.0121355001
539, 0.00625000009, 0.0121355001
540, 0.00749999983, 0.0121355001
541, 0.00875000004, 0.0121355001
542, 0.00999999978, 0.0121355001
543, 0.0112500004, 0.0121355001
544, 0.0125000002, 0.0121355001
545, 0.0137499999, 0.0121355001
546, 0.0149999997, 0.0121355001
547, 0.0162499994, 0.0121355001

548, 0.0175000001, 0.0121355001
549, 0.0187500007, 0.0121355001
550, 0.0199999996, 0.0121355001
551, 0.0212500002, 0.0121355001
552, 0.0225000009, 0.0121355001
553, 0.0237499997, 0.0121355001
554, 0.0250000004, 0.0121355001
555, 0.0262499992, 0.0121355001
556, 0.0274999999, 0.0121355001
557, 0.0287500005, 0.0121355001
558, 0.0299999993, 0.0121355001
559, 0.03125, 0.0121355001
560, 0.0324999988, 0.0121355001
561, 0.0337500013, 0.0121355001
562, 0.0350000001, 0.0121355001
563, 0.036249999, 0.0121355001
564, 0.0375000015, 0.0121355001
565, 0.0387500003, 0.0121355001
566, 0.0399999991, 0.0121355001
567, 0.0412500016, 0.0121355001
568, 0.0425000004, 0.0121355001
569, 0.0437499993, 0.0121355001
570, 0.0450000018, 0.0121355001
571, 0.0462500006, 0.0121355001
572, 0.0474999994, 0.0121355001
573, 0.0487499982, 0.0121355001
574, 0.0500000007, 0.0121355001
575, 0., 0.0130690001
576, 0.00124999997, 0.0130690001
577, 0.00249999994, 0.0130690001
578, 0.00374999992, 0.0130690001
579, 0.00499999989, 0.0130690001
580, 0.00625000009, 0.0130690001
581, 0.00749999983, 0.0130690001
582, 0.00875000004, 0.0130690001
583, 0.00999999978, 0.0130690001
584, 0.0112500004, 0.0130690001
585, 0.0125000002, 0.0130690001
586, 0.0137499999, 0.0130690001
587, 0.0149999997, 0.0130690001
588, 0.0162499994, 0.0130690001
589, 0.0175000001, 0.0130690001
590, 0.0187500007, 0.0130690001
591, 0.0199999996, 0.0130690001
592, 0.0212500002, 0.0130690001
593, 0.0225000009, 0.0130690001
594, 0.0237499997, 0.0130690001
595, 0.0250000004, 0.0130690001
596, 0.0262499992, 0.0130690001
597, 0.0274999999, 0.0130690001
598, 0.0287500005, 0.0130690001
599, 0.0299999993, 0.0130690001
600, 0.03125, 0.0130690001
601, 0.0324999988, 0.0130690001
602, 0.0337500013, 0.0130690001
603, 0.0350000001, 0.0130690001
604, 0.036249999, 0.0130690001
605, 0.0375000015, 0.0130690001
606, 0.0387500003, 0.0130690001
607, 0.0399999991, 0.0130690001
608, 0.0412500016, 0.0130690001
609, 0.0425000004, 0.0130690001
610, 0.0437499993, 0.0130690001
611, 0.0450000018, 0.0130690001
612, 0.0462500006, 0.0130690001
613, 0.0474999994, 0.0130690001
614, 0.0487499982, 0.0130690001
615, 0.0500000007, 0.0130690001
616, 0., 0.0140025001
617, 0.00124999997, 0.0140025001
618, 0.00249999994, 0.0140025001
619, 0.00374999992, 0.0140025001
620, 0.00499999989, 0.0140025001
621, 0.00625000009, 0.0140025001
622, 0.00749999983, 0.0140025001
623, 0.00875000004, 0.0140025001
624, 0.00999999978, 0.0140025001
625, 0.0112500004, 0.0140025001
626, 0.0125000002, 0.0140025001
627, 0.0137499999, 0.0140025001
628, 0.0149999997, 0.0140025001
629, 0.0162499994, 0.0140025001
630, 0.0175000001, 0.0140025001
631, 0.0187500007, 0.0140025001
632, 0.0199999996, 0.0140025001
633, 0.0212500002, 0.0140025001
634, 0.0225000009, 0.0140025001
635, 0.0237499997, 0.0140025001
636, 0.0250000004, 0.0140025001
637, 0.0262499992, 0.0140025001
638, 0.0274999999, 0.0140025001
639, 0.0287500005, 0.0140025001
640, 0.0299999993, 0.0140025001
641, 0.03125, 0.0140025001
642, 0.0324999988, 0.0140025001
643, 0.0337500013, 0.0140025001
644, 0.0350000001, 0.0140025001
645, 0.036249999, 0.0140025001
646, 0.0375000015, 0.0140025001
647, 0.0387500003, 0.0140025001
648, 0.0399999991, 0.0140025001
649, 0.0412500016, 0.0140025001
650, 0.0425000004, 0.0140025001
651, 0.0437499993, 0.0140025001
652, 0.0450000018, 0.0140025001
653, 0.0462500006, 0.0140025001
654, 0.0474999994, 0.0140025001
655, 0.0487499982, 0.0140025001
656, 0.0500000007, 0.0140025001
657, 0., 0.0149360001
658, 0.00124999997, 0.0149360001
659, 0.00249999994, 0.0149360001
660, 0.00374999992, 0.0149360001
661, 0.00499999989, 0.0149360001
662, 0.00625000009, 0.0149360001
663, 0.00749999983, 0.0149360001
664, 0.00875000004, 0.0149360001
665, 0.00999999978, 0.0149360001
666, 0.0112500004, 0.0149360001
667, 0.0125000002, 0.0149360001
668, 0.0137499999, 0.0149360001
669, 0.0149999997, 0.0149360001
670, 0.0162499994, 0.0149360001
671, 0.0175000001, 0.0149360001
672, 0.0187500007, 0.0149360001
673, 0.0199999996, 0.0149360001
674, 0.0212500002, 0.0149360001
675, 0.0225000009, 0.0149360001
676, 0.0237499997, 0.0149360001
677, 0.0250000004, 0.0149360001
678, 0.0262499992, 0.0149360001
679, 0.0274999999, 0.0149360001
680, 0.0287500005, 0.0149360001
681, 0.0299999993, 0.0149360001
682, 0.03125, 0.0149360001
683, 0.0324999988, 0.0149360001
684, 0.0337500013, 0.0149360001
685, 0.0350000001, 0.0149360001
686, 0.036249999, 0.0149360001
687, 0.0375000015, 0.0149360001
688, 0.0387500003, 0.0149360001
689, 0.0399999991, 0.0149360001
690, 0.0412500016, 0.0149360001
691, 0.0425000004, 0.0149360001
692, 0.0437499993, 0.0149360001
693, 0.0450000018, 0.0149360001
694, 0.0462500006, 0.0149360001
695, 0.0474999994, 0.0149360001
696, 0.0487499982, 0.0149360001
697, 0.0500000007, 0.0149360001

```
698,           0., 0.0158695001
699, 0.00124999997, 0.0158695001
700, 0.00249999994, 0.0158695001
701, 0.00374999992, 0.0158695001
702, 0.00499999989, 0.0158695001
703, 0.00625000009, 0.0158695001
704, 0.00749999983, 0.0158695001
705, 0.00875000004, 0.0158695001
706, 0.00999999978, 0.0158695001
707, 0.0112500004, 0.0158695001
708, 0.0125000002, 0.0158695001
709, 0.0137499999, 0.0158695001
710, 0.0149999997, 0.0158695001
711, 0.0162499994, 0.0158695001
712, 0.0175000001, 0.0158695001
713, 0.0187500007, 0.0158695001
714, 0.0199999996, 0.0158695001
715, 0.0212500002, 0.0158695001
716, 0.0225000009, 0.0158695001
717, 0.0237499997, 0.0158695001
718, 0.0250000004, 0.0158695001
719, 0.0262499992, 0.0158695001
720, 0.0274999999, 0.0158695001
721, 0.0287500005, 0.0158695001
722, 0.0299999993, 0.0158695001
723,      0.03125, 0.0158695001
724, 0.0324999988, 0.0158695001
725, 0.0337500013, 0.0158695001
726, 0.0350000001, 0.0158695001
727,  0.036249999, 0.0158695001
728, 0.0375000015, 0.0158695001
729, 0.0387500003, 0.0158695001
730, 0.0399999991, 0.0158695001
731, 0.0412500016, 0.0158695001
732, 0.0425000004, 0.0158695001
733, 0.0437499993, 0.0158695001
734, 0.0450000018, 0.0158695001
735, 0.0462500006, 0.0158695001
736, 0.0474999994, 0.0158695001
737, 0.0487499982, 0.0158695001
738, 0.0500000007, 0.0158695001
739,           0., 0.0168030001
740, 0.00124999997, 0.0168030001
741, 0.00249999994, 0.0168030001
742, 0.00374999992, 0.0168030001
743, 0.00499999989, 0.0168030001
744, 0.00625000009, 0.0168030001
745, 0.00749999983, 0.0168030001
746, 0.00875000004, 0.0168030001
747, 0.00999999978, 0.0168030001
748, 0.0112500004, 0.0168030001
749, 0.0125000002, 0.0168030001
750, 0.0137499999, 0.0168030001
751, 0.0149999997, 0.0168030001
752, 0.0162499994, 0.0168030001
753, 0.0175000001, 0.0168030001
754, 0.0187500007, 0.0168030001
755, 0.0199999996, 0.0168030001
756, 0.0212500002, 0.0168030001
757, 0.0225000009, 0.0168030001
758, 0.0237499997, 0.0168030001
759, 0.0250000004, 0.0168030001
760, 0.0262499992, 0.0168030001
761, 0.0274999999, 0.0168030001
762, 0.0287500005, 0.0168030001
763, 0.0299999993, 0.0168030001
764,      0.03125, 0.0168030001
765, 0.0324999988, 0.0168030001
766, 0.0337500013, 0.0168030001
767, 0.0350000001, 0.0168030001
768,  0.036249999, 0.0168030001
769, 0.0375000015, 0.0168030001
770, 0.0387500003, 0.0168030001
771, 0.0399999991, 0.0168030001
772, 0.0412500016, 0.0168030001
773, 0.0425000004, 0.0168030001
774, 0.0437499993, 0.0168030001
775, 0.0450000018, 0.0168030001
776, 0.0462500006, 0.0168030001
777, 0.0474999994, 0.0168030001
778, 0.0487499982, 0.0168030001
779, 0.0500000007, 0.0168030001
780,           0., 0.0177365001
781, 0.00124999997, 0.0177365001
782, 0.00249999994, 0.0177365001
783, 0.00374999992, 0.0177365001
784, 0.00499999989, 0.0177365001
785, 0.00625000009, 0.0177365001
786, 0.00749999983, 0.0177365001
787, 0.00875000004, 0.0177365001
788, 0.00999999978, 0.0177365001
789, 0.0112500004, 0.0177365001
790, 0.0125000002, 0.0177365001
791, 0.0137499999, 0.0177365001
792, 0.0149999997, 0.0177365001
793, 0.0162499994, 0.0177365001
794, 0.0175000001, 0.0177365001
795, 0.0187500007, 0.0177365001
796, 0.0199999996, 0.0177365001
797, 0.0212500002, 0.0177365001
798, 0.0225000009, 0.0177365001
799, 0.0237499997, 0.0177365001
800, 0.0250000004, 0.0177365001
801, 0.0262499992, 0.0177365001
802, 0.0274999999, 0.0177365001
803, 0.0287500005, 0.0177365001
804, 0.0299999993, 0.0177365001
805,      0.03125, 0.0177365001
806, 0.0324999988, 0.0177365001
807, 0.0337500013, 0.0177365001
808, 0.0350000001, 0.0177365001
809,  0.036249999, 0.0177365001
810, 0.0375000015, 0.0177365001
811, 0.0387500003, 0.0177365001
812, 0.0399999991, 0.0177365001
813, 0.0412500016, 0.0177365001
814, 0.0425000004, 0.0177365001
815, 0.0437499993, 0.0177365001
816, 0.0450000018, 0.0177365001
817, 0.0462500006, 0.0177365001
818, 0.0474999994, 0.0177365001
819, 0.0487499982, 0.0177365001
820, 0.0500000007, 0.0177365001
821,           0., 0.0186700001
822, 0.00124999997, 0.0186700001
823, 0.00249999994, 0.0186700001
824, 0.00374999992, 0.0186700001
825, 0.00499999989, 0.0186700001
826, 0.00625000009, 0.0186700001
827, 0.00749999983, 0.0186700001
828, 0.00875000004, 0.0186700001
829, 0.00999999978, 0.0186700001
830, 0.0112500004, 0.0186700001
831, 0.0125000002, 0.0186700001
832, 0.0137499999, 0.0186700001
833, 0.0149999997, 0.0186700001
834, 0.0162499994, 0.0186700001
835, 0.0175000001, 0.0186700001
836, 0.0187500007, 0.0186700001
837, 0.0199999996, 0.0186700001
838, 0.0212500002, 0.0186700001
839, 0.0225000009, 0.0186700001
840, 0.0237499997, 0.0186700001
841, 0.0250000004, 0.0186700001
842, 0.0262499992, 0.0186700001
843, 0.0274999999, 0.0186700001
844, 0.0287500005, 0.0186700001
845, 0.0299999993, 0.0186700001
846,      0.03125, 0.0186700001
847, 0.0324999988, 0.0186700001
```

```
848, 0.0337500013, 0.0186700001
849, 0.0350000001, 0.0186700001
850,  0.036249999, 0.0186700001
851, 0.0375000015, 0.0186700001
852, 0.0387500003, 0.0186700001
853, 0.0399999991, 0.0186700001
854, 0.0412500016, 0.0186700001
855, 0.0425000004, 0.0186700001
856, 0.0437499993, 0.0186700001
857, 0.0450000018, 0.0186700001
858, 0.0462500006, 0.0186700001
859, 0.0474999994, 0.0186700001
860, 0.0487499982, 0.0186700001
861, 0.0500000007, 0.0186700001
*Element, type=CPE4P
 1,  1,  2, 43, 42
 2,  2,  3, 44, 43
 3,  3,  4, 45, 44
 4,  4,  5, 46, 45
 5,  5,  6, 47, 46
 6,  6,  7, 48, 47
 7,  7,  8, 49, 48
 8,  8,  9, 50, 49
 9,  9, 10, 51, 50
10, 10, 11, 52, 51
11, 11, 12, 53, 52
12, 12, 13, 54, 53
13, 13, 14, 55, 54
14, 14, 15, 56, 55
15, 15, 16, 57, 56
16, 16, 17, 58, 57
17, 17, 18, 59, 58
18, 18, 19, 60, 59
19, 19, 20, 61, 60
20, 20, 21, 62, 61
21, 21, 22, 63, 62
22, 22, 23, 64, 63
23, 23, 24, 65, 64
24, 24, 25, 66, 65
25, 25, 26, 67, 66
26, 26, 27, 68, 67
27, 27, 28, 69, 68
28, 28, 29, 70, 69
29, 29, 30, 71, 70
30, 30, 31, 72, 71
31, 31, 32, 73, 72
32, 32, 33, 74, 73
33, 33, 34, 75, 74
34, 34, 35, 76, 75
35, 35, 36, 77, 76
36, 36, 37, 78, 77
37, 37, 38, 79, 78
38, 38, 39, 80, 79
39, 39, 40, 81, 80
40, 40, 41, 82, 81
41, 42, 43, 84, 83
42, 43, 44, 85, 84
43, 44, 45, 86, 85
44, 45, 46, 87, 86
45, 46, 47, 88, 87
46, 47, 48, 89, 88
47, 48, 49, 90, 89
48, 49, 50, 91, 90
49, 50, 51, 92, 91
50, 51, 52, 93, 92
51, 52, 53, 94, 93
52, 53, 54, 95, 94
53, 54, 55, 96, 95
54, 55, 56, 97, 96
55, 56, 57, 98, 97
56, 57, 58, 99, 98
57, 58, 59, 100, 99
58, 59, 60, 101, 100
59, 60, 61, 102, 101
60, 61, 62, 103, 102
61, 62, 63, 104, 103
62, 63, 64, 105, 104
63, 64, 65, 106, 105
64, 65, 66, 107, 106
65, 66, 67, 108, 107
66, 67, 68, 109, 108
67, 68, 69, 110, 109
68, 69, 70, 111, 110
69, 70, 71, 112, 111
70, 71, 72, 113, 112
71, 72, 73, 114, 113
72, 73, 74, 115, 114
73, 74, 75, 116, 115
74, 75, 76, 117, 116
75, 76, 77, 118, 117
76, 77, 78, 119, 118
77, 78, 79, 120, 119
78, 79, 80, 121, 120
79, 80, 81, 122, 121
80, 81, 82, 123, 122
81, 83, 84, 125, 124
82, 84, 85, 126, 125
83, 85, 86, 127, 126
84, 86, 87, 128, 127
85, 87, 88, 129, 128
86, 88, 89, 130, 129
87, 89, 90, 131, 130
88, 90, 91, 132, 131
89, 91, 92, 133, 132
90, 92, 93, 134, 133
91, 93, 94, 135, 134
92, 94, 95, 136, 135
93, 95, 96, 137, 136
94, 96, 97, 138, 137
95, 97, 98, 139, 138
96, 98, 99, 140, 139
97, 99, 100, 141, 140
98, 100, 101, 142, 141
99, 101, 102, 143, 142
100, 102, 103, 144, 143
101, 103, 104, 145, 144
102, 104, 105, 146, 145
103, 105, 106, 147, 146
104, 106, 107, 148, 147
105, 107, 108, 149, 148
106, 108, 109, 150, 149
107, 109, 110, 151, 150
108, 110, 111, 152, 151
109, 111, 112, 153, 152
110, 112, 113, 154, 153
111, 113, 114, 155, 154
112, 114, 115, 156, 155
113, 115, 116, 157, 156
114, 116, 117, 158, 157
115, 117, 118, 159, 158
116, 118, 119, 160, 159
117, 119, 120, 161, 160
118, 120, 121, 162, 161
119, 121, 122, 163, 162
120, 122, 123, 164, 163
121, 124, 125, 166, 165
122, 125, 126, 167, 166
123, 126, 127, 168, 167
124, 127, 128, 169, 168
125, 128, 129, 170, 169
126, 129, 130, 171, 170
127, 130, 131, 172, 171
128, 131, 132, 173, 172
129, 132, 133, 174, 173
130, 133, 134, 175, 174
131, 134, 135, 176, 175
132, 135, 136, 177, 176
133, 136, 137, 178, 177
134, 137, 138, 179, 178
135, 138, 139, 180, 179
```

136, 139, 140, 181, 180
137, 140, 141, 182, 181
138, 141, 142, 183, 182
139, 142, 143, 184, 183
140, 143, 144, 185, 184
141, 144, 145, 186, 185
142, 145, 146, 187, 186
143, 146, 147, 188, 187
144, 147, 148, 189, 188
145, 148, 149, 190, 189
146, 149, 150, 191, 190
147, 150, 151, 192, 191
148, 151, 152, 193, 192
149, 152, 153, 194, 193
150, 153, 154, 195, 194
151, 154, 155, 196, 195
152, 155, 156, 197, 196
153, 156, 157, 198, 197
154, 157, 158, 199, 198
155, 158, 159, 200, 199
156, 159, 160, 201, 200
157, 160, 161, 202, 201
158, 161, 162, 203, 202
159, 162, 163, 204, 203
160, 163, 164, 205, 204
161, 165, 166, 207, 206
162, 166, 167, 208, 207
163, 167, 168, 209, 208
164, 168, 169, 210, 209
165, 169, 170, 211, 210
166, 170, 171, 212, 211
167, 171, 172, 213, 212
168, 172, 173, 214, 213
169, 173, 174, 215, 214
170, 174, 175, 216, 215
171, 175, 176, 217, 216
172, 176, 177, 218, 217
173, 177, 178, 219, 218
174, 178, 179, 220, 219
175, 179, 180, 221, 220
176, 180, 181, 222, 221
177, 181, 182, 223, 222
178, 182, 183, 224, 223
179, 183, 184, 225, 224
180, 184, 185, 226, 225
181, 185, 186, 227, 226
182, 186, 187, 228, 227
183, 187, 188, 229, 228
184, 188, 189, 230, 229
185, 189, 190, 231, 230
186, 190, 191, 232, 231
187, 191, 192, 233, 232
188, 192, 193, 234, 233
189, 193, 194, 235, 234
190, 194, 195, 236, 235
191, 195, 196, 237, 236
192, 196, 197, 238, 237
193, 197, 198, 239, 238
194, 198, 199, 240, 239
195, 199, 200, 241, 240
196, 200, 201, 242, 241
197, 201, 202, 243, 242
198, 202, 203, 244, 243
199, 203, 204, 245, 244
200, 204, 205, 246, 245
201, 206, 207, 248, 247
202, 207, 208, 249, 248
203, 208, 209, 250, 249
204, 209, 210, 251, 250
205, 210, 211, 252, 251
206, 211, 212, 253, 252
207, 212, 213, 254, 253
208, 213, 214, 255, 254
209, 214, 215, 256, 255
210, 215, 216, 257, 256
211, 216, 217, 258, 257
212, 217, 218, 259, 258
213, 218, 219, 260, 259
214, 219, 220, 261, 260
215, 220, 221, 262, 261
216, 221, 222, 263, 262
217, 222, 223, 264, 263
218, 223, 224, 265, 264
219, 224, 225, 266, 265
220, 225, 226, 267, 266
221, 226, 227, 268, 267
222, 227, 228, 269, 268
223, 228, 229, 270, 269
224, 229, 230, 271, 270
225, 230, 231, 272, 271
226, 231, 232, 273, 272
227, 232, 233, 274, 273
228, 233, 234, 275, 274
229, 234, 235, 276, 275
230, 235, 236, 277, 276
231, 236, 237, 278, 277
232, 237, 238, 279, 278
233, 238, 239, 280, 279
234, 239, 240, 281, 280
235, 240, 241, 282, 281
236, 241, 242, 283, 282
237, 242, 243, 284, 283
238, 243, 244, 285, 284
239, 244, 245, 286, 285
240, 245, 246, 287, 286
241, 247, 248, 289, 288
242, 248, 249, 290, 289
243, 249, 250, 291, 290
244, 250, 251, 292, 291
245, 251, 252, 293, 292
246, 252, 253, 294, 293
247, 253, 254, 295, 294
248, 254, 255, 296, 295
249, 255, 256, 297, 296
250, 256, 257, 298, 297
251, 257, 258, 299, 298
252, 258, 259, 300, 299
253, 259, 260, 301, 300
254, 260, 261, 302, 301
255, 261, 262, 303, 302
256, 262, 263, 304, 303
257, 263, 264, 305, 304
258, 264, 265, 306, 305
259, 265, 266, 307, 306
260, 266, 267, 308, 307
261, 267, 268, 309, 308
262, 268, 269, 310, 309
263, 269, 270, 311, 310
264, 270, 271, 312, 311
265, 271, 272, 313, 312
266, 272, 273, 314, 313
267, 273, 274, 315, 314
268, 274, 275, 316, 315
269, 275, 276, 317, 316
270, 276, 277, 318, 317
271, 277, 278, 319, 318
272, 278, 279, 320, 319
273, 279, 280, 321, 320
274, 280, 281, 322, 321
275, 281, 282, 323, 322
276, 282, 283, 324, 323
277, 283, 284, 325, 324
278, 284, 285, 326, 325
279, 285, 286, 327, 326
280, 286, 287, 328, 327
281, 288, 289, 330, 329
282, 289, 290, 331, 330
283, 290, 291, 332, 331
284, 291, 292, 333, 332
285, 292, 293, 334, 333

286, 293, 294, 335, 334
287, 294, 295, 336, 335
288, 295, 296, 337, 336
289, 296, 297, 338, 337
290, 297, 298, 339, 338
291, 298, 299, 340, 339
292, 299, 300, 341, 340
293, 300, 301, 342, 341
294, 301, 302, 343, 342
295, 302, 303, 344, 343
296, 303, 304, 345, 344
297, 304, 305, 346, 345
298, 305, 306, 347, 346
299, 306, 307, 348, 347
300, 307, 308, 349, 348
301, 308, 309, 350, 349
302, 309, 310, 351, 350
303, 310, 311, 352, 351
304, 311, 312, 353, 352
305, 312, 313, 354, 353
306, 313, 314, 355, 354
307, 314, 315, 356, 355
308, 315, 316, 357, 356
309, 316, 317, 358, 357
310, 317, 318, 359, 358
311, 318, 319, 360, 359
312, 319, 320, 361, 360
313, 320, 321, 362, 361
314, 321, 322, 363, 362
315, 322, 323, 364, 363
316, 323, 324, 365, 364
317, 324, 325, 366, 365
318, 325, 326, 367, 366
319, 326, 327, 368, 367
320, 327, 328, 369, 368
321, 329, 330, 371, 370
322, 330, 331, 372, 371
323, 331, 332, 373, 372
324, 332, 333, 374, 373
325, 333, 334, 375, 374
326, 334, 335, 376, 375
327, 335, 336, 377, 376
328, 336, 337, 378, 377
329, 337, 338, 379, 378
330, 338, 339, 380, 379
331, 339, 340, 381, 380
332, 340, 341, 382, 381
333, 341, 342, 383, 382
334, 342, 343, 384, 383
335, 343, 344, 385, 384
336, 344, 345, 386, 385
337, 345, 346, 387, 386
338, 346, 347, 388, 387
339, 347, 348, 389, 388
340, 348, 349, 390, 389
341, 349, 350, 391, 390
342, 350, 351, 392, 391
343, 351, 352, 393, 392
344, 352, 353, 394, 393
345, 353, 354, 395, 394
346, 354, 355, 396, 395
347, 355, 356, 397, 396
348, 356, 357, 398, 397
349, 357, 358, 399, 398
350, 358, 359, 400, 399
351, 359, 360, 401, 400
352, 360, 361, 402, 401
353, 361, 362, 403, 402
354, 362, 363, 404, 403
355, 363, 364, 405, 404
356, 364, 365, 406, 405
357, 365, 366, 407, 406
358, 366, 367, 408, 407
359, 367, 368, 409, 408
360, 368, 369, 410, 409
361, 370, 371, 412, 411
362, 371, 372, 413, 412
363, 372, 373, 414, 413
364, 373, 374, 415, 414
365, 374, 375, 416, 415
366, 375, 376, 417, 416
367, 376, 377, 418, 417
368, 377, 378, 419, 418
369, 378, 379, 420, 419
370, 379, 380, 421, 420
371, 380, 381, 422, 421
372, 381, 382, 423, 422
373, 382, 383, 424, 423
374, 383, 384, 425, 424
375, 384, 385, 426, 425
376, 385, 386, 427, 426
377, 386, 387, 428, 427
378, 387, 388, 429, 428
379, 388, 389, 430, 429
380, 389, 390, 431, 430
381, 390, 391, 432, 431
382, 391, 392, 433, 432
383, 392, 393, 434, 433
384, 393, 394, 435, 434
385, 394, 395, 436, 435
386, 395, 396, 437, 436
387, 396, 397, 438, 437
388, 397, 398, 439, 438
389, 398, 399, 440, 439
390, 399, 400, 441, 440
391, 400, 401, 442, 441
392, 401, 402, 443, 442
393, 402, 403, 444, 443
394, 403, 404, 445, 444
395, 404, 405, 446, 445
396, 405, 406, 447, 446
397, 406, 407, 448, 447
398, 407, 408, 449, 448
399, 408, 409, 450, 449
400, 409, 410, 451, 450
401, 411, 412, 453, 452
402, 412, 413, 454, 453
403, 413, 414, 455, 454
404, 414, 415, 456, 455
405, 415, 416, 457, 456
406, 416, 417, 458, 457
407, 417, 418, 459, 458
408, 418, 419, 460, 459
409, 419, 420, 461, 460
410, 420, 421, 462, 461
411, 421, 422, 463, 462
412, 422, 423, 464, 463
413, 423, 424, 465, 464
414, 424, 425, 466, 465
415, 425, 426, 467, 466
416, 426, 427, 468, 467
417, 427, 428, 469, 468
418, 428, 429, 470, 469
419, 429, 430, 471, 470
420, 430, 431, 472, 471
421, 431, 432, 473, 472
422, 432, 433, 474, 473
423, 433, 434, 475, 474
424, 434, 435, 476, 475
425, 435, 436, 477, 476
426, 436, 437, 478, 477
427, 437, 438, 479, 478
428, 438, 439, 480, 479
429, 439, 440, 481, 480
430, 440, 441, 482, 481
431, 441, 442, 483, 482
432, 442, 443, 484, 483
433, 443, 444, 485, 484
434, 444, 445, 486, 485
435, 445, 446, 487, 486

436, 446, 447, 488, 487
437, 447, 448, 489, 488
438, 448, 449, 490, 489
439, 449, 450, 491, 490
440, 450, 451, 492, 491
441, 452, 453, 494, 493
442, 453, 454, 495, 494
443, 454, 455, 496, 495
444, 455, 456, 497, 496
445, 456, 457, 498, 497
446, 457, 458, 499, 498
447, 458, 459, 500, 499
448, 459, 460, 501, 500
449, 460, 461, 502, 501
450, 461, 462, 503, 502
451, 462, 463, 504, 503
452, 463, 464, 505, 504
453, 464, 465, 506, 505
454, 465, 466, 507, 506
455, 466, 467, 508, 507
456, 467, 468, 509, 508
457, 468, 469, 510, 509
458, 469, 470, 511, 510
459, 470, 471, 512, 511
460, 471, 472, 513, 512
461, 472, 473, 514, 513
462, 473, 474, 515, 514
463, 474, 475, 516, 515
464, 475, 476, 517, 516
465, 476, 477, 518, 517
466, 477, 478, 519, 518
467, 478, 479, 520, 519
468, 479, 480, 521, 520
469, 480, 481, 522, 521
470, 481, 482, 523, 522
471, 482, 483, 524, 523
472, 483, 484, 525, 524
473, 484, 485, 526, 525
474, 485, 486, 527, 526
475, 486, 487, 528, 527
476, 487, 488, 529, 528
477, 488, 489, 530, 529
478, 489, 490, 531, 530
479, 490, 491, 532, 531
480, 491, 492, 533, 532
481, 493, 494, 535, 534
482, 494, 495, 536, 535
483, 495, 496, 537, 536
484, 496, 497, 538, 537
485, 497, 498, 539, 538
486, 498, 499, 540, 539
487, 499, 500, 541, 540
488, 500, 501, 542, 541
489, 501, 502, 543, 542
490, 502, 503, 544, 543
491, 503, 504, 545, 544
492, 504, 505, 546, 545
493, 505, 506, 547, 546
494, 506, 507, 548, 547
495, 507, 508, 549, 548
496, 508, 509, 550, 549
497, 509, 510, 551, 550
498, 510, 511, 552, 551
499, 511, 512, 553, 552
500, 512, 513, 554, 553
501, 513, 514, 555, 554
502, 514, 515, 556, 555
503, 515, 516, 557, 556
504, 516, 517, 558, 557
505, 517, 518, 559, 558
506, 518, 519, 560, 559
507, 519, 520, 561, 560
508, 520, 521, 562, 561
509, 521, 522, 563, 562
510, 522, 523, 564, 563
511, 523, 524, 565, 564
512, 524, 525, 566, 565
513, 525, 526, 567, 566
514, 526, 527, 568, 567
515, 527, 528, 569, 568
516, 528, 529, 570, 569
517, 529, 530, 571, 570
518, 530, 531, 572, 571
519, 531, 532, 573, 572
520, 532, 533, 574, 573
521, 534, 535, 576, 575
522, 535, 536, 577, 576
523, 536, 537, 578, 577
524, 537, 538, 579, 578
525, 538, 539, 580, 579
526, 539, 540, 581, 580
527, 540, 541, 582, 581
528, 541, 542, 583, 582
529, 542, 543, 584, 583
530, 543, 544, 585, 584
531, 544, 545, 586, 585
532, 545, 546, 587, 586
533, 546, 547, 588, 587
534, 547, 548, 589, 588
535, 548, 549, 590, 589
536, 549, 550, 591, 590
537, 550, 551, 592, 591
538, 551, 552, 593, 592
539, 552, 553, 594, 593
540, 553, 554, 595, 594
541, 554, 555, 596, 595
542, 555, 556, 597, 596
543, 556, 557, 598, 597
544, 557, 558, 599, 598
545, 558, 559, 600, 599
546, 559, 560, 601, 600
547, 560, 561, 602, 601
548, 561, 562, 603, 602
549, 562, 563, 604, 603
550, 563, 564, 605, 604
551, 564, 565, 606, 605
552, 565, 566, 607, 606
553, 566, 567, 608, 607
554, 567, 568, 609, 608
555, 568, 569, 610, 609
556, 569, 570, 611, 610
557, 570, 571, 612, 611
558, 571, 572, 613, 612
559, 572, 573, 614, 613
560, 573, 574, 615, 614
561, 575, 576, 617, 616
562, 576, 577, 618, 617
563, 577, 578, 619, 618
564, 578, 579, 620, 619
565, 579, 580, 621, 620
566, 580, 581, 622, 621
567, 581, 582, 623, 622
568, 582, 583, 624, 623
569, 583, 584, 625, 624
570, 584, 585, 626, 625
571, 585, 586, 627, 626
572, 586, 587, 628, 627
573, 587, 588, 629, 628
574, 588, 589, 630, 629
575, 589, 590, 631, 630
576, 590, 591, 632, 631
577, 591, 592, 633, 632
578, 592, 593, 634, 633
579, 593, 594, 635, 634
580, 594, 595, 636, 635
581, 595, 596, 637, 636
582, 596, 597, 638, 637
583, 597, 598, 639, 638
584, 598, 599, 640, 639
585, 599, 600, 641, 640

586, 600, 601, 642, 641
587, 601, 602, 643, 642
588, 602, 603, 644, 643
589, 603, 604, 645, 644
590, 604, 605, 646, 645
591, 605, 606, 647, 646
592, 606, 607, 648, 647
593, 607, 608, 649, 648
594, 608, 609, 650, 649
595, 609, 610, 651, 650
596, 610, 611, 652, 651
597, 611, 612, 653, 652
598, 612, 613, 654, 653
599, 613, 614, 655, 654
600, 614, 615, 656, 655
601, 616, 617, 658, 657
602, 617, 618, 659, 658
603, 618, 619, 660, 659
604, 619, 620, 661, 660
605, 620, 621, 662, 661
606, 621, 622, 663, 662
607, 622, 623, 664, 663
608, 623, 624, 665, 664
609, 624, 625, 666, 665
610, 625, 626, 667, 666
611, 626, 627, 668, 667
612, 627, 628, 669, 668
613, 628, 629, 670, 669
614, 629, 630, 671, 670
615, 630, 631, 672, 671
616, 631, 632, 673, 672
617, 632, 633, 674, 673
618, 633, 634, 675, 674
619, 634, 635, 676, 675
620, 635, 636, 677, 676
621, 636, 637, 678, 677
622, 637, 638, 679, 678
623, 638, 639, 680, 679
624, 639, 640, 681, 680
625, 640, 641, 682, 681
626, 641, 642, 683, 682
627, 642, 643, 684, 683
628, 643, 644, 685, 684
629, 644, 645, 686, 685
630, 645, 646, 687, 686
631, 646, 647, 688, 687
632, 647, 648, 689, 688
633, 648, 649, 690, 689
634, 649, 650, 691, 690
635, 650, 651, 692, 691
636, 651, 652, 693, 692
637, 652, 653, 694, 693
638, 653, 654, 695, 694
639, 654, 655, 696, 695
640, 655, 656, 697, 696
641, 657, 658, 699, 698
642, 658, 659, 700, 699
643, 659, 660, 701, 700
644, 660, 661, 702, 701
645, 661, 662, 703, 702
646, 662, 663, 704, 703
647, 663, 664, 705, 704
648, 664, 665, 706, 705
649, 665, 666, 707, 706
650, 666, 667, 708, 707
651, 667, 668, 709, 708
652, 668, 669, 710, 709
653, 669, 670, 711, 710
654, 670, 671, 712, 711
655, 671, 672, 713, 712
656, 672, 673, 714, 713
657, 673, 674, 715, 714
658, 674, 675, 716, 715
659, 675, 676, 717, 716
660, 676, 677, 718, 717
661, 677, 678, 719, 718
662, 678, 679, 720, 719
663, 679, 680, 721, 720
664, 680, 681, 722, 721
665, 681, 682, 723, 722
666, 682, 683, 724, 723
667, 683, 684, 725, 724
668, 684, 685, 726, 725
669, 685, 686, 727, 726
670, 686, 687, 728, 727
671, 687, 688, 729, 728
672, 688, 689, 730, 729
673, 689, 690, 731, 730
674, 690, 691, 732, 731
675, 691, 692, 733, 732
676, 692, 693, 734, 733
677, 693, 694, 735, 734
678, 694, 695, 736, 735
679, 695, 696, 737, 736
680, 696, 697, 738, 737
681, 698, 699, 740, 739
682, 699, 700, 741, 740
683, 700, 701, 742, 741
684, 701, 702, 743, 742
685, 702, 703, 744, 743
686, 703, 704, 745, 744
687, 704, 705, 746, 745
688, 705, 706, 747, 746
689, 706, 707, 748, 747
690, 707, 708, 749, 748
691, 708, 709, 750, 749
692, 709, 710, 751, 750
693, 710, 711, 752, 751
694, 711, 712, 753, 752
695, 712, 713, 754, 753
696, 713, 714, 755, 754
697, 714, 715, 756, 755
698, 715, 716, 757, 756
699, 716, 717, 758, 757
700, 717, 718, 759, 758
701, 718, 719, 760, 759
702, 719, 720, 761, 760
703, 720, 721, 762, 761
704, 721, 722, 763, 762
705, 722, 723, 764, 763
706, 723, 724, 765, 764
707, 724, 725, 766, 765
708, 725, 726, 767, 766
709, 726, 727, 768, 767
710, 727, 728, 769, 768
711, 728, 729, 770, 769
712, 729, 730, 771, 770
713, 730, 731, 772, 771
714, 731, 732, 773, 772
715, 732, 733, 774, 773
716, 733, 734, 775, 774
717, 734, 735, 776, 775
718, 735, 736, 777, 776
719, 736, 737, 778, 777
720, 737, 738, 779, 778
721, 739, 740, 781, 780
722, 740, 741, 782, 781
723, 741, 742, 783, 782
724, 742, 743, 784, 783
725, 743, 744, 785, 784
726, 744, 745, 786, 785
727, 745, 746, 787, 786
728, 746, 747, 788, 787
729, 747, 748, 789, 788
730, 748, 749, 790, 789
731, 749, 750, 791, 790
732, 750, 751, 792, 791
733, 751, 752, 793, 792
734, 752, 753, 794, 793
735, 753, 754, 795, 794

```
736, 754, 755, 796, 795
737, 755, 756, 797, 796
738, 756, 757, 798, 797
739, 757, 758, 799, 798
740, 758, 759, 800, 799
741, 759, 760, 801, 800
742, 760, 761, 802, 801
743, 761, 762, 803, 802
744, 762, 763, 804, 803
745, 763, 764, 805, 804
746, 764, 765, 806, 805
747, 765, 766, 807, 806
748, 766, 767, 808, 807
749, 767, 768, 809, 808
750, 768, 769, 810, 809
751, 769, 770, 811, 810
752, 770, 771, 812, 811
753, 771, 772, 813, 812
754, 772, 773, 814, 813
755, 773, 774, 815, 814
756, 774, 775, 816, 815
757, 775, 776, 817, 816
758, 776, 777, 818, 817
759, 777, 778, 819, 818
760, 778, 779, 820, 819
761, 780, 781, 822, 821
762, 781, 782, 823, 822
763, 782, 783, 824, 823
764, 783, 784, 825, 824
765, 784, 785, 826, 825
766, 785, 786, 827, 826
767, 786, 787, 828, 827
768, 787, 788, 829, 828
769, 788, 789, 830, 829
770, 789, 790, 831, 830
771, 790, 791, 832, 831
772, 791, 792, 833, 832
773, 792, 793, 834, 833
774, 793, 794, 835, 834
775, 794, 795, 836, 835
776, 795, 796, 837, 836
777, 796, 797, 838, 837
778, 797, 798, 839, 838
779, 798, 799, 840, 839
780, 799, 800, 841, 840
781, 800, 801, 842, 841
782, 801, 802, 843, 842
783, 802, 803, 844, 843
784, 803, 804, 845, 844
785, 804, 805, 846, 845
786, 805, 806, 847, 846
787, 806, 807, 848, 847
788, 807, 808, 849, 848
789, 808, 809, 850, 849
790, 809, 810, 851, 850
791, 810, 811, 852, 851
792, 811, 812, 853, 852
793, 812, 813, 854, 853
794, 813, 814, 855, 854
795, 814, 815, 856, 855
796, 815, 816, 857, 856
797, 816, 817, 858, 857
798, 817, 818, 859, 858
799, 818, 819, 860, 859
800, 819, 820, 861, 860
*Nset, nset=_PickedSet2, internal, generate
  1, 861,   1
*Elset, elset=_PickedSet2, internal, generate
  1, 800,   1
** Section: soil
*Solid Section, elset=_PickedSet2, material=camclay
,
*End Instance
**
***************************************************
************************************
*Nset, nset=bottom, instance=soil-1, generate
 1, 41,  1
*Elset, elset=bottom, instance=soil-1, generate
 1, 40,  1
*Nset, nset=top, instance=soil-1, generate
 821, 861,   1
*Elset, elset=top, instance=soil-1, generate
 761, 800,   1
*Nset, nset=sides, instance=soil-1
   1,  41,  42,  82,  83, 123, 124, 164, 165, 205, 206, 246, 247,
287, 288, 328
 329, 369, 370, 410, 411, 451, 452, 492, 493, 533, 534, 574, 575,
615, 616, 656
 657, 697, 698, 738, 739, 779, 780, 820, 821, 861
*Elset, elset=sides, instance=soil-1
  1,  40,  41,  80,  81, 120, 121, 160, 161, 200, 201, 240, 241,
280, 281, 320
 321, 360, 361, 400, 401, 440, 441, 480, 481, 520, 521, 560, 561,
600, 601, 640
 641, 680, 681, 720, 721, 760, 761, 800
*Nset, nset=soil, instance=soil-1, generate
  1, 861,   1
*Elset, elset=soil, instance=soil-1, generate
  1, 800,   1
*Nset, nset=_PickedSet9, internal, instance=soil-1, generate
 821, 861,   1
*Elset, elset=_PickedSet9, internal, instance=soil-1, generate
 761, 800,   1
*Elset, elset=_top_S3, internal, instance=soil-1, generate
 761, 800,   1
*Surface, type=ELEMENT, name=top
_top_S3, S3
*Nset, nset=bottom_PP_, internal, instance=soil-1, generate
 1, 41,  1
*Nset, nset=_PickedSet9_PP_, internal, instance=soil-1,
generate
 821, 861,   1
*Nset, nset=top_PP_, internal, instance=soil-1, generate
 821, 861,   1
*End Assembly
**
*************Defining Layer Sets
*Nset, nset=Layer-1, instance=soil-1
 821, 861
*Nset, nset=Layer-2, instance=soil-1
 780, 820
*Nset, nset=Layer-3, instance=soil-1
 739, 779
*Nset, nset=Layer-4, instance=soil-1
 698, 738
*Nset, nset=Layer-5, instance=soil-1
 657, 697
*Nset, nset=Layer-6, instance=soil-1
 616, 656
*Nset, nset=Layer-7, instance=soil-1
 575, 615
*Nset, nset=Layer-8, instance=soil-1
 534, 574
*Nset, nset=Layer-9, instance=soil-1
 493, 533
*Nset, nset=Layer-10, instance=soil-1
 452, 492
*Nset, nset=Layer-11, instance=soil-1
 411, 451
*Nset, nset=Layer-12, instance=soil-1
 370, 410
*Nset, nset=Layer-13, instance=soil-1
 329, 369
*Nset, nset=Layer-14, instance=soil-1
 288, 328
*Nset, nset=Layer-15, instance=soil-1
 247, 287
*Nset, nset=Layer-16, instance=soil-1
```

```
 206, 246
*Nset, nset=Layer-17, instance=soil-1
 165, 205
*Nset, nset=Layer-18, instance=soil-1
 124, 164
*Nset, nset=Layer-19, instance=soil-1
 83, 123
*Nset, nset=Layer-20, instance=soil-1
 42, 82
**
****************************************************
*End Assembly
**
** Define the sinusoidal function for the horizontal/shear displacement
*Amplitude, name=Cyclic_Shearing_Amp, definition=PERIODIC
1,     0.02964,           0.,           0.
          0.,          1.59
**
** Shearing Rate = 0.03mm/s
** Shearing Amplitude = 1.59mm
** Period T=212s
** Circular frequency = 2pi/T = 0.02964rad/s
**
** MATERIALS
**
** Define the modified Cam-Clay model
*Material, name=camclay
*Density
 1.57,
*POROUS ELASTIC, SHEAR=POISSON
** kappa v
  0.04,  0.3
*CLAY PLASTICITY, INTERCEPT=2.1
**Lam  M   ao   beta  K  T
0.174,  0.85,   ,  1.,   1., ,
**
** Define Horizontal and Vertical Permeability at Different Void Ratio Level
*Permeability, specific=10.
 2.6184e-10, 0.8
 3.7991e-10, 0.9
   5.3e-10,  1.
 7.1627e-10, 1.1
 9.4295e-10, 1.2
 1.2143e-09, 1.3
 1.5348e-09, 1.4
 1.9086e-09, 1.5
 2.3404e-09, 1.6
 2.8346e-09, 1.7
 3.3958e-09, 1.8
 4.0284e-09, 1.9
 4.7373e-09,  2.
  5.527e-09, 2.1
 6.4022e-09, 2.2
 7.3678e-09, 2.3
 8.4284e-09, 2.4
 9.5888e-09, 2.5
****************************************************
******
*INITIAL CONDITIONS, TYPE=STRESS, GEOSTATIC
soil, 0.0, 0.01867, -0.104, 0., 0.4, 0.4
*Initial Conditions, TYPE=RATIO
Soil, 1.827
*Initial Conditions, TYPE=SATURATION
Soil, 1.0
*Initial Conditions, Type=PORE PRESSURE
Soil, 0, 0.01867, 0.1867, 0.0
** BOUNDARY CONDITIONS
**
** Name: bottom Type: Displacement/Rotation
*Boundary
bottom, 2, 2
** Name: sides Type: Displacement/Rotation
*Boundary
sides, 1, 1
** ----------------------------------------------------------------
**
** STEP: Step-1
**
*Step, name=Step-1, nlgeom=YES, unsymm=YES
*Geostatic
**
** BOUNDARY CONDITIONS
**
** Name: botpore Type: Pore pressure
*Boundary
bottom_PP_, 8, 8, 0.1867
** Name: toppore Type: Pore pressure
*Boundary
_PickedSet9_PP_, 8, 8
**
** LOADS
**
** Name: Load-1   Type: Gravity
*Dload
soil, GRAV, 9.81, 0., -1.
**
** OUTPUT REQUESTS
**
*Restart, write, frequency=0
**
** FIELD OUTPUT: F-Output-1
**
*Output, field, variable=PRESELECT
**
** HISTORY OUTPUT: H-Output-1
**
*Output, history, variable=PRESELECT
*End Step
** ----------------------------------------------------------------
**
** STEP: Step-2
**
*Step, name=Step-2, nlgeom=YES, inc=10000, unsymm=YES, AMPLITUDE=RAMP
*Soils, consolidation, end=PERIOD, utol=1000.
0.001, 50., 1e-25, 5.,
**
** BOUNDARY CONDITIONS
**
** Name: botpore Type: Pore pressure
*Boundary, op=NEW
** Name: bottom Type: Displacement/Rotation
*Boundary, op=NEW
bottom, 2, 2
** Name: sides Type: Displacement/Rotation
*Boundary, op=NEW
sides, 1, 1
** Name: toppore Type: Pore pressure
*Boundary, op=NEW
**
** LOADS
**
** Name: Load-2   Type: Pressure
*DsLoad
top, P, 60.
**
** OUTPUT REQUESTS
**
*Restart, write, frequency=0
**
** FIELD OUTPUT: F-Output-1
**
*Output, field, variable=PRESELECT
**
** HISTORY OUTPUT: H-Output-1
**
*Output, history, variable=PRESELECT
```

```
*End Step
** ----------------------------------------------------------------
**
** STEP: Step-3
**
*Step, name=Step-3, nlgeom=YES, inc=10000, unsymm=YES,
AMPLITUDE=RAMP
*Soils, consolidation, end=ss, utol=100.
0.001, 172800., 1e-25, 500., 1e-15
** END=SS end when steady step is reached
** 0.001= initial increment size, 172800=period=48hrs, 1e-25=
min increment size,
** 500= max increment size
** End the consolidation when the pore pressure change is less
than 1e-15kPa
**
** BOUNDARY CONDITIONS
**
** Name: topporestep3 Type: Pore pressure
*Boundary
top_PP_, 8, 8, 0
**
** OUTPUT REQUESTS
**
*Restart, write, frequency=0
**
** FIELD OUTPUT: F-Output-1
**
*Output, field, variable=PRESELECT
**
** HISTORY OUTPUT: H-Output-1
**
*Output, history, variable=PRESELECT
*End Step
** ----------------------------------------------------------------
**
** STEP: Step-4
**
*Step, name=Step-4, nlgeom=YES, inc=100000
*Soils, consolidation, end=PERIOD, utol=100.
0.001, 4240, 1e-25, 5.,
** 0.001=initial increment size, 4240=period, 1e-25=min inc
size, 5=max inc size
**
** Period = 212s, Number of Cycles = 20, Total Time=4240s
** BOUNDARY CONDITIONS
**
** Name: bottom Type: Displacement/Rotation
*Boundary, op=NEW
bottom, 2, 2
bottom, 1, 1
** Name: sides Type: Displacement/Rotation
*Boundary, op=NEW
** Name: topporestep3 Type: Pore pressure
** The pore pressure at top is set as 0kPa
*Boundary, op=NEW
top_PP_, 8, 8, 0
*****************************Define Top Shearing BCs
** Name: Shearing-Layer-1 Type: Displacement/Rotation
*Boundary, op=NEW, amplitude=Cyclic_Shearing_Amp
top, 1, 1, 0.001
*****************************Define Linear Side BCs
** The following lines define the cyclic shear/horiozntal
displacement of nodes at the vertical edges
** Name: Shearing-Layer-2 Type: Displacement/Rotation
*Boundary, op=NEW, amplitude=Cyclic_Shearing_Amp
Layer-2, 1, 1, 0.00095
** Name: Shearing-Layer-3 Type: Displacement/Rotation
*Boundary, op=NEW, amplitude=Cyclic_Shearing_Amp
Layer-3, 1, 1, 0.0009
** Name: Shearing-Layer-4 Type: Displacement/Rotation
*Boundary, op=NEW, amplitude=Cyclic_Shearing_Amp
Layer-4, 1, 1, 0.00085
** Name: Shearing-Layer-5 Type: Displacement/Rotation
*Boundary, op=NEW, amplitude=Cyclic_Shearing_Amp
Layer-5, 1, 1, 0.0008
** Name: Shearing-Layer-6 Type: Displacement/Rotation
*Boundary, op=NEW, amplitude=Cyclic_Shearing_Amp
Layer-6, 1, 1, 0.00075
** Name: Shearing-Layer-7 Type: Displacement/Rotation
*Boundary, op=NEW, amplitude=Cyclic_Shearing_Amp
Layer-7, 1, 1, 0.0007
** Name: Shearing-Layer-8 Type: Displacement/Rotation
*Boundary, op=NEW, amplitude=Cyclic_Shearing_Amp
Layer-8, 1, 1, 0.00065
** Name: Shearing-Layer-9 Type: Displacement/Rotation
*Boundary, op=NEW, amplitude=Cyclic_Shearing_Amp
Layer-9, 1, 1, 0.0006
** Name: Shearing-Layer-10 Type: Displacement/Rotation
*Boundary, op=NEW, amplitude=Cyclic_Shearing_Amp
Layer-10, 1, 1, 0.00055
** Name: Shearing-Layer-11 Type: Displacement/Rotation
*Boundary, op=NEW, amplitude=Cyclic_Shearing_Amp
Layer-11, 1, 1, 0.0005
** Name: Shearing-Layer-12 Type: Displacement/Rotation
*Boundary, op=NEW, amplitude=Cyclic_Shearing_Amp
Layer-12, 1, 1, 0.00045
** Name: Shearing-Layer-13 Type: Displacement/Rotation
*Boundary, op=NEW, amplitude=Cyclic_Shearing_Amp
Layer-13, 1, 1, 0.0004
** Name: Shearing-Layer-14 Type: Displacement/Rotation
*Boundary, op=NEW, amplitude=Cyclic_Shearing_Amp
Layer-14, 1, 1, 0.00035
** Name: Shearing-Layer-15 Type: Displacement/Rotation
*Boundary, op=NEW, amplitude=Cyclic_Shearing_Amp
Layer-15, 1, 1, 0.0003
** Name: Shearing-Layer-16 Type: Displacement/Rotation
*Boundary, op=NEW, amplitude=Cyclic_Shearing_Amp
Layer-16, 1, 1, 0.00025
** Name: Shearing-Layer-17 Type: Displacement/Rotation
*Boundary, op=NEW, amplitude=Cyclic_Shearing_Amp
Layer-17, 1, 1, 0.0002
** Name: Shearing-Layer-18 Type: Displacement/Rotation
*Boundary, op=NEW, amplitude=Cyclic_Shearing_Amp
Layer-18, 1, 1, 0.00015
** Name: Shearing-Layer-19 Type: Displacement/Rotation
*Boundary, op=NEW, amplitude=Cyclic_Shearing_Amp
Layer-19, 1, 1, 0.0001
** Name: Shearing-Layer-20 Type: Displacement/Rotation
*Boundary, op=NEW, amplitude=Cyclic_Shearing_Amp
Layer-20, 1, 1, 0.00005
**************************************************
*******
** OUTPUT REQUESTS
**
*Restart, write, frequency=0
**
** FIELD OUTPUT: F-Output-1
**
*Output, field, variable=ALL
**
** HISTORY OUTPUT: H-Output-1
**
*Output, history, variable=PRESELECT
*End Step
```